UTS UNIVERSITY OF TECHNOLOGY SYDNEY

# DEVELOPMENT OF PRECISION 3D-PRINTED MEDICAL IMPLANTS

**by Hakim Ullah Wazir**

Thesis submitted in fulfilment of the requirements for
the degree of

**Doctor of Philosophy**

Under the supervision of Dr. Joshua Chou & Dr. Nico Pietroni

University of Technology Sydney
Faculty of Engineering and IT
School of Biomedical Engineering

August 2023

# CERTIFICATE OF ORIGINAL AUTHORSHIP

I, Hakim Ullah Wazir declare that this thesis, is submitted in fulfilment of the requirements for the award of Doctor of Philosophy, in the School of Biomedical Engineering, Faculty of Engineering and Information Technology at the University of Technology Sydney.

This thesis is wholly my own work unless otherwise referenced or acknowledged. In addition, I certify that all information sources and literature used are indicated in the thesis.

This document has not been submitted for qualifications at any other academic institution.

This research is supported by the Australian Government Research Training Program.

Signature: Production Note:
Signature removed prior to publication.

Date: 13/08/2023

# Disclaimer

This project has been impacted by the global ongoing COVID-19 pandemic and the lockdown restriction that has been implemented by the Australian government to slow down the infection rate by restricting citizens' movements and to reduce people to gather with other people outside their household. Due to such circumstances, I could not go on campus at UTS to access the laboratory to conduct experiments and finish my project on time. We also had to make critical changes to my project proposal as my 3rd aim to conduct animal studies could not happen due to COVID-19 strict global lockdown circumstances.

The 1st major setback for this project occurred during the initial stages of COVID-19 outbreak at the start of 2020 when WHO officially declared COVID-19 a pandemic. By mid-late March 2020 the Australian government progressively implemented the lockdown restrictions. Easing of lockdown restriction was gradually reinstated across Australia by end of May. During this time, major changes were taking place to this project. The 3rd aim of this project was animal studies, what involved examining porous 3D printed dental implants in beagle dog, that was supposed to take place in China. Due to the COVID-19 outbreak, the 3rd aim of this project was changed from conducting animal studies to further examining medical implants in an in-vitro study using implant-on-chip. Implant-on-chip allows certain conditions such as mechanical force applied on cells in an in-vitro setting to help reproduce and mimic an *in vivo* cellular microenvironment. The implant-on-chip study would paint a better picture by examining the cellular response on medical implants in an in-vitro setting by artificially creating an *in vivo* microenvironment.

Whilst undertaking the final aim for this study, which involved designing and optimisation the chip features to hold together for 24 hours, continuous fluid shear stress run at ~0.5-1 dynes/cm$^2$ without leakage. Australia went through another major lockdown by end of June 2021 in NSW due to COVID-19 delta variant transmissions within the communities. Strict measures were taken by UTS to revoke research students' card access to buildings/labs, where permission were only granted to final year students, who were not living within the local government areas (LGA) of concern and making sure each student had one dose of Pfizer or AstraZeneca vaccine before being granted approval for particular

days and times during the week. My access was unfortunately revoked due to my residency being in one of the LGA's of concern and was told to not come to UTS campus until further notice. During this 3 month long delays, I was not able to execute my gene analysis experiment and complete my final chapter for my thesis. I have asked for extension, to complete my experiments and write my final chapter before submission. This long delays also caused major setbacks due to majority of the ddPCR consumables being expired by the end of the year and had to be repurchased, which took about a month to arrive.

# Acknowledgements

To my supervisor and mentor Dr. Joshua Chou. Thank you for your patient guidance, encouragement, advice and continuous support that you have provided me throughout my candidature as your student. I have been extremely lucky to have a supervisor who cared so much about my work and focused on my strengths to excel me in so many other areas. It has been an honour and a privilege to be your student. I wouldn't have been at this current stage in life without you and your continuous support. Thank you for giving me this podium to enhance my skills that are going to be vital for the betterment of society.

To my co-supervisor Dr. Nico Pietroni, thank you for guiding me with technical matters to further enhance my skillset in 3D modelling. You have been instrumental towards my project and I appreciate your helping hand. Thank you for sharing with me your innovative ideas to implement in my project.

To my friends and group members, Andrew Shehata, Andrew Li, Parker Liang and Ipek Karacan Soylu as well as the rest of Dr. Joshua Chou group members over the years; thank you for your continuous support and contribution towards my project.

Finally, I would like to thank my mum and dad for their continuous support during this long tedious PhD journey. It would not have been possible or an easy journey without your support. Especially to my little brother Sibghat who has been heavily invested in my crazy ideas to bring them into fruition. Thank you for your continuous support and encouragement.

# Contents

# List of Tables



# List of Figures

# Abbreviation

| | |
|---|---|
| AI | Artificial Intelligence |
| µL | Microlitre |
| AD | Alzheimer's disease |
| Ag | Sliver |
| AI | Artificial Intelligence |
| ALP | Alkaline phosphatase |
| Bglap2 | bone gamma-carboxyglutamate protein 2 |
| BMPs | Bone Morphogenetic Proteins |
| cDNA | Complementary Deoxyribonucleic Acid |
| Col1α1 | Collagen type I alpha 1 |
| CPT | commercialised pure titanium |
| CT | Computed tomography |
| CTRL | Control |
| ddPCR | Droplet Digital polymerase chain reaction |
| DMP1 | Dentin Matrix Acidic Phosphoprotein 1 |
| DNA | Deoxyribonucleic Acid |
| EBL | Electron Beam Lithography |
| ECM | Extracellular matrix |
| FBS | Foetal bovine serum |
| FGF | Fibroblast Growth Factors |
| FIJI | FIJI Is Just Image J Software |
| FSS | Fluid shear stress |
| GAPDH | Glyceraldehyde 3-phosphate dehydrogenase |
| GPa | Gigapascals |

| | |
|---|---|
| HMSCs | Human mesenchymal stem cells |
| IGF-1 | Insulin-like growth factor 1 |
| Mef2c | Myocyte enhancer-binding factor 2C |
| MEMα | Minimum Essential Medium Alpha |
| MPa | Megapascal |
| MRI | Magnetic resonance imaging |
| SMSCs | Skeletal Mesenchymal Stem Cells |
| NB | Niobium |
| OC | Osteocalcin |
| OPG | Osteoprotegerin |
| OPN | Osteopontin |
| P/S | Penicillin/Streptomycin |
| PDGF | Platelet-Derived Growth Factor |
| PHEX | Phosphate Regulating Endopeptidase Homolog X-Linked |
| PRGF | Plasma Rich in Growth Factors |
| PTH | Parathyroid hormone |
| RANK | Receptor activator of nuclear factor κ B |
| RANKL | Receptor activator of nuclear factor kappa-B ligand |
| RD | Relative density |
| RNA | Ribonucleic acid |
| RT-qPCR | reverse Transcription-quantitative polymerase chain reaction |
| RUNX2 | Runt-related transcription factor 2 |
| SAB | staphylococcus aureus bacteraemia |
| SLA | Sand-blasted, Large grit, Acid etched |
| SLS | Selective laser sintering |
| Sn | Tin |
| SOST | Sclerostin |
| SPP1 | Secreted phosphoprotein 1 |
| Ta | Tantalum |
| TGF-β | Transforming Growth Factor Beta |
| Ti | Titanium |
| Ti-12Nb-12Zr-12Sn (T12) | Titanium-12Niobium-12Zirconium-12Tin |
| Ti-6Al-4V (T64) | Titanium-6Aluminium-4Vanadium |
| $TiO_2$ | Titanium oxide |
| VEGF | Vascular Endothelial Growth Factor |
| Zr | Zirconium |

# Chapter 1 - Introduction

# Chapter 1 - Introduction

This chapter provides context for my research, delivers detailed bone biology, contributes the basis for all commercialised medical implants and describes the aetiology for failure of current medical implant. It then outlines key strategies and interventions to overcome the challenges that current medical implant faces, and how such strategies will improve long-term fixation and enhance osseointegration. Thereby, this background helps provide the framework for the aim and scope of this project and defines its research questions.

The thesis aims and hypothesis for the overall project is set out at the end of this chapter.

# 1. Background

In Australia each year we spend $11.8 billion on medical implants (*Industry Statistics - MTAA*, 2014). Bone fracture is common especially within the elderly population, which includes 28% of the population over the age of 55 (CIA, 2018). Due to metal implants' high mechanical reliability, approximately 80% of medical devices and 95% of orthopaedic devices are all currently produced from metal and thereby, plays an integral role in medical treatment. The most basic expectations of these implants is to reinforce mechanical stabilization, ensure alignment and enable normal function of skeleton (Hanawa, 2021). During implant placement, osseointegration occurs, which refers to the bonding between the implant and the surrounding bone tissue. That way the implant is held strongly in place. If this bonding doesn't occur, implant fails (Li et al., 2018). If individual areas of implant placement are observed, for example, in Australia about 45,000 spinal implants are placed every year, where Australians spend about $486 million and within the first two years 23% of spinal implants fails that leads to a revision surgery (Apos E, 2019). Similarly, approximately 50,000 hip implants and 64,000 knee implants are placed every year costing Australians about $1.2 billion; and about 20-24% implants fail within the first two years leading to a revision surgery due to poor osseointegration (Ackerman et al., 2019). So there is still a high failure and revision surgery rate of medical implants. This causes a significant social-economic burden on patients and on the healthcare system. There is a

current need for innovative solutions to increase the efficiency and recovery of medical bone implants and to achieve that will require better and improved osseointegration, which is the bonding between the implant and the surrounding tissue. The current challenge lies in that every patient is anatomically different and therefore recovery is also different. With the introduction of 3D printing especially with metallic printing, opens a new era where personalized 3D printed implants is now becoming a possibility. To that end this background will cover the research gap that is lacking within current bone medical implants and what is needed to help improve long term fixation. This will not only enhance osseointegration but the recovery time as well.

## 1.1 Bone biology and remodelling

Human bones go through continuous repair and remodelling. Osteoblast are the cells responsible for the repair mechanism by synthesizing and mineralizing bones during both periods of initial bone formation and the later phase in life when bone remodelling is taking place (Britannica, 2016). In this case bone repair and remodelling mechanism are coordinated by the action of two main cell types, which are bone-resorbing osteoclasts and bone-forming osteoblasts (Fakhry et al., 2013).

### 1.1.1 Skeletal mesenchymal stem cells and bone cells

Bones are constantly being demineralised and reformed, which is to maintain bone volume and calcium homeostasis. Human bones are stiff, slightly flexible, and light enough for locomotion as well as to make loading possible. Bones are made out of cells and an extracellular matrix that develops from being mineralised by the calcium hydroxyapatite, which gives bone its rigidity and strength. There are three types of cells that facilitate born formation, remodel and maintain bone, which are osteoblast (bone forming cells), osteoclast (bone resorbing cells), and osteocytes (which are basically osteoblasts cells that differentiates into osteocyte by being entrapped within lacunae). So osteocytes are cells that lies within a fully formed bone structure, located in a small chamber called lacuna from where it communicates with its surroundings via tiny channels called canaliculi as seen in Figure 1 (Katagiri & Takahashi, 2002). Furthermore, osteocyte cells act as mechnosensors that has the ability to detect

mechanical stimuli and help initiate bone remodelling by sending signals to other effector cells that regulate bone formation and resorption (You et al., 2008).

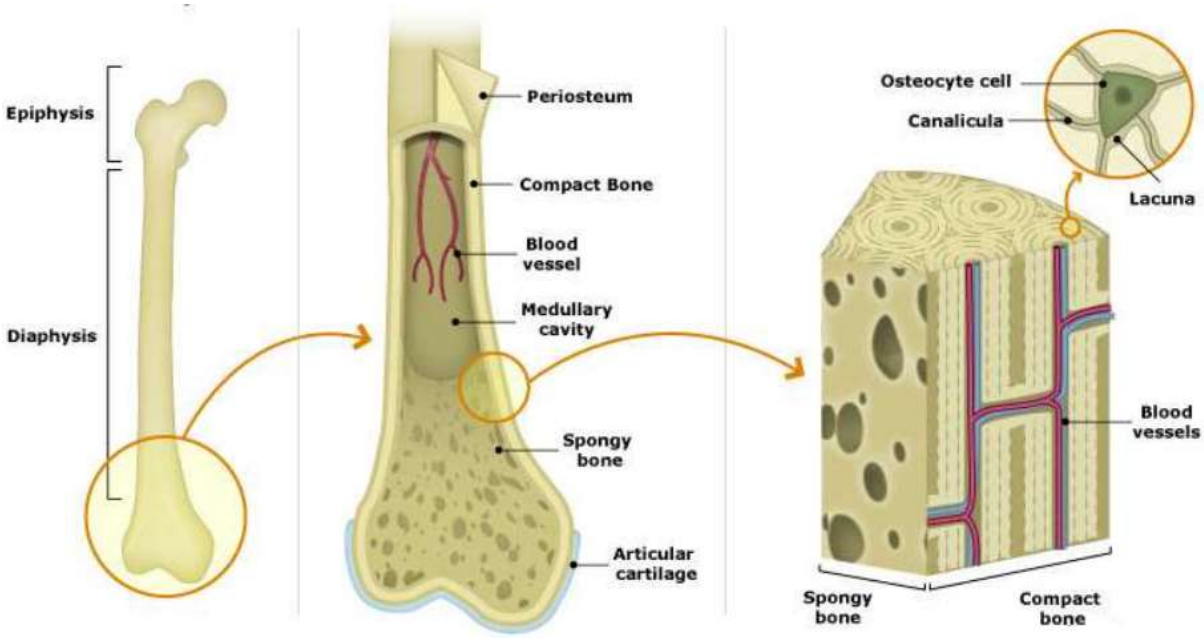


**Figure 1.** Osteocyte cells are located within the small chambers called lacuna. They communicate with its surroundings via tiny channels called canaliculi (Zayed, 2018).

The production of osteoblasts is called osteoblastogenesis that is defined by four major phases, which are "lineage commitment, proliferative expansion, synthesis of extracellular matrix and mineralization" (Javed et al., 2010). Skeletal stem cells (SSCs) are a rare multipotent stem cells residing in the bone marrow stroma that can differentiate into osteoblasts, chondrocytes, adipocytes, and stromal cells depending on their microenvironment (Figure 2) (Van Gastel & Carmeliet, 2021). SSCs ability to generate cartilage, bone, stroma, and marrow adipocytes have distinct skeletal lineages and controlled by specific developmental processes. Regulation of lineage commitment to chondrogenesis, osteogenesis and adipogenesis is regulated by three master transcription factors, which are Sox9 (chondrogenic), Runx2 (osteogenic), CXCL12 (Stromal cell formation) and PPARϒ2 (adipogenic). In the osteogenic lineage commitment, BMP acts via Msx/Dlx homeoproteins to upregulate Runx2

expression, which as a result increases OSX expression (Bianco & Robey, 2015; Cook & Genever, 2013). PTHrP protein contributes to the upregulation of Col1a1 in osteoblasts, influencing the osteoblasts lineage commitment from SSCs (Feng et al., 2022). Furthermore, OCN is strictly secreted by osteoblasts and is specifically responsible for the synthesis and mineralization of bone matrix during the development of the skeleton; in this case it is indicative of matured osteoblasts successfully differentiated from SSCs (Petersen et al., 2000).

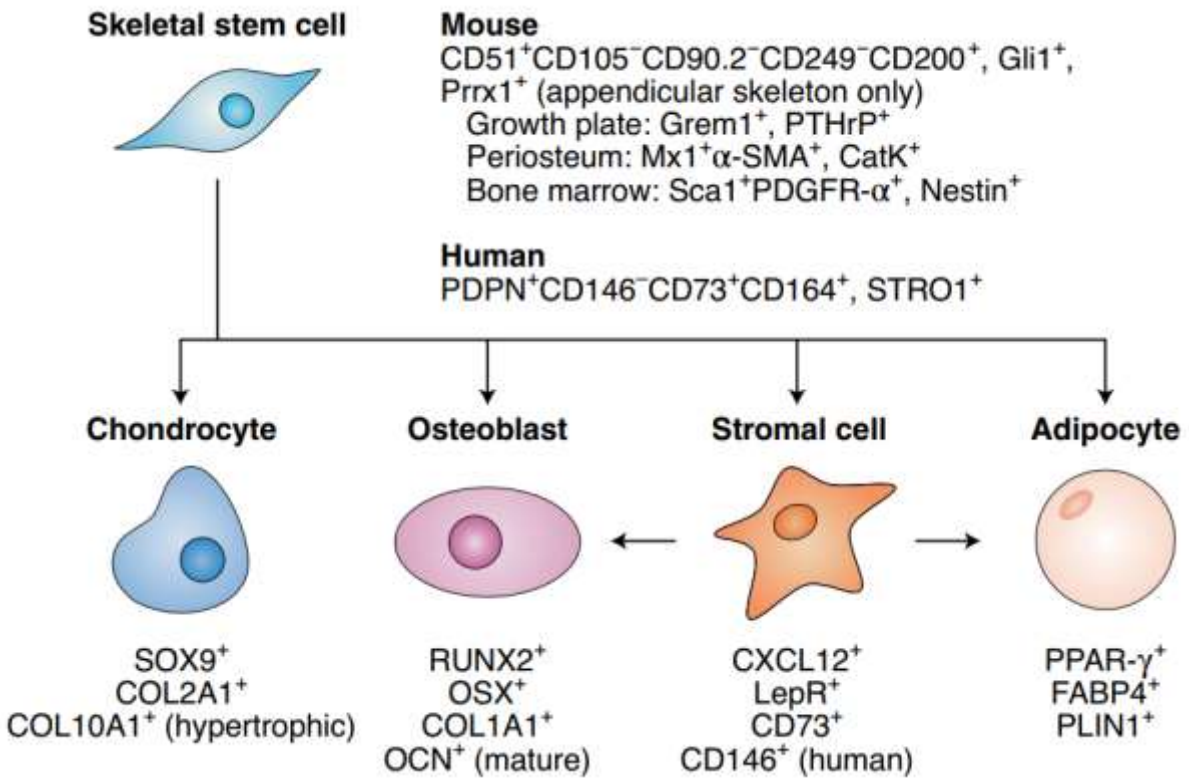


**Figure 2.** Shows the flow diagram of Skeletal stem cell differentiating into all the different cell type such as chondrocyte, osteoblast, stromal cells and adipocyte that are directed by the indicated transcription factors. The osteoblast differentiation pathway is mediated through the transcription factors of Runx2, Osx, COL1A1 and OCN. The most commonly used markers for identification or isolation are listed for both mouse and human cell type (Van Gastel & Carmeliet, 2021).

The expression of matrix genes also takes place during this stage such as type-l collagen and fibronectin, alongside the growth factors counterparts BMP2/TGFβ. The third stage involves osteoblast cells clustering, multi-layering of the cells and initialise the synthesise of matured extracellular matrix. In the final stage of osteoblastogenesis involves minerals deposits in the extracellular matrix. These include the non-collagenous extracellular matrix protein expression of bone sialoprotein, osteocalcin

and osteopontin. Approximately 85% of osteoblast cells does not achieve the phenotypic transition of an osteocyte as they undergo apoptosis by the end of this stage. Osteocyte cells are bone cells, which are basically formed by an osteoblast cell differentiating into osteocyte cells where they embed themselves in the materials that it has secreted. Hence, osteocytes are both spatially and morphologically different to that of osteoblast cells, in the sense that they are completely encapsulated in bone and have dendritic processes. The dendritic long branched processes enables osteocytes to communicate with each other as well as to communicate with osteoblasts cells and lining cells that are present on the surface of the bone, along with the marrow stromal cells that are present on the endosteum (Javed et al., 2010).

### 1.1.2 The bone remodelling process

There are five stages within the bone remodelling process as seen in Figure 3. Osteocytes dendritic factors senses external stimulation that respond with the production of a protein called sclerostin, which helps inhibit osteoblast cells activity and initiate osteoclast activity (Feng et al., 2006). Also osteoblasts secrete cytokines to stimulate nearby osteoclast progenitors (Ducy et al., 1997). The osteoclast progenitors differentiate into osteoclasts to start the resorption of bone. After the resorption phase, osteoclast moves away from the demineralised bone area. Macrophages initiates the reversal process by removing debris left behind from osteoclast resorption phase. Once all the debris is cleared out and macrophage moves away from the area, osteoblast progenitors differentiate into osteoblasts. These osteoblasts initiate the formation of proteinaceous matrix called osteoid which becomes mineralised during the formation stage. The bone remodelling process is ended when the same amount of bone is created that was resorbed and the process comes to the resting stage (Kohli et al., 2018).

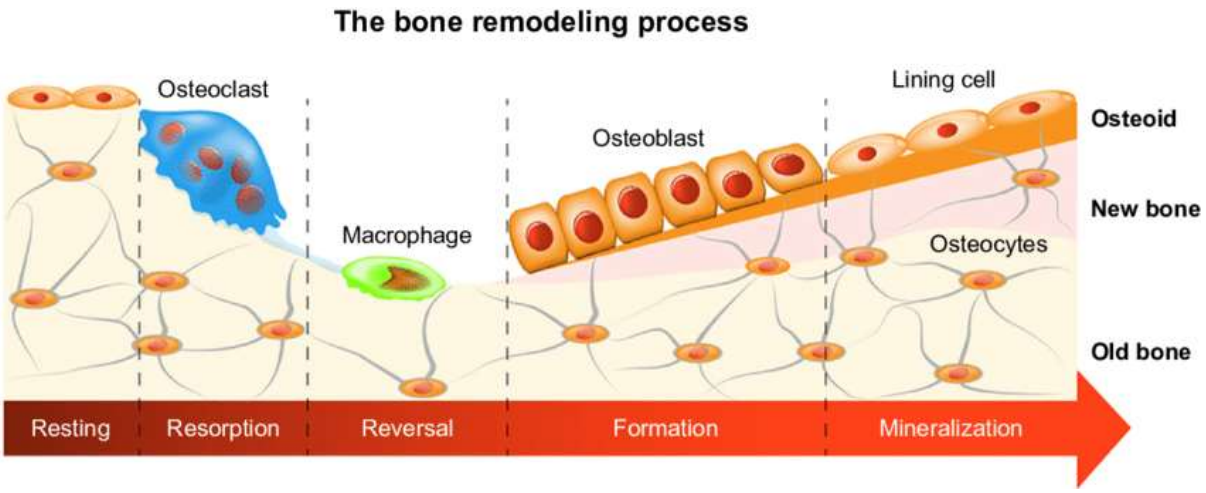


**Figure 3.** Flow diagram showing the bone remodelling stages. It initialises with a resorption stage by the osteoclast cells. Followed by reversal stage of macrophage to clear out the demineralise bone. Once the demineralised bone is cleared out, formation stage initiates with osteoblast cells to form the new layer of bone. Osteoblasts initiate the formation of proteinaceous matrix called osteoid during the mineralization stage. The cycle comes to a resting stage when the same amount of bone is created that was resorbed (Lisowska et al., 2018).

### 1.1.3 Interaction between osteoblasts, osteocytes and osteoclast cells

Osteoblast cells help build new bone matrix, which is soft initially but hardens up under various hormones and chemicals that are secreted out by the osteoblast cells. Whereas osteoclast cells have the responsibility to resorb/break down bone matrix. Continuous bone production and bone resorption in a balance manner is necessary to help remodel and renew the skeleton. Since osteoblast, chondrocytes, myocytes and adipocytes are derived from a common progenitor stem cells called skeletal mesenchymal cells. It is the bone morphogenetic proteins (BMPs) that help regulate differentiation of osteoblast cells from skeletal mesenchymal stem cells. Runx2 and Osterix are the two main transcription factors that are responsible for inducting osteoblast differentiation. On the other hand, osteoclasts are multinucleated cells that are differentiated from haemopoietic stem cells from the lineage of monocyte and macrophage under bone microenvironment conditions. Osteoblast plays a critical role in the induction of osteoclast differentiation through the receptor activation called NF-$_k$B ligand, and (RANKL)-RANK interaction. Osteoblasts expresses RANKL, which is a membrane associated factor and osteoclast expresses RANK, which is a receptor to recognise RANKL during cell-cell interaction

that leads to the differentiation of osteoclast cells as seen in Figure 4 (Caetano-Lopes et al., 2007; Katagiri & Takahashi, 2002).

Even though osteoblast cells regulate the differentiation of osteoclast cells, it is osteocytes that secrete factors to regulate both osteoblast and osteoclast cells. Bone resorption through osteoclast takes 2-3 weeks, whereas osteoblast bone forming cells that rebuild the bone takes three months (Caetano-Lopes et al., 2007). Osteocyte cells in response to mechanical stimuli produces sclerostin, RANKL and osteoprotegerin (OPG) for the initiation of bone remodelling machnism starting with osteoclast cells and then followed by osteoblast cells (Morrell et al., 2018; Tanaka et al., 2005). Sclerostin is a negative regulator of bone formation promoted by the SOST gene in osteocytes. When sclerostin is upregulated, it influences OPG to be downregulated and in return upregulating RANKL in greater number resulting in the activation of bone resorbing osteoclast through RANKL binding to the receptor RANK on osteoclast cells. Henceforth, Sclerostin supresses bone formation by inhibiting the differentiation of osteoblasts (Van Bezooijen et al., 2004). On the other hand, when sclerostin is downregulated, it leads to the upregulation of OPG in greater number and supresses RANKL, resulting in OPG binding to RANK thereby blocking RANKL from binding to RANK receptor on osteoclast leading to reduced bone resorption activity and increased bone formation activity via osteoblasts activation (Lara-Castillo et al., 2015; Pflanz et al., 2017; Van Bezooijen et al., 2004). Furthermore, osteoblast cells can also secrete a soluble decoy receptor called OPG that block RANK/RANKL interaction by binding to the RANKL; leading to the deactivation of osteoclast differentiation and help stop bone resorption as seen in figure 4 (Caetano-Lopes et al., 2007).

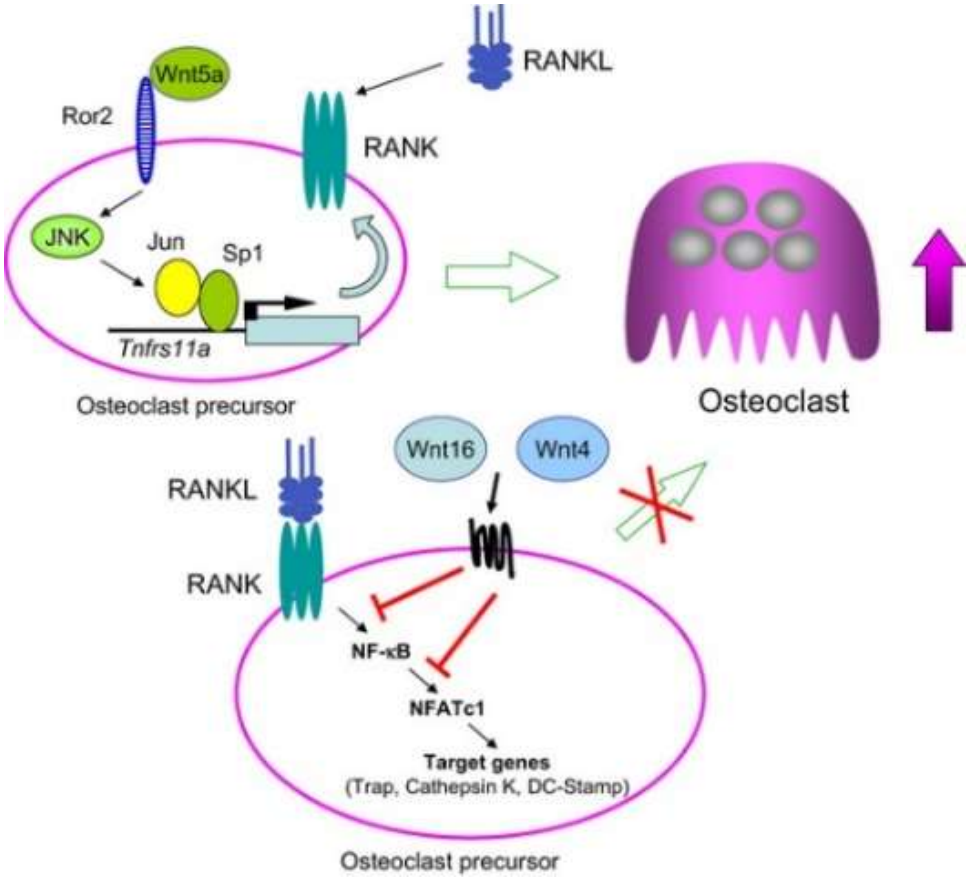


**Figure 4.** Shows the non-canonical Wnt signalling in relation to osteoclast differentiation. Osteoblasts secretes Wnt5A when it binds with the Ror2 precursors in osteoclast cells. The signals from the mediated Ror2 promotes the expression of Rank in osteoclast precursors, which enhance the Rankl induced osteoclast differentiation. On the other hand, both Wnt4 and Wnt16 that are also secreted by osteoblast cells can lead to the inhibition of Rankl-induced activation of NF-κB and NFATc1 signals; resulting in the inhibition of osteoclast differentiation (Y. Kobayashi et al., 2015).

In addition, 95% of the living adult bone cells are made up of osteocytes, whereas about 4-6% are osteoblast cells and a small portion of about 1-2% are osteoclast cells(Javed et al., 2010). Hence, osteocytes are known for their longevity and can survive for decades within their bony chambers. They are spread throughout the bone matrix that communicates with nearby osteocytes, osteoblasts, osteoclasts and other distinct tissues and organs through a direct contact, using their tentacle like dendrites that extends throughout the canaliculi. They control the activity of osteoblast and osteoclast by secreting factors through the dendrites, influencing the remodelling of bone structure directly. One study has found that only osteocytes secrete this protein called sclerostin, that helps inhibit osteoblast cells activity and initiate osteoclast activity. When osteocytes are producing more sclerostin, bone regeneration slows down, but when bones are under physical stress, osteocyte secrete less sclerostin,

initiating bone production via osteoblasts in areas where the bone is under stressful conditions. So osteocyte has the ability to sense areas around the bone that are under stress and know the difference between healthy bone and injured (worn and torn area on the bone) that may occur on the healthy skeleton (Lewiecki, 2014). Under the circumstances of a fracture or a break in the bone, osteocytes secrete insulin-like growth factor 1 (IGF-1) that help stimulate the activity of osteoblast cells to accelerate the formation of new bone in the injured area. Therefore, osteocyte main purpose is to help sense injury and communicate with osteoblasts and osteoclasts to regulate the necessary repairs around the skeleton (Sheng et al., 2014).

## 1.2 Cell Interaction with bone implants

3D printing technology has the capability to fully control the 3D modelling features at a nano-level to help replicate natural cellular environment that can influence and regulate molecular behaviour at nanoscale. Majority of the inorganic component of bone is hydroxyapatite, measured to be between 2 to 5nm in width and around 50 nm in length. Whereas the major organic component of bone is collagen I, measured to be around 300 nm in length and 0.5 nm in width. The surface roughness of natural bone was calculated to range between 25-32 nm. Thereby, natural bone surface roughness holds nanometric features. This can be overcome by nanophase titanium surface roughness using 3D printing technology, to help replicate surface roughness of bone (Rodriguez y Baena et al., 2017). In relation to surface roughness of cortical bone, the pore size of cancellous bone has a much greater diameter than cortical bone. Approximately 75-85% of the cancellous bone structure is porous that ranges between 300-600 μm in diameter. Whereas 5-10% of cortical bone structure is porous which ranges between 10-50 μm in diameter. Cortical bone has a compressive strength between 110-150 megapascal (MPa). While cancellous bone has a compressive strength of around 2-6 MPa (Lee et al., 2012).

In the case of using MSCs on implant materials; research findings have shown that structural design, surface microstructural topography, surface chemistry or surface energy/wettability, as well as environmental factors can all affect biological response, cells behaviour, cell adhesion, cell proliferation and cell migration (Feller et al., 2015). These factors need constant regulation and optimisation for

healthy osteoblast cells differentiation. Furthermore, research findings have shown that nano-topography of moderately rough surface of an implant helps to promote the production of mediators such as BMPs, Runx2 and Osterix, stimulating osteoblast cells proliferation as well as osteogenic maturation. Hence, rough surface features on implants that has high surface energy have shown to promote osteogenesis (bone formation), increase ratio of bone to implant contact, and increase the bonding strength of van der waal, electrostatic forces and mechanical anchorage between the osteoblast cells and the implant surface. Cells have the ability to recognise and react differently on different characteristics of an implant surface. This is done through the use of cell surface receptors and specific ligand molecules which are secreted and deposited on over the biomaterial (Boyan et al., 2016).

As such, medical implant materials need to be biocompatible, chemically inert, hypoallergenic, corrosion resistant and stable. The most common biomaterial used in medical bone implants are titanium and zirconium, due to their suitable mechanical properties and their excellent biocompatibility (Bruschi et al., 2015; Zareidoost et al., 2012). Despite the fact that bulk properties are important part of an implant due to their mechanical stability, it is the surface design in the end, which ultimately contributes to osseointegration. Recent studies that has been conducted on surface roughness at a microscale, shows that surface roughness is an important parameter in osseointegration for bone medical implants (Li et al., 2018). Surface roughness has been studied at a micron, submicron, and nano-surface roughness alongside with surface wettability. Prior studies' findings illustrate that integrins, which are transmembrane proteins that are involved in cell adhesion play a vital role in sensing the environment, controlling cell shape and motility (Boyan et al., 2016). They are known for providing communication channels for cells to interact with adjacent surfaces. The integrin is a heterodimeric protein receptor, consists of alpha and beta integrin subunits that binds to peptide ligands and also within the cell to cell's signalling machinery and the cytoskeleton. During cell-cell interaction, the integrin will recognise a ligand to attach to the surface of another cell for cellular interaction. The ligand that is widely used and most often recognised by nearly half of over 20 known integrins is the ligand sequence that is made up of arginine, glycine, aspartic acid (RGD) sequence. (Dalby et al., 2014). This means integrins are responsible for recognising changes to a surface, which leads to a downstream

signalling pathway. More specifically it leads to the Wnt5a pathway, when osteoblast cell differentiation takes place on the surface of a titanium implant (Boyan et al., 2016).

### 1.2.1 Medical Bone Implants

Medical bone implants are used mainly in orthopaedic surgeries to help fix fractures caused to the human skeleton through injury. The most basic expectations of these implants is to reinforce mechanical stabilization, ensure alignment and normal function of skeleton. Bone implants are continuously being improved over the years to enhance osseointegration, biocompatibility, corrosion resistance, and improve mechanical properties (de Viteri & Fuentes, 2013; Le Guéhennec et al., 2007). There are numerous type of bone implants such as spinal, dental, maxillofacial implants and hip bone and knee implants.

### 1.2.2 Spinal implant

Manufacturers cut down on cost by standardising one implant design to accustom all patients. Since every individual is anatomically different. By implementing the same implant to be used by everyone, it can result in the implant to break because of the misalignment to a particular patient body type; leading to further complications for the patient to undergo another surgical procedure. This can be clearly seen in the case of a spinal implant called pedicle screw fixation, which is required to treat thoracolumbar fractures and other spinal disorders. In Figure 5, it shows various age groups from 14 to 47 years involving both men and women, where a broken screw or rod resulted after 8-24 months of implantation. This clearly shows how every patient is anatomically different and would require a personalised 3D-printed implant to help reduce stress applied during movement, which will help avoid implants from being broken after it has been successfully implanted (H. Wang et al., 2017).

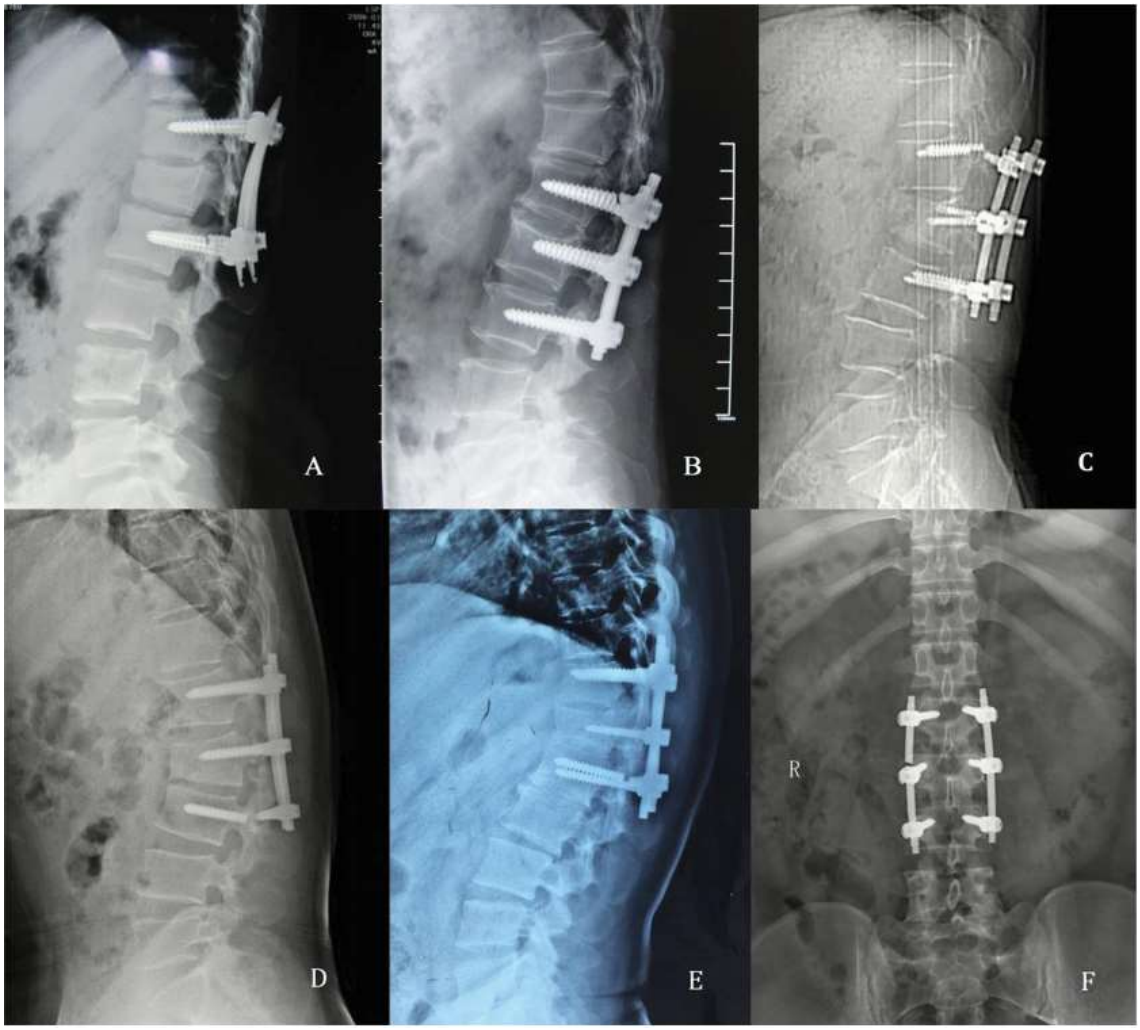


**Figure 5.** Shows various cases involving spinal implant's pedicle screw and rod breakage. A. 14 months after surgery the pedicle screw broke, which involved a 14-year-old girl that had a L1 fracture. B. 10 months after surgery the pedicle screw broke, which involves a 47-year-old man that had a L2 fracture. C. 18 months after surgery the pedicle screw broke, which involved a 39-year-old woman that had a T12 fracture. D. 8 months after surgery the pedicle screw broke, which involved a 35-year-old man that had a L2 fracture. E. 12 months after surgery the pedicle screw broke, which involved a 45-year-old man that had a T12 fracture. F. 24 months after surgery the rod broke, which involved a 27-year-old man that had a L3 fracture (H. Wang et al., 2017).

### 1.2.3 Dental Implants

Current dental implants are 3D printed using the traditional top down approach, which is then followed by sand blasting and acid-etching technique to roughen the implant so that osseointegration can occur between the surrounding bone and the dental implant as seen in Figure 6. Dental implants are made out of titanium grade 4 that is combined with SLA (Sand-blasted, Large grit, Acid etched). SLA involves large-grit (250-500 µm) sandblasting technique using corundum particles of aluminium oxide that help creates a micro rough surface on the titanium implant. This is then followed by a strong acid-etching bath in $HCl/H_2SO_4$ at high temperatures for several minutes. This results in creating a 2-4µm pits on the rough sanded titanium surface. The resulting structure has shown to be an ideal surface for cell attachment. This tedious procedure can be overcome by the 3D-printing bottom-up fabrication approach as it has made it possible to control each layer at a micro level to create predefined surface topography and porosity for optimum osseointegration. Henceforth, this will cut down on cost as well as chemical waste during acid etching procedure using $HCl/ H_2SO_4$, which needs to be properly disposed of every time during the post treatment of the dental implant under SLA procedure (Vazouras, 2013).

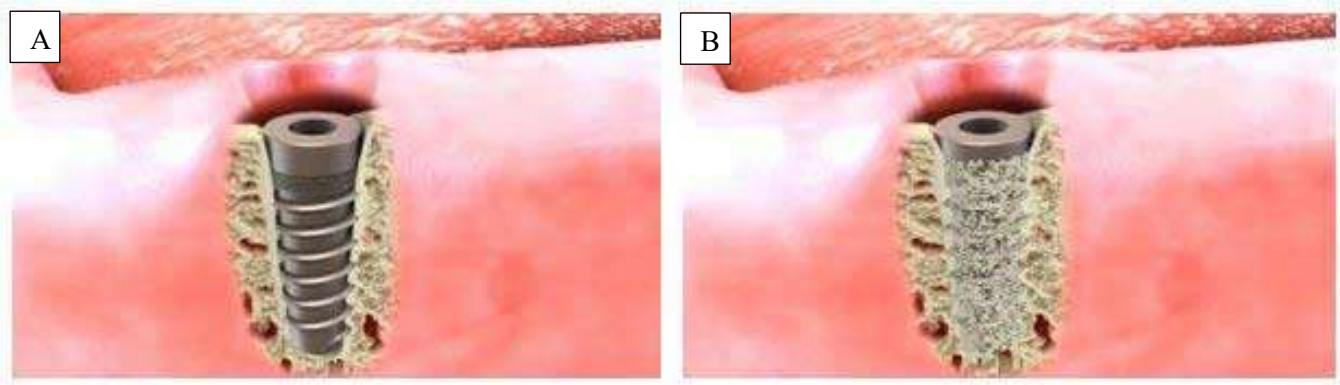


**Figure 6.** Image (A) shows pre-osseointegration when the implant is freshly inserted into the missing tooth area in the jawbone. Image (B) shows osseointegration occurring after several months where new bone cells begin to grow on the dental implant. This helps hold the new dental implant in place securely, which ensures that it will be strong enough to support the new tooth (Rahmani, 2018).

### 1.2.4 Craniofacial implants

Craniofacial implants are used in restorative procedures and titanium alloy material has long being the gold standard for fabrication of craniofacial implants (Neumann & Kevenhoerster, 2009). One of the many challenges in this type of surgery is outlined in a study conducted by Subramaniam et al. (2018) to analyse the long-term outcomes of craniofacial implants for facial defects restoration. Three different implant sites in the craniofacial region were selected for this study which were the temporal (ear reconstruction), orbital (eye reconstruction) as seen in Figure 7a and b, and nasal (nose reconstruction) as seen in Figure 8. Within this study, 53 patients had auricular implants, 42 had orbital implants insertion and 15 nasal implant insertion. The osseointegration success rate differed at each site. The osseointegration for temporal implant had 97% success rate, orbital implants had 63.3% success rate, and nasal implants had 87.5% success rate. This results clearly demonstrates that there is room for improvements. Such implants needs to be personalised so it can fit perfectly in place as this will avoid unnecessary pressure from the surrounding tissue that may eventually dislodge the implant due to aseptic loosening or osseous pressure necrosis (Meltzer et al., 2009; Takakubo et al., 2013). To overcome this issue, personalised 3D-printed implants needs to be created for each individual as every patient anatomical structure is different. The personalised craniofacial implants will be able to fit perfectly in position and would avoid parafunction that has a negative impact on bone-implant integration as mentioned before during the initial healing stage. Furthermore, using the 3D-printing bottom-up approach can help further optimise the surface topography at a micro level for optimum osseointegration.

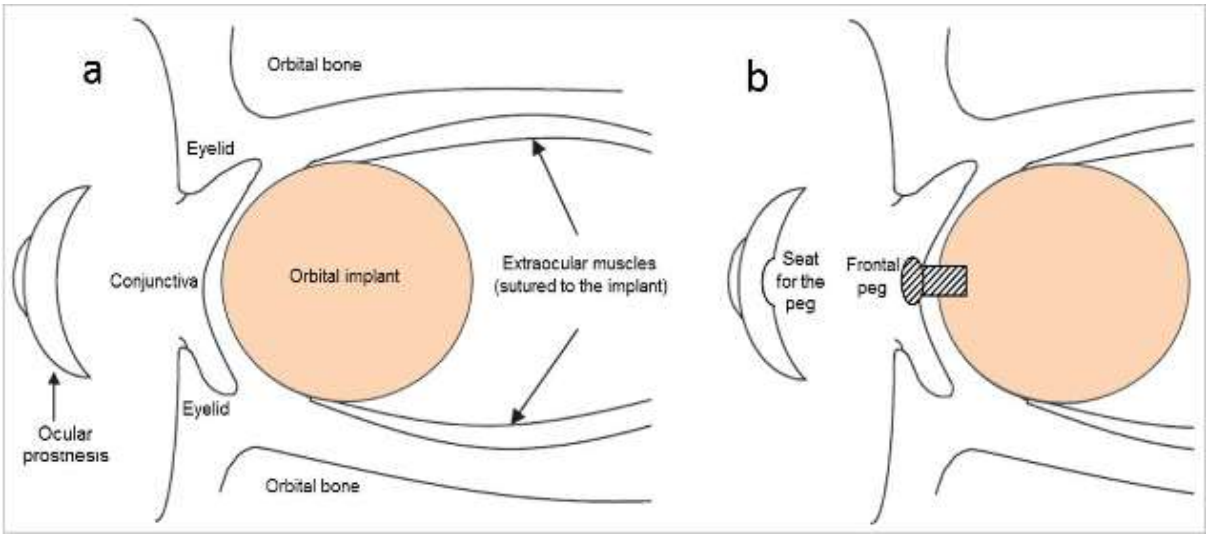


**Figure 7a.** The drawing shows the orbital implant placement within the eye socket during the eye reconstruction procedure. **b.** Shows the frontal peg that helps hold the ocular prosthesis on the orbital implant (Salerno et al., 2018).

**Figure 8.** Osseointegrated bone anchored nasal implant to help hold the nose prosthesis in place. This surgical procedure replaces various adhesives used to hold the prosthetic nose (Nasal Nose Prosthetics, 2018).

### 1.2.5 Hip bone implants

The hip joint is made up of a ball and socket, where the hip has the open pocket and the round head of the femoral bone creates the ball-and-socket joint. When the natural ball-and-socket joint is damaged, a new durable artificial synthetic replacement will be surgically inserted to mimic the ball-and-socket join of the hip (Grundei & Gerdesmeyer, 2009). One of the key factors of bone implant failure is aseptic loosening. Aseptic loosening is a term used to describe the bonding between the bone and implant (osseointegration) failure without the presence of infection. A review conducted by Apostu et al. (2018) to study the aseptic loosening of the osseointegrated titanium implant in cementless total hip arthroplasty (hip replacement implant). Survival rate of cementless titanium implants at 10 years stands at 85%, but this rate decreases to 70% after 15 years. It is noted that if proper osseointegration doesn't occur between the titanium implant and the bone, then it leads to aseptic loosening which results in complications for the patient i.e. causing pain and instability during mobility or when applying pressure onto the implant. The key factors stated by Apostu et al. (2018) which plays a major role in aseptic loosening are due to 'low biocompatibility of implants, surface and design of the implants, bone quality, surgical technique, loading conditions and insufficient bone turnover'. Apart from surgical technique which is due to human error by not fitting the implant properly in place. Surgical technique can be improved by designing patient specific implants using imaging technology to model the implant that perfectly aligns with the patient bone structure in this case the hip joint. The other risk factors can be significantly improved by implementing 3D printing bottom-up approach to create implant surface topography that cells prefer and hence improving osseointegration. Inert titanium alloys can also increase biocompatibility and osseointegration as it avoids the oxide layer from forming onto the pure titanium implant surface (Bruschi et al., 2015; Zareidoost et al., 2012).

To further increase the survival rate of the newly inserted hip implant, monitoring the healing stage needs to be implemented as it depends on the type of individual. Prior studies have indicated that diabetes plays a major role in the bone healing stage as the bone healing and regeneration takes twice as long compared to patients without diabetes. This means longer courses of antibiotics (7-10 days) is required for a diabetic patient compared to 3 days for a patient without diabetes. At least 30 days needs

to be implemented to not disturb bone-implant integration i.e. by avoiding placing pressure on the implant, which can result in aseptic loosening of the hip implant as seen in Figure 9 (Apostu et al., 2018; Sussman & Volker, 2013).

**Figure 9.** The two black arrows at the femoral stem shows aseptic loosening with a zone of 2 mm of the hip joint implant against the surrounding bone structure (Apostu et al., 2018).

## 1.3 Improving Bioactivities of Implants

Titanium and its alloys are well established biomaterials used in various implants such as hip and knee implants, bone screws, plates implants and in dental applications. This is due to their excellent biocompatibility, corrosion resistant, and mechanical properties. To enhance osseointegration, which is required for long term fixation of the implant within the surrounding bone tissue; many techniques have been implemented such as plasma spraying technique to coat hydroxyapatite onto the implant, use of

nanotubes, growth factors and creating nanotopography structures onto the implant surface (Wang et al., 2015).

### 1.3.1 Plasma coating

Plasma spraying technique involves super-high temperature and super-fast cooling rate. This allows the ceramic and metal powders to melt and combine together. When the melted ceramic/metal powder undergoes rapid solidification under the fast cooling conditions, which results in the suppressed crystal growth producing less than 100 nm surface topography. Plasma spraying technique is one way to utilize nano-sized powders to produced nanostructured coating onto the metal implant (Wang et al., 2015).

### 1.3.2 Nanotubes

One way to synthesize Nanotubes onto the titanium oxide ($TiO_2$) layer of the metallic titanium substrate is by a process called electrochemical oxidation reaction set under specific environmental conditions. This process can achieve $TiO_2$ tubes at various diameters ranging between 10-250nm onto the titanium surface as seen in figure 10 (Sathish, 2016). Sathish (2016) have successfully demonstrated that the $TiO_2$ nanotubes with a diameter of 15nm strongly promote cell adhesion, proliferation and differentiation as seen in figure 11. On the other hand, $TiO_2$ nanotubes with a diameter of 100nm induced apoptosis (Sathish, 2016).

Nanotube surface provides nano-topography where osteoblast cells can go into the pores to produce the interlocking cell structure. Hence, this provides significantly greater osteoblast cells adhesion compared to other conventional aluminium and titanium surfaces. To further enhance osseointegration, electrochemical anodization and Ag doping techniques can establish antibacterial coating onto the $TiO_2$ nanotubes surface, which has shown to be effective against periodontal pathogens such as *A. actinomycetemcomitans*, *T. forsythia* and *C. rectus* (Sathish, 2016).

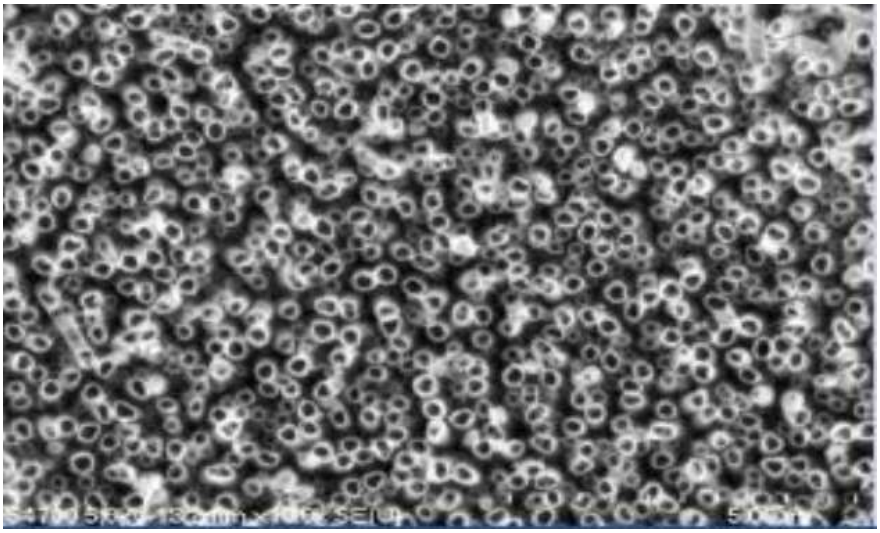

**Figure 10.** Cluster of $TiO_2$ tubes (Sathish, 2016).

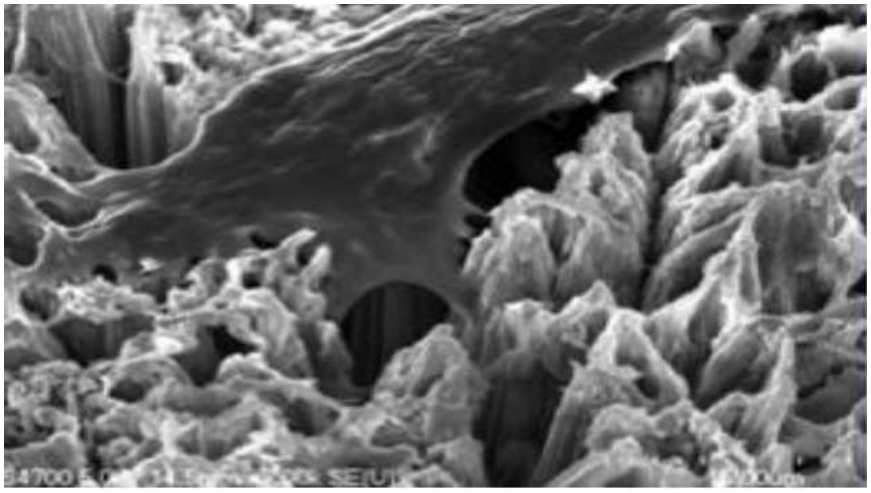

**Figure 11.** Osteoblast cells anchoring to the surface of titanium dioxide nanotubes (Sathish, 2016).

### 1.3.3 Growth factors

There are numerous biological growth factors used to boost bone healing by regulating cellular proliferation, migration, differentiation, and stimulating various other cellular processes. Some of the growth factors that are used are Vascular Endothelial Growth Factor (VEGF), Transforming Growth Factor Beta (TGF-β), Plasma Rich in Growth Factors (PRGF), Platelet-Derived Growth Factor (PDGF), Fibroblast Growth Factors (FGF), Bone Morphogenetic Proteins (BMP-2,4 7) (Ghiasi et al., 2017). PRGF being one of the most commonly used growth factor in the field of dentistry. They are extracted from the patient own blood and are prepared at the same time before the surgical procedure.

PRGF does not contain leukocytes, but consists of platelet and plasma growth factors, fibrin, fibronectin and vitronectin that are directly involved in the repair mechanism. Growth factor treatment has shown to reduce osseointegration time and improves primary stability after successfully placing the implant in its position within the bone (Anitua et al., 2007; Ghiasi et al., 2017).

### 1.3.4 Nanotopography

Natural bone surface roughness holds nanometric features. There are numerous 3D printing technologies that are used to replicate the surface roughness of bone onto a titanium implant. One such technology called Electron Beam Lithography (EBL) that has been used to construct ultra-precise nano-topographies of pore size less than 10 nm in size in a particular pattern of arrays. A study conducted on comparing the effects of stimulating the differentiation of osteogenic cells from human mesenchymal stem cells (HMSCs) cultured on periodic arrays nano-pores, which are then compared against the disorganised arrays of the same nano-pores using EBL as seen in Figure 12. The results indicated that the disorganised arrays of nano-pores showed better stimulation of HMSCs differentiating into osteogenic cells (Rodriguez y Baena et al., 2017). EBL creates the nano-sized patterns on the surface of materials using the de Broglie wave, this is where the wavelength of the electron being much shorter than light beams. The use of EBL to create patterns can only be possible if the surface of the material is sensitive to electrons. Despite the high spatial resolution down to nano-scale, EBL has some limitations, where this technique costs a lot and has a low throughput. So it can't be used in an industrialised scale and hence, EBL is being limited to laboratory use only for research purposes (Qiu et al., 2014).

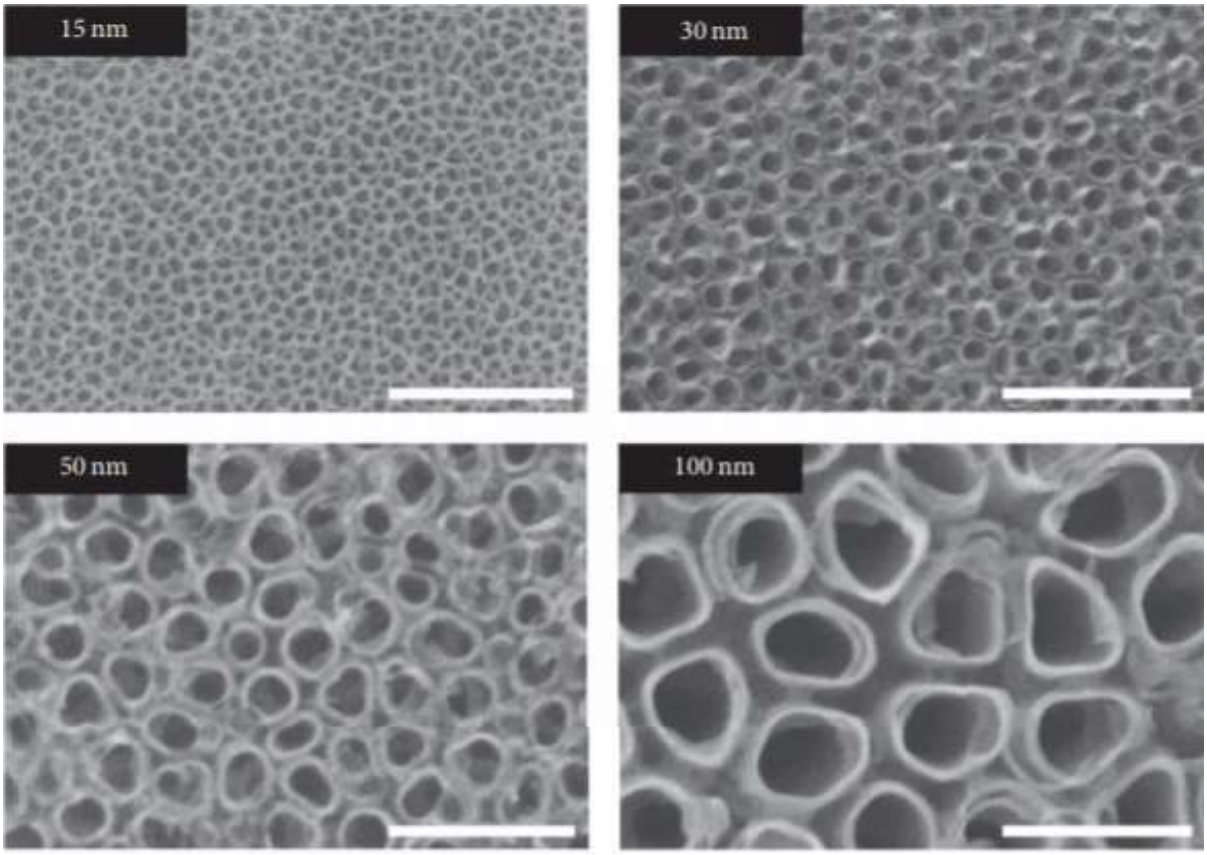


**Figure 12.** SEM images that shows $TiO_2$ nanotubes with different size diameters (Rodriguez y Baena et al., 2017).

## 1.4 Designer Biomaterials & 3D Metal Printing

3D-printing technology allows the fabrication of scaffolds and metal implants with complex internal structures and high resolution. It also uses less material than traditional manufacturing methods. CT scan and MRI images can obtain custom tailored implant that would be able to fit perfectly in place, since every individual anatomical structure is different. This will also help with avoiding implants to break due to load bearing within the implanted region that did not align perfectly within the surrounding bone structure. Furthermore, the implant surface topography and porosity can also be implemented using metal 3D printers to enhance osseointegration (Leukers et al., 2005). Although, 3D printing technology has opened up a new era in medical implant. There is still a lot of room for improvements and optimisation of the printing process, material selection, and design of implants to ensure

biocompatibility, corrosion resistance, inert and be able to with stand mechanical load bearing within the body (de Viteri & Fuentes, 2013).

### 1.4.1 Material selection

Materials selected for medical bone implants are mainly metallic type of materials. These include stainless steel, cobalt chromium alloys, titanium alloys, tantalum, gold, dental amalgams and various other metals. Out of all of these metals, titanium alloys are mostly preferred to be implemented in majority of medical implants. This is due to their high strength, low density, corrosion resistant, inertness, biocompatibility, and most importantly it has low young's modulus compared to other alloys such as stainless steels or cobalt-based alloys. High young's modulus means the material is stiff, whereas low young's modulus means that the material is flexible. Cobalt-chromium alloy has an average Young's modulus of 210 Gpa (Moharrami et al., 2013). While the Young's modulus for SUS 316 L stainless steel that is used in medical implants stands at around 200 GPa (Niinomi & Nakai, 2014). Due to titanium alloy's low Young's modulus, corrosion resistance, superior biocompatibility compared to other metals such as stainless steels or cobalt-based alloys. This makes them an ideal choice to be used in medical implants such as in artificial bones, joints and dental implants (de Viteri & Fuentes, 2013).

The natural human bone is a hard and rigid structure, which makes it useful for weight bearing attributable to the high resistance to bending and torsion. Human bone has a Young's modulus that ranges between 10-30 GPa (Niinomi & Nakai, 2014; Rho et al., 1993). While currently approved titanium and its alloys for medical implant ranges between 110-120 GPa (de Viteri & Fuentes, 2013; Wu et al., 2019). This results in a stress shielding effect due to the mismatch Young's modulus of implants to that of bone, causing bone to atrophy within the implanted region, leading to the loosening of the implant, increasing the risk of re-fracture of the cortical bone, in addition to subsequent damage to the surrounding tissue. This causes a significant socio-economic burden on patients and on the healthcare system, with the need for revision or emergency surgical procedures a common occurrence

following implant surgeries. To overcome the stress shielding effect, medical implant's Young's modulus needs to be equal to that of bone (Niinomi & Nakai, 2014; Wu et al., 2019).

### 1.4.2 Material selection with antibacterial properties

A nosocomial infection is a hospital acquired infection where a patient is exposed to an infection within a health care or a hospital facility. Patients are prone to infections especially in the case of acquiring an implant. Hence, implant nosocomial infections imposes significant complications that impacts patients' quality of life, leading to long-term administration of antibiotics, multiple operations, and prolonged hospitalisation. Patients in such cases are further effected by the prolonged absence from work and the significant loss of income (Holinka et al., 2013).

To overcome nosocomial infection, researcher have been trying to implement antibacterial coating onto medical implants. They have shown to successfully inhibit bacterial adhesion and simultaneously promote bone forming cell (osteoblast cells) adhesion during *in vitro* studies (Barth et al., 1989; Holinka et al., 2013). However, efficacy of antibacterial coating needs to be demonstrated in a randomised clinical trial to confirm the effectiveness in a long-term implantation (Darouiche, 2003).

A study conducted by Shimabukuro et al. (2019) that have shown that elements like Niobium (NB) and Tantalum (Ta) have the ability to inhibit bacteria like S. *aureus* and oppose no harm to bone forming cells as osteoblast cells. Other elements like Titanium (Ti), Zirconium (Zr) and Tin (Sn) possesses no harm to both bacteria and bone forming cells (Ďurišin et al., 2019; Shimabukuro et al., 2019; Yasuyuki et al., 2010). On the other hand, elements like Silver (Ag) can inhibit both bone forming cells as well as bacteria (Shimabukuro et al., 2019). Therefore, elements selected for metallic medical implants alloys should not be cytotoxic like Ag. It should either possess no harmful effects to both bone cells and bacterial cells like Ti, Zr and Sn or have the capability to inhibit bacteria while simultaneously exhibit no harmful effects on bone cells such as the elements like NB and Ta.

### 1.4.3 Current 3D-printing technologies

3D-printing technology have vastly improved over the last 25 years. 3D-printing industry is continuously improving and evolving rapidly into a manufacturing focused enterprise. Current 3D-printing technology such as 'selective laser sintering' (SLS) is a multipurpose 3D-printing technology that can be applied to plastics, glass, ceramics and several different metals and metal alloys to form various models designed by the user. This technique uses heat to melt and bond the powdered materials. The object is created by a bottom-up approach, where each layer from the fine powdered material is lasered selectively to fuse the particles together. For more complex object, a support structure is required for most of the downwards facing surfaces to help stabilise the build architecture. SLS has the ability to create each layer with a thickness that ranges between 20 to 60 μm, dependent on the powdered materials used. Each layer of the powdered material is melted with a powerful 200 Watt Yb-fibre laser, which is controlled in the X and Y-direction and the platform moves down in the Z-direction as seen in figure 13. Metal objects produced using this technique are extremely dense and the mechanical

properties are comparable to that of a cast or machined component. Hence, SLS 3D-printing technology have replaced majority of the components produced through various traditional methods (Bogue, 2013).

**Figure 13.** Schematic diagram of 'Selective Laser Sintering' (SLS) 3D-printer's components (Singh et al., 2016).

### 1.4.4 Advantages

3D printing technology is an additive manufacturing technique to help fabricate patient specific scaffolds or metal implants with great structural complexity, high accuracy and precision of the implant design. This is achieved through medical imaging techniques such as computed tomography (CT) and magnetic resonance imaging (MRI) to capture the anatomical structure of the patient body part where the implant needs to be implanted. 3D modelling software can design implant models that would be able to perfectly fit within the injured area of the patient. This is not possible with the conventional

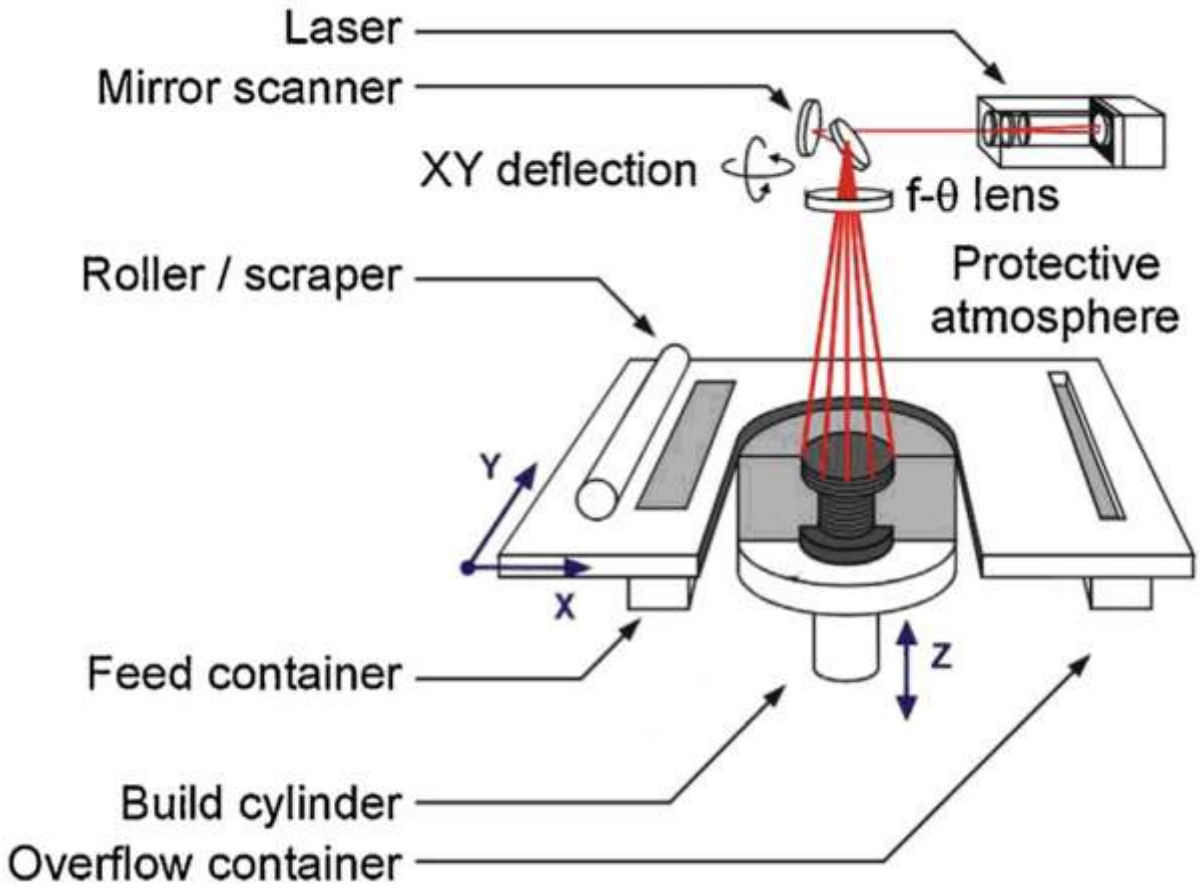


fabrication techniques (Guvendiren et al., 2016). Also, metal printing technology has the ability to construct ultra-precise nano-topographies of pore size less than 10 nm, in a particular pattern of array

for optimum osseointegration. This can be achieved with EBL, where it is only effective on surfaces that is sensitive to electrons (Rodriguez y Baena et al., 2017).

Furthermore, the advantages of porous structures of a scaffold is that it helps facilities diffusion of biological fluids, it provides sufficient nutrients for the maturation of tissues, and helps with removal of metabolic waste. More importantly, the porous structure would provide cell ingrowth, reorganization, and neovascularization (formation of new blood vessels) from the surrounding tissue. Hence, a 3D printed scaffold that has well defined porosity i.e. pores size, geometry, distribution and interconnectivity that can mimic the natural bone matrix, can thereby boost bone ingrowth. The pore size between 100 to 400 μm seems to support formation of mineralized bone within the porous scaffolds. Thereby, 3D printing/additive manufacturing techniques have been able to provide full control over the porous structure of each layer during the fabrication of the titanium implant. The procedure is cost effective in the way that it doesn't require decontamination after production as the titanium implants are not machined and hence no oils or other contaminants are present in and around the implant. Hence, the 3D printed titanium implant does not require surface treatments (Tunchel et al., 2016).

### 1.4.5 Disadvantages

3D-printing technology also has limited capabilities. Although processing speed, printing speed and printing resolution has improved over the past years, yet in many cases it still lags behind optimal levels. Also many 3D-printable biomaterials have excellent properties for *in vitro* applications, but for implantable biomaterials multiple conditions still needs to be adjusted. These conditions include biocompatibility, the biomaterial should be printable, have appropriate mechanical properties, have good degradation kinetics, the degradation by-products should not be toxic, and has the ability to integrate with the surrounding tissue. Fulfilling all of these conditions for medical implants are still challenging particularly for bone implants. Biomaterial implants for bone implants are desirable to have stiff materials for osseointegration and load barring with slow to non-existent degradation. Biomaterials still lack that capability in bone implants as they start to degrade over time (Guvendiren et al., 2016).

Whereas, 3D-printing for metal implant is not cost effective and also has a low throughput which can't be used at an industrial scale (Qiu et al., 2014).

### 1.4.6 Challenges and hope

Repair and restauration of bone defects caused by various diseases and traumas, can be treated through the use of inert implants. Medical implants are shifting towards customised designs for patient/customer through the use of specific data, that is provided by and accomplished through the advancement of 3D printing technology. The traditional approach to fabrication of implants was done through the use of the top-down approach. In this case, the surface topographies are evaluated after the medical implant design is created. Henceforth, the surface features cannot be customised or controlled as its fully depended on the synthesis process. 3D printed medical implants have still not been fully evaluated in the direction towards finding out which type of surface topography and design is most optimal for host tissue-implant integration. The finalised 3D-printed medical implant's mechanical properties will also need to be evaluated and optimised to make sure they will be safe to use in the long term and can withstand all major forces within the body.

This project will focus on using 3D printing technology to design inert implants from the bottom-up approach as it allows the user to have full control over the design and surface topography of an implant. This will help answer such questions as to, what type of surface features promote better bone integration? What type of surface or materials do cells prefer? Hence, this project will help promote and standardise surface topography for all medical implants that require host tissue-implant integration. It will focus on designing implants from the bottom up approach with the help of AI (Artificial Intelligence) machine learning to help evaluate cellular mechanisms behind bone-implant integration. The biological response to the most optimised implant design will be evaluated in animal studies.

### 1.4.7 Current development in 3D printed Metal Bone Implants

Aseptic loosening as mentioned before plays a vital role in implant failure due to the bonding failure between the bone and implant. Aseptic loosening has been a major problem in the acetabular component of the ball-and-socket hip joint implants as seen in Figure 9 (Apostu et al., 2018). To overcome this issue, research has been conducted to optimise the surface characteristics of implants to enhance bone ingrowth within the implant structure. This will ensure the long term use of implant without failure and help avoid revision hip surgery (Hosny et al., 2018).

Global medical device manufacturing company 'Stryker' has been fully committed to 3D-printing technology. They have developed a highly porous acetabular implant, which has a high coefficient of friction that is able to enhance initial fixation and the porous structure helps with bone ingrowth to help with optimum osseointegration. The clinical trial conducted on 35 revision surgery cases using titanium tritanium acetabular shell with a follow of 6 years. They achieved 97% success rate. Another similar clinical trial undertaken that has also shown similar excellent results with 98.4% success rate after 97 months follow up, which had 1 out of 62 patients that required re-revision correction surgery. Therefore, titanium tritanium acetabular shell achieved excellent results with high success rate under complex revisions conditions where patients had massive bone loss from prior hip implant (Hosny et al., 2018).

### 1.4.8 Challenges with SLS 3D-printing metal components

SLS 3D-printers for the fabrication of tailored medical implants models still require further optimisation to decrease the time of printing, while simultaneously making sure the accuracy and quality of the printed metal implant is not affected. This will overall help increase the productivity rate. Although, SLS has the ability to manufacture components from materials like titanium or nylon which are difficult to construct using traditional methods. SLS metal parts are limited in application for industrial use as the materials used for processing is limited. Aerospace grade aluminium among other metal powders are still in development (Rangappa et al., 2015).

### 1.4.9 Manufacturing

SLS 3D-printed metal components are useful for industrial applications. SLS 3D-printed model's mechanical properties such as hardness and tensile strength have been evaluated to be equivalent to that of conventional processed materials. It also has the ability to print titanium alloy (Ti-6Al-4V) components, with high accuracy and reliability. Hence, SLS 3D-printers once high throughput is achieved and optimised, it will be able to replace conventional 3D printers (Rangappa et al., 2015).

## 1.5 Material design utilising 3D metal printing technology

Software development allows for the creation of structures that would otherwise be impossible with current 3D printers. For this project, we use the Reinshaw AM400 metallic 3D printer and in preliminary design samples using Ti6Al4V. It has been demonstrated that we can improve osseointegration significantly as seen in figure 14 (Lei et al., 2022).

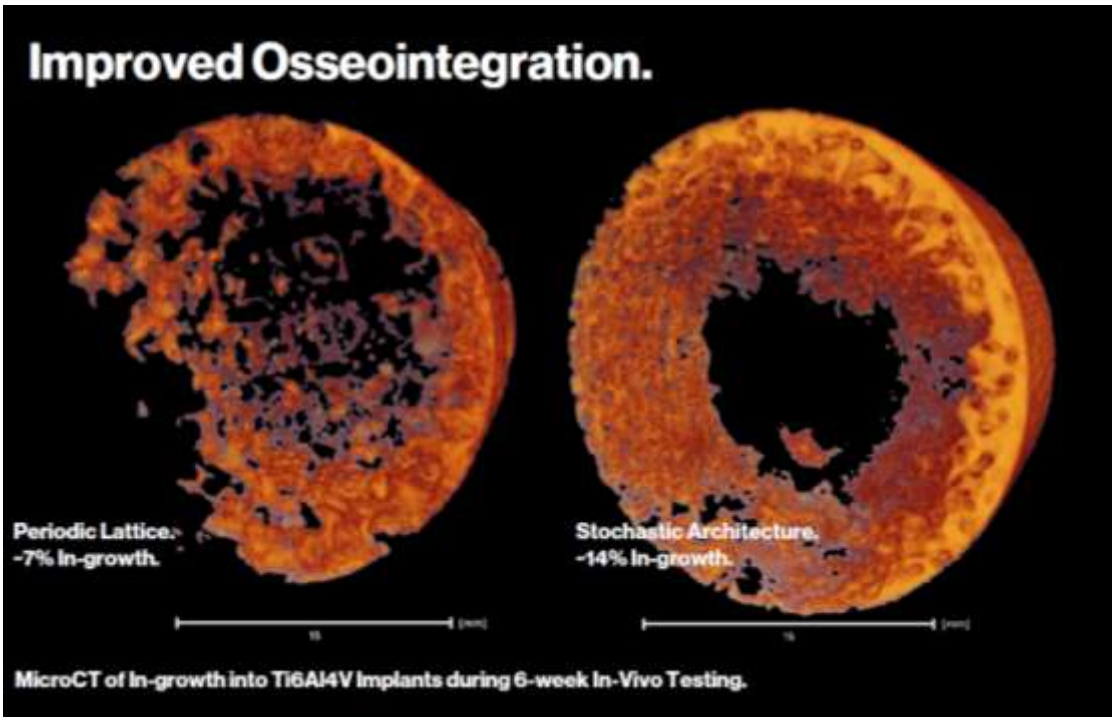

**Figure 14.** The microCT images shows the bone ingrowth into Ti6Al4V implants during 6-weeks in vivo test (Lei et al., 2022).

Furthermore, the production process can be optimized to deliver high quality implant samples in the same production process. Reinshaw AM400 metallic 3D printer uses selective laser melting (SLM) 3D printing technology to help melt and fuses metallic powders with a powerful laser beam to build models using the bottom-up approach. The fibre laser having a spot size of 75 μm using the bottom-up approach to control each layer at a micro level. Hence, this achieves high quality implant samples as seen in the figure 15 (D. Wang et al., 2017).

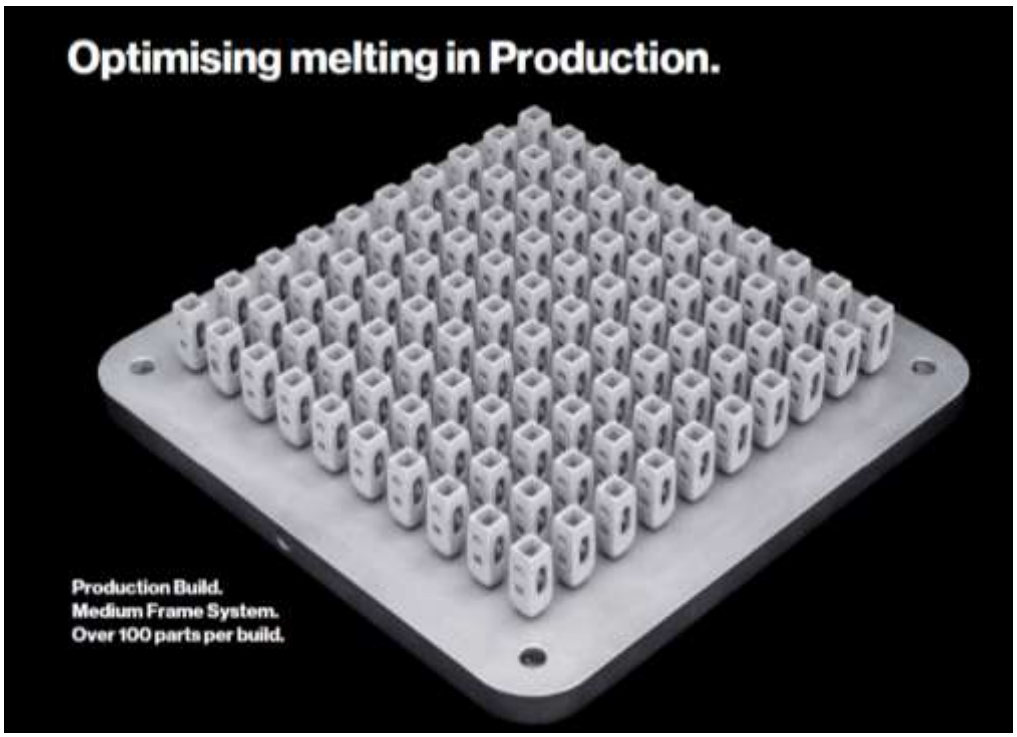


**Figure 15.** Using Reinshaw AM400 metallic 3D printer that printed high quality implant samples in the same production process (D. Wang et al., 2017).

As an example of the finer details, we can achieve under optimised laser scanning compared with standard laser scanning. It is evident we can achieve higher resolution structures as seen the figure 16 (Patel et al., 2021).

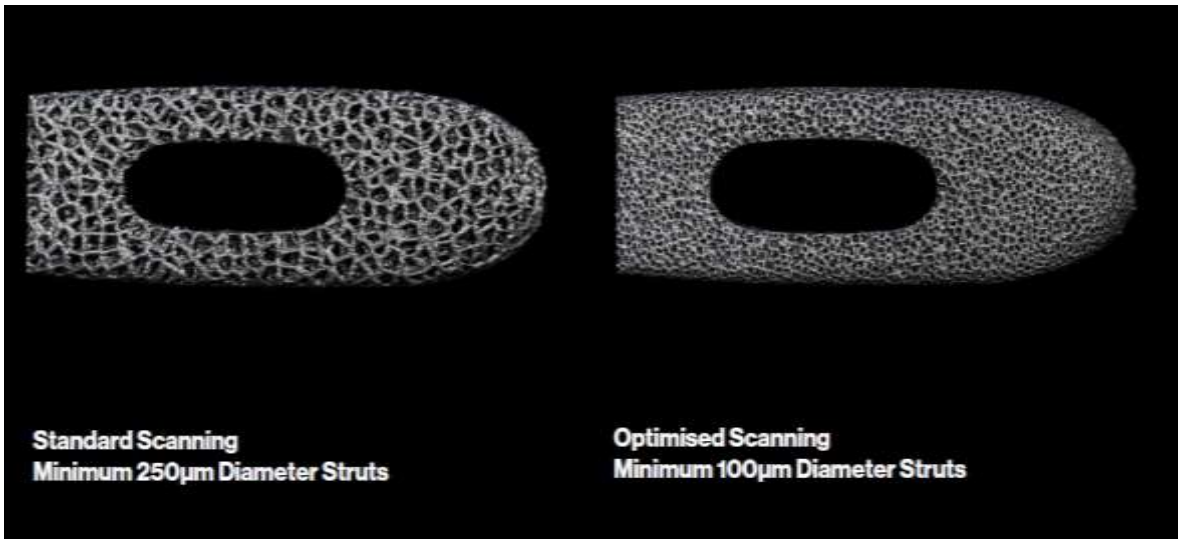


**Figure 16.** Shows the comparison between standard scanning and optimised scanning quality when 3D printing detailed samples (Patel et al., 2021).

For my research I have being conducting investigation into the effect of different level of porosity of our specialized 3D printed implants as shown in the following Figure 17. They represent increasing porosity of the implant and now that we have the capability to do so the next step is to conduct cellular

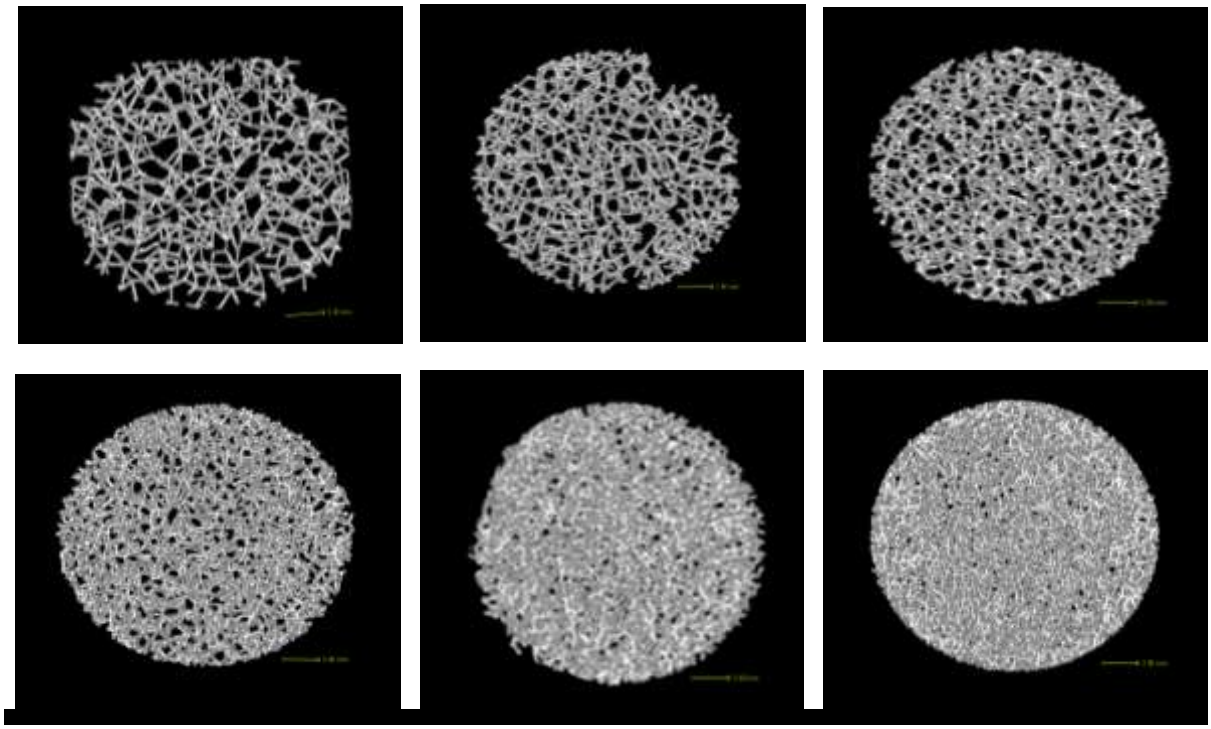

response assays. This will include examining bone cells such as osteoblasts and osteocytes cellular response to the different level of 3D printed implant's porosity. I will examine gene expression profile using digital droplet PCR.

**Figure 17.** Development of New Class of Titanium alloy using machine learning algorithm. It shows the porous structure of titanium alloy samples that can be controlled at different levels of porosity (Alloyed, 2021).

Taking Ti-6Al-4V (in wt. %) for example, vanadium could cause potential cytotoxicity and adverse tissue reaction being imposed on by oxidative stress (Cortizo et al., 2000), and emission of aluminium ions into the human body could cause Alzheimer disease (Tomljenovic, 2011). Therefore, biocompatible solute elements, such as niobium, molybdenum, zirconium, tantalum, or tin, are used when developing new Ti alloys for biomedical implants (Davidson & Tuneberg, 2001; López et al., 2001).

The issue of mechanical incompatibility arises due to Wolff's law, as Ti alloys are four to five times stronger than natural bone in terms of Young's modulus, causing complications of mechanical and structural incompatibility between the implant and the host bone. According to Wolff's law, the high stiffness of the implant will cause a reduction of mechanical stress, which gradually leads to bone resorption. Every change of a bone is in response to changes in its internal structure and its external conformation (Frost, 2004). Human bone has a Young's modulus of below 40 GPa, which is much lower than most metals and alloys. For example, the Young's modulus is 105 GPa for pure titanium, and 110 GPa for Ti-6Al-4V. Stress shielding as a result of the significant difference of stiffness between bone and implant causes abnormal degradation of bone in the vicinity of the implant (Cansizoglu et al., 2008; Wen et al., 2001; Zysset et al., 1999). Hence, designing alloys with a bone-like Young's modulus is still an issue. Although magnesium and its alloys have low moduli of about 45 GPa, their degradation rates must be well controlled clinically (Wen et al., 2001; Wen et al., 2004).

Apart from developing low Young's modulus titanium alloys to overcome the stress shielding effects. Another approach to reducing the Young's modulus or the stiffness of current

medical implants' material is by applying porous structure to medical implants as mentioned earlier, which can be 3D printed. In this case the porous structure needs to be further evaluated and optimised as the differences in stiffness from using thick struts to thin struts effects the rate of osseointegration.

## 1.6 AI machine learning to speed up research and development

The conventional approach to the development of new materials is through using the 'Trial and Error' process, which results in a very expensive and slow progression in advancement. One way to overcome this issue and enhance advancement in material science is through AI machine learning approach. Artificial intelligence and machine learning approach can analyse large datasets that can be used to classify and to pattern out distinct properties of material compositions to then predict new set of novel composition output that a user might be interested in with 90-95% accuracy. This helps speed up the process of material development. It saves cost from long term R&D process and it overall results in cheaper material to manufacture and market (Yu et al., 2021).

Artificial neural network (ANN) is a machine learning method that generally used for regression and classification (Haykin et al., 2009). ANNs are proficient data driven modelling tools that are widely used for nonlinear systems, dynamic modelling and identification, which are normally due to their universal approximation capabilities and flexible structure that allows for capturing complex nonlinear behaviours (Radl et al., 2018). The ANN machine encloses the relationship between inputs and outputs by black-box, which have been trained with labelled data in self-amending (Figure 18). Actually, the relationship is transparent in the black-box with multiple weights and activation functions, but it might be too complicated to present into simple formula (Gardner & Dorling, 1998; Olden et al., 2004).

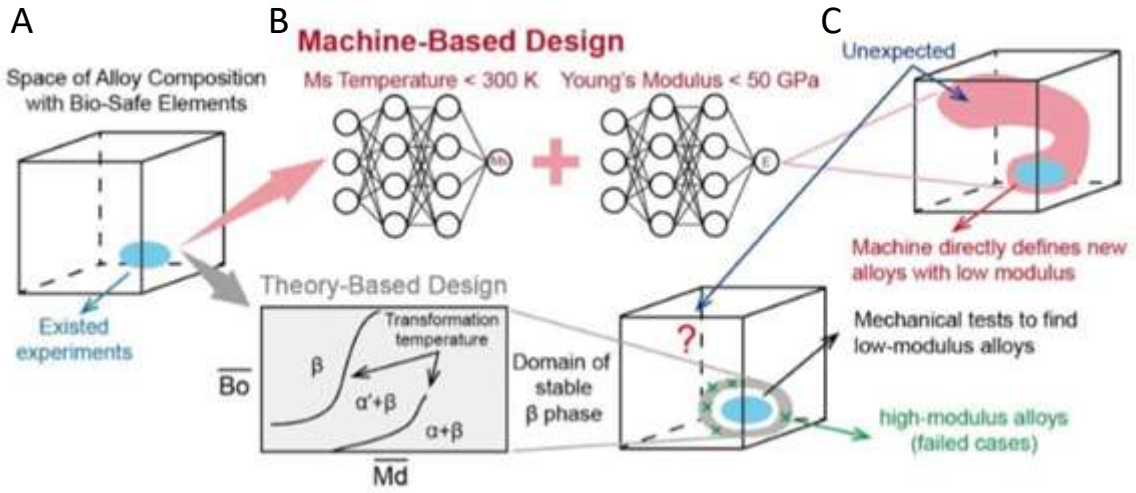


**Figure 18.** Illustration of how βLow works. **A.** Sequence network provide valid prediction of Young's modulus of β phase titanium alloy that can help to find new region of low modulus alloying constituent. **B and C.** Validations of the prediction of βLow (Wu et al., 2019).

## 1.7 Hypothesis

AI generated titanium alloy with low Young's modulus together with geometric design can stimulate osteocytes and osteoblasts bone formation mechanism and functions that is comparable to current titanium alloy Ti-6Al-4V.

## 1.8 Aims and Objectives

The medical implant field is shifting towards the era of personalized implants based on patient/customer specific data made available by the advancement of 3D printing. However, 3D printed medical implants have yet to be evaluated in-depth as to what type of surface topography and design is most optimal to promote host tissue-implant integration. This project will evaluate the mechanical properties and biological response to the AI recommended titanium alloy with low Young's modulus comparable to that of cortical bone to ensure it is biocompatible and safe to use in the long-term implantation.

This project will achieve the following aims and objectives:

**Aim 1: Development and evaluation of AI-developed titanium alloy.**

The objective of this aim is to develop and evaluate the AI recommended titanium alloy composition. The fabricated implant will than undergo material characterization based on FDA/TGA standards.

**Aim 2: *In-vitro* evaluation of AI developed titanium alloy for bone regeneration.**

The objective of this aim is to evaluate the cellular response from bone cells (Osteocytes and osteoblast cells) to the AI developed T12 titanium alloy. The cell morphological response to the surface features will be analysed by immunofluorescent imaging and evaluated by deep learning algorithms. The genes expression will be examined by digital droplet PCR (ddPCR). Cytokines released from osteocyte cells will be examined by high throughput antibody array membrane assay.

**Aim 3: Evaluation of geometric design in 3D printed implants**

The objective of this aim is to evaluate the cellular response of osteocytes and osteoblast cells on the 3D printed titanium alloy substrates. The cell morphological response to the porous surface features will be analysed by immunofluorescent imaging and evaluated by deep learning algorithms. The genes expression will be examined by dd-PCR.

# Chapter 2 - Development and Characterization of AI generated biomimetic titanium alloy for bone implant

# Chapter 2 - Development and Characterization of AI generated biomimetic titanium alloy for bone implant

This chapter focuses on the development and characterization of a new class AI generated biomimetic titanium alloy to be considered and used for bone implants. It will initiate with a brief background of current approved titanium alloys that are used for medical implants with a cross comparison to the AI generated biomimetic titanium alloy in terms of mechanical properties, biocompatibility of elements used within the alloy, and mechanical biocompatibility. This chapter will then go through the methodology used to obtain results and then discuss these findings in relations to the mechanical properties of the titanium alloys and where does the new AI generated titanium alloy compares against the current approved titanium alloys.

## 2.1 Introduction

Titanium and its alloys possess high strength, low weight and outstanding corrosion resistance properties, allowing greater suitability and demand for use in medical implants. More than 1000 tonnes of titanium are manufactured around the world for the purpose of medical implantation in patients each year (Veiga et al., 2012). Globally the life expectancy is ever increasing with an average life expectancy of 72 years (Roser et al., 2013). The demand for joint replacement surgery is continually growing due to the increase in life expectancy; where approximately 70-80% of all total hip joint replacement implants are manufactured from titanium alloys particularly Ti-6Al-4V (Tan et al., 2019). Titanium is one of the few materials that is able to match the requirements needed to be successfully implanted within the human body as it is light weight, strong, inert, non-magnetic, immune to corrosion and fully biocompatible. Due to these properties, titanium is able to integrate very well within the human bone and the surrounding tissue (Sidambe, 2014). The young's modulus for pure titanium and titanium alloys range between 103-120 gigapascals (GPa), whereas the stiffness of bone can range between 10-30 GPa (Elias et al., 2008; Liu et al., 2017). Henceforth, titanium and it's alloy such as Ti-6Al-4V is prone to the stress shielding effect due to the mismatch of stiffness to that of the adjacent bone, leading to greater

bone resorption and bone cell death causing implant failure (Oldani & Dominguez, 2012; Tan et al., 2019). To overcome this issue, cost-effective and biocompatible materials with low young's modulus are highly desirable to avoid stress shielding in bone implants (Wu et al., 2019).

The characteristic of Young's modulus describes the response of a material to stress and strain. This can be used to help with the understanding of mechanical biocompatibility. To achieve mechanical biocompatibility, metal used in various prostheses and orthopaedic implants must be mechanically harmonized with the surrounding bone tissue (Niinomi & Nakai, 2014). Due to the big differences between the current metal implants and natural bone's Young's modulus, the load transferred between implant to bone is non-homogeneous, leading to the reduction of stress stimulation of bone (Niinomi & Nakai, 2014; Oldani & Dominguez, 2012). This phenomenon is known as the stress shielding effect and under such conditions, bone is more likely to atrophy, leading to the loosening of the implant where it can easily re-fracture the cortical bone and damage the surrounding tissue (Niinomi & Nakai, 2014). With that said, it is believed that metals with Young's moduli that is equal to that of bone will be an ideal metal implant to for mitigate the stress shielding effect (Niinomi et al., 2012).

Apart from having a low Young's modulus, the material selected must be biocompatible, and non-toxic or harmful to the living tissue in the human body. The current approved titanium alloy Ti-6Al-4V for example consists of the elements aluminium and vanadium. Vanadium ions (Guan et al., 2017; Kawahara & Kato-Negishi, 2011; Siemers et al., 2016) contents from Ti-6Al-4V has been reported to cause toxicity in the body and aluminium is reported to be a neurotoxic element (Gomes et al., 2011; Gray et al., 2018; Khadija et al., 2018; Mravcová et al., 1993; Sommer et al., 2019).

Henceforth, our group have developed a low Young's modulus titanium alloy that is composed of non-toxic and non-allergenic elements for biomedical applications. This novel titanium alloy with a composition of Ti-12Nb-12Zr-12Sn (T12) (in wt. %) was produced through AI machine learning approach called "βLow". The elements used within the titanium alloy composition are cost effective, and all elements are biocompatible. T12 has a Young's modulus closer to that of bone, at 35 gigapascal (GPa). Therefore, a Young's modulus this low maybe effective in supressing the stress shielding effects in bone (Wu et al., 2019). Nevertheless, this chapter will focus on the development and characterization

of AI generated biomimetic titanium alloy T12 for bone implants in comparison to the currently approved titanium alloy Ti-6Al-4V and commercially pure titanium (CPT).

# 2.2 Methodology

## 2.2.1 Collaboration and contribution of AI developed T12 alloy

All the titanium alloy substrates including CPT, T64 and T12 for this study were developed and supplied by Wu et al. (2019). This was a cross collaboration between National Taiwan University, Tsing

Hua University, China Steel Corporation based in Taiwan, and my supervisor Dr. Joshua Chou; to develop a cost-effective titanium alloy with bone-like Young's modulus. In this project, I evaluated all titanium alloy substrates characteristics including microhardness test, SEM/EDS elemental composition analysis, and EDS mapping, which was to confirm all the titanium alloy properties as well as to ensure we had the correct samples and how the new AI developed T12 titanium alloy would perform against the currently approved titanium alloys CPT and T64.

### 2.2.2 Production of T12

Ti-12Nb-12Zr-12Sn (T12) material was sourced from our previous study's findings where machine learning approach called βLow was used to help determine titanium alloy composition with bone-like Young's modulus. βLow machine learning algorithm used datasets for Young's modulus and Ms temperature derived from biocompatible titanium alloy materials that were previously studied to then predict the combination of a new titanium alloy composition with a specified bone-like Young's modulus (Wu et al., 2019). All the titanium alloys including T12, commercially pure titanium (CPT), Ti-6Al-4V (T64) were fabricated by an arc-melting method within a vacuum melting furnace under argon atmosphere as described in our previous study's findings (Wu et al., 2019).

### 2.2.3 Microscopy surface structure evaluation

Scanning Electron Microscope (SEM) was used to examine the surface topography of each of the titanium alloy substrates: commercially pure titanium (CPT), Ti-6Al-4V (T64) or Ti-12Nb-12Zr-12Sn (T12). Prior to imaging, the titanium alloy samples were mounted on to carbon adhesive discs/tabs (ProSciTech, Australia). Each sample was examined using the Zeiss SUPRA 55-VP SEM (Carl Zeiss, Germany). Images of low magnification at 100x and a high magnification at 9000x were taken from each of the titanium alloy substrate.

### 2.2.4 Material hardness

The hardness test is the basic mechanical property of a material. Hardness is defined as the resistance offered by the material to indentation such as permanent deformation and cracking. Henceforth, a direct measurement of hardness is a simple and useful technique for examining the base-line mechanical properties of materials (Poondla et al., 2009). In this study, the microhardness of the titanium alloy substrates was measured using Leco M400-H2 microhardness testing machine (Leco, USA) with a Vickers indenter at a load of 2 kg. The indenter creates a diamond shape geometry on the polished titanium alloy substrate, where the diagonal length and width are measured using a low magnification optical microscope. Each substrate was indented at three different random locations on the surface and their measurements were taken. The experiment was repeated in triplicate, where the readings were taken from three different samples per substrate. Statistical analysis was performed using GraphPad Prism 7 (GraphPad Software, CA, USA). Significance was determined using one-way ANOVA with a Tukey post-hoc analysis. All values are presented as mean ± SEM (standard error of the mean). P values less than 0.05 were considered statistically significant.

### 2.2.5 SEM/EDS elemental composition analysis

The titanium alloy substrates' chemical composition was investigated by Scanning electron microscope (SEM) using Zeiss SUPRA 55-VP SEM (Carl Zeiss, Germany) in combination with X-Ray energy dispersive spectroscopy (EDS). The titanium alloy substrates were first mounted on to carbon adhesive discs/tabs, then they were coated with gold and palladium using Leica EM ACE600 (Leica, Germany). Each sample was examined using the Zeiss SUPRA 55-VP SEM. Images of low magnification at 500x were taken followed by EDS mapping.

## 2.3 Results

### 2.3.1 Hardness and chemical composition of titanium alloy substrates

In this study, we propose a new titanium alloy T12 to be used for medical implants based from previous research findings that has a Young's modulus of 35 GPa closer to that of natural bone to help overcome the stress shielding effect (Wu et al., 2019). As seen in the schematic diagram in Figure 19, the T12 titanium alloy was created using a machine learning approach called βlow where temperature and Young's modulus of various titanium alloys are used to predict a new titanium alloy at a specified low Young's modulus (Wu et al., 2019). Scanning electron microscope (SEM) images of the titanium alloy substrates CPT, T64 and T12 for both low magnification (100x) and high magnification (9000x) are presented in Figure 20 with their respective photographs of CPT, T64 and T12; to show the micro-rough topography of the three titanium substrates, which overall possess relatively smooth surfaces.

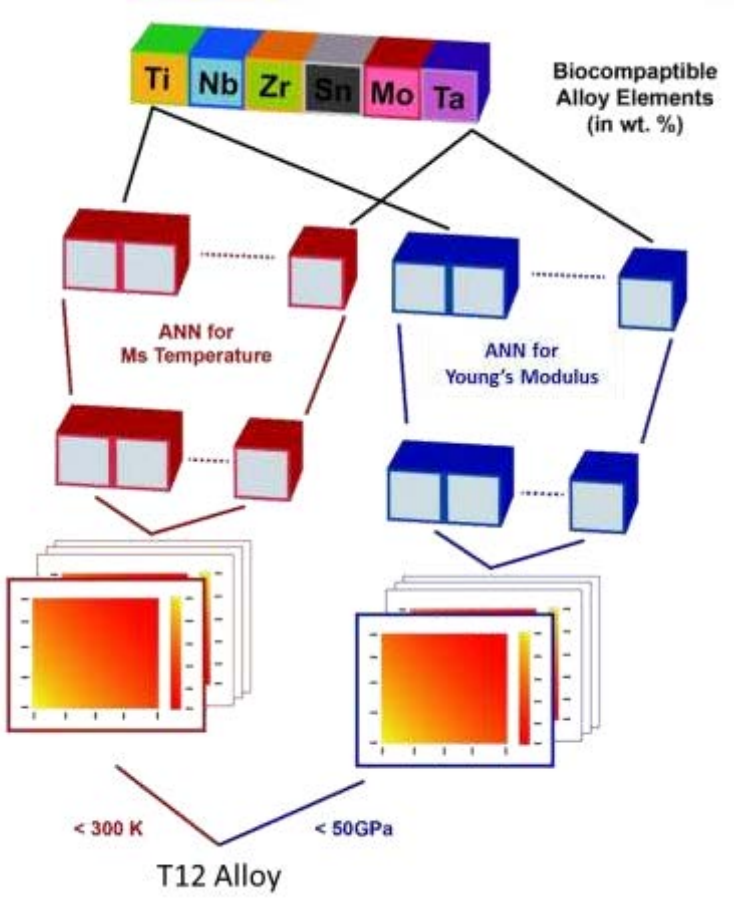


**Figure 19.** Schematic diagram of machine learning approach called βlow to create Ti-12Nb-12Zr-12Sn (T12) alloy. The schematic diagram was reproduced with permission from the authors from a previous research findings (Wu et al., 2019).

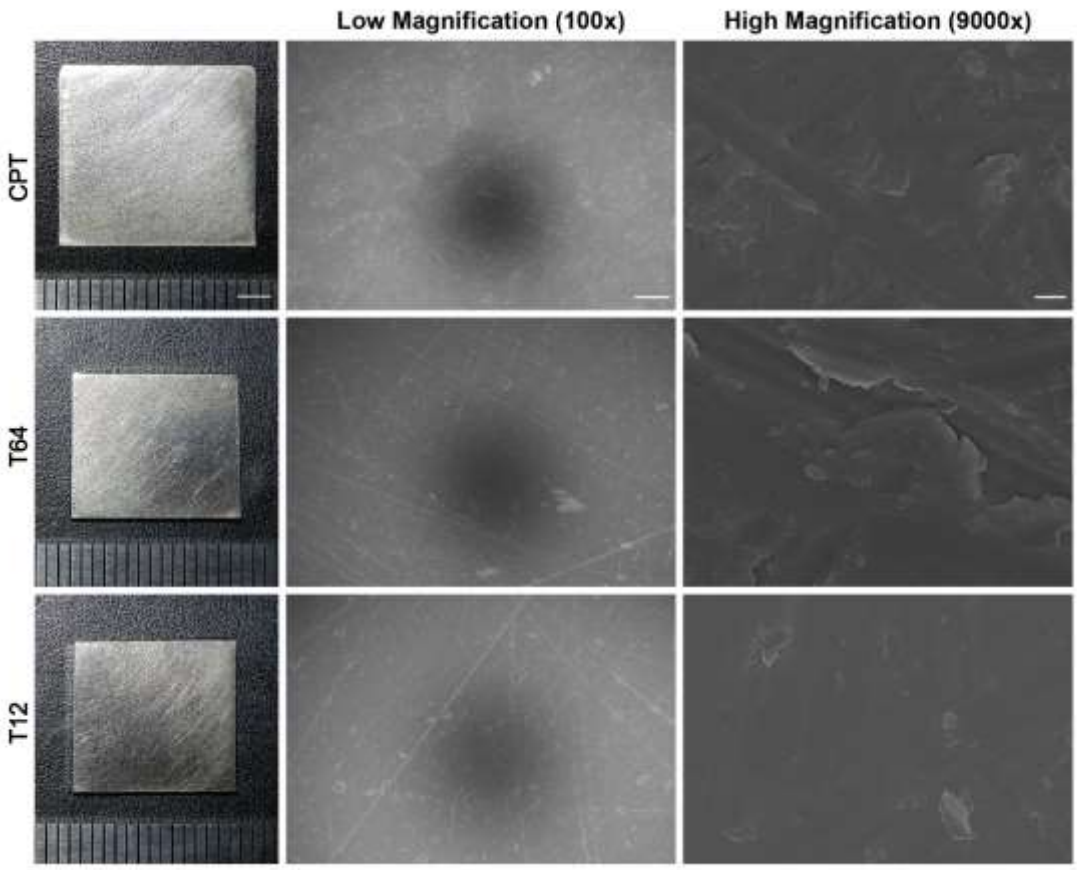


**Figure 20.** Surface topography of titanium substrates CPT, T64 and T12. Image of titanium substrates (scale bar = 3 mm). Scanning electron microscope (SEM) micrographs showing surface topography of titanium substrates at low magnification (100x) (scale bar = 100 µm) and high magnification (9000x) (scale bar = 1 µm).

The Vickers microhardness measurements taken from the three different titanium alloy substrates as seen in Figure 21, shows that CPT (184.6 ± 6.429 HV) is significantly lower than both the titanium alloy substrates T64 (379.7 ± 4.999 HV) and T12 (310.7 ± 0.5316 HV) ($p < 0.0001$; one-way ANOVA with Tukey's post Hoc analysis). Moreover, T64 substrate was significantly higher in terms of Vickers microhardness compared to T12, suggesting that CPT is notably softer than their titanium alloyed counterparts, whereas T64 is the hardest substrate followed by T12.

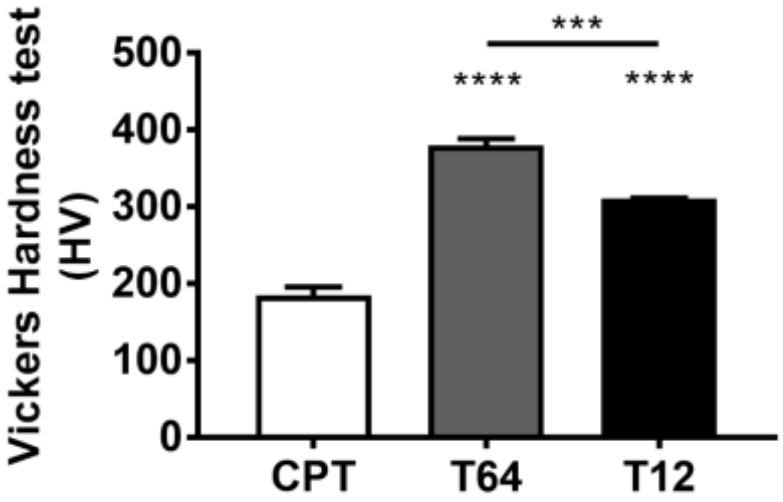


**Figure 21.** Microhardness test data using Leco M400-H2 microhardness testing machine with a Vickers indenter at a load of 2 kg performed on the titanium alloy substrates including CPT, T64 and T12.

### 2.3.2 SEM/EDS elemental composition analysis of titanium alloys

The energy dispersive spectroscopy (EDS) technique was used to determine the elemental composition of CPT, T64 and T12 material as shown in table 1, 2 and 3, which shows the distinct elements peaks that makes up the titanium alloy substrates. EDS mapping of the elements in Figure 22 under EDS mapping, suggest that all the elements are evenly distributed across the surface in CPT, T64 and T12 substrates. EDS analysis shows that on CPT, it detected the element concentration of titanium at 100 wt. % (weight percentage) (Table 4). Table 5 shows the EDS spectrum acquisition of the titanium alloy substrate T64, where EDS detected the element concentration of titanium at approximately 90.89 wt. %, aluminium at 6.68 wt. % and vanadium at 2.43 wt. %. Table 6 shows the EDS spectrum acquisition of the titanium alloy substrate T12, where EDS detected the element concentration of titanium at 63.76 wt. %, zirconium at 12.24 wt. %, niobium at 10.61 wt. % and tin at 8.2 wt. %.

**2.3.3 Tables.** Energy-dispersive x-ray spectroscopy **(**EDS) spectrum analysis and elemental composition of titanium alloy substrates CPT, T64 and T12.

**Table 1.** EDS spectrum analysis to distinguish the elemental composition of the commercially pure titanium (CPT) substrate, containing titanium and the substrate coated with gold and palladium, which helps with high resolution SEM imaging.

| CPT EDS elemental analysis | KeV | cps/eV |
|---|---|---|
| Ti-La | 0.41 | 3.47 |
| Au | 1.73 | 0.94 |
| Pd | 2.13 | 0.99 |
| Ti-Ka | 4.51 | 16.97 |
| Ti-Kb | 4.93 | 2.36 |

**Table 2.** EDS spectrum analysis to distinguish the elemental composition of the titanium alloy substrate T64, containing titanium, aluminium, vanadium, and the substrate coated with gold and palladium, which helps with high resolution SEM imaging.

| T64 EDS elemental analysis | KeV | cps/eV |
|---|---|---|
| V-Lα | 0.40 | 4.22 |
| Ti-Lα | 0.46 | 3.76 |
| Al-Kα | 1.48 | 5.05 |
| Au | 1.73 | 0.94 |
| Pd | 2.13 | 0.99 |
| Ti-Kβ | 4.50 | 21.86 |
| V-Kβ | 4.91 | 3.74 |
| Ti-Kβ | 4.93 | 2.36 |

**Table 3.** EDS spectrum analysis to distinguish the elemental composition of the titanium alloy substrate T12, containing titanium, zirconium, niobium and tin and the substrate coated with gold and palladium, which helps with high resolution SEM imaging.

| T12 EDS elemental analysis | KeV | cps/eV |
|---|---|---|
| Sn-M | 0.38 | 2.07 |
| Ti-La | 0.46 | 2.07 |
| Au | 1.73 | 0.94 |
| Zr-La | 2.04 | 5.87 |
| Pd | 2.13 | 0.99 |
| Nb-La | 2.15 | 6.92 |
| Sn-La | 3.45 | 2.26 |
| Sn-Lb | 3.67 | 1.44 |
| Ti-Ka | 4.51 | 15.48 |
| Ti-Kb | 4.92 | 2.27 |

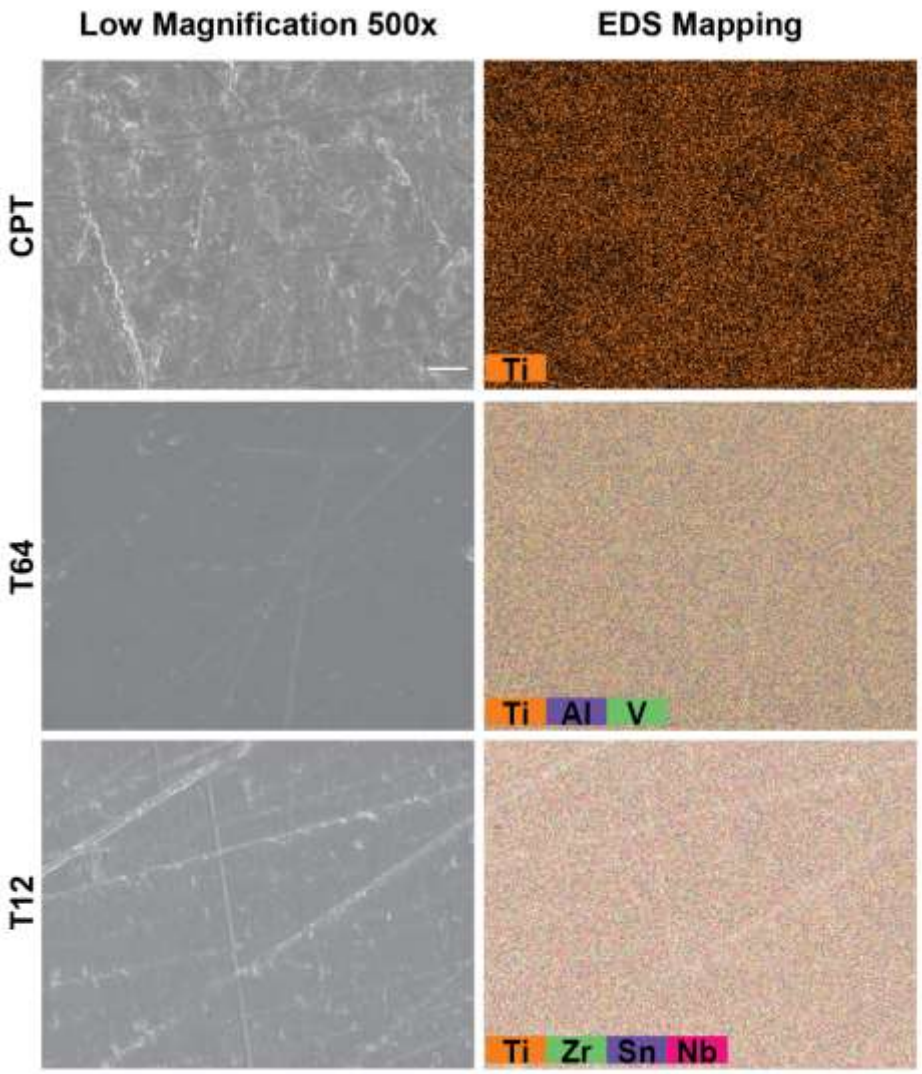


**Figure 22.** EDS spectrum to distinguish the chemical composition of the titanium alloy substrates CPT, T64 and T12. SEM micrographs showing surface topography of titanium substrates coated with gold and palladium at low magnification (500x). EDS maps of CPT, T64 and T12 substrates were examined, where the same location were used from the SEM micrographs that were taken at low magnification (500x) (scale bar = 10 μm).

**Table 4.** EDS elemental spectrum acquisition of CPT.

| Element | Atomic number | Normalised concentration in weight percentage (wt. %) of the element | Atomic weight percentage (at. %) |
|---|---|---|---|
| Ti | 22 | 100 | 100 |

**Table 5.** EDS elemental spectrum acquisition of T64.

| Element | Atomic number | Normalised concentration in weight percentage (wt. %) of the element | Atomic weight percentage (at. %) |
|---|---|---|---|
| Ti | 22 | 90.89 | 86.54 |
| Al | 13 | 6.68 | 11.28 |
| V | 23 | 2.43 | 2.18 |

**Table 6.** EDS elemental spectrum acquisition of T12.

| Element | Atomic number | Normalised concentration in weight percentage (wt. %) of the element | Atomic weight percentage (at. %) |
|---|---|---|---|
| Ti | 22 | 63.76 | 63.96 |
| Zr | 40 | 12.24 | 6.44 |
| Nb | 41 | 10.61 | 5.48 |
| Sn | 50 | 8.2 | 3.32 |

## 2.4 Discussion

### 2.4.1 Fabrication and characterisation of T12

The integration between bone and implant is an intricate process with various challenges including the effects of stress shielding where implants' stiffness are mismatched in terms of Young's modulus to that of bone, causing bone to atrophy over time leading to implant failure (Niinomi & Nakai, 2014). To address this challenge, researchers have been developing titanium alloys that more closely mimic the stiffness of bone ~33GPa. Whilst there are potential titanium alloys developed, their introduction as mainstream implant materials have been limited by high costs, bulk manufacturing, and efficacy. The development of biomaterials with different compositional compounds have been limited by the scale and time it takes to develop and characterize these materials. As such, we have developed βLOW which is a machine learning platform to establish a high-throughput process in which biomaterials such as titanium alloys can be quickly assessed and produced and characterized. One of these new class of titanium alloy is Ti-12Nb-12Zr-12Sn (T12) which have been shown to display stiffness similar to bone ~35GPa. Previous study on the T12 material was focused on the development and physio-chemical characterization to determine its feasibility as a titanium alloy for biomedical applications and bulk production (Wu et al., 2019). The focus of this chapter is to evaluate the development and characterisation of AI generated biomimetic titanium alloy T12 for bone medical implants.

The importance of hardness testing is to help evaluate material's properties including strength, ductility and wear resistance as to ensure quality control and acceptance of materials to be suitable for its target application (Verdins et al., 2013). Hardness test is typically used to measure the metal's resistance to localized surface deformation (Alsaeedi & Ozdemir, 2018). Henceforth, in this study Vickers microhardness test was used to determine the hardness of the titanium alloy substrates. Poondla et al. (2009) used Vickers microhardness test to measure the hardness of CPT and T64, whereby on average CPT had a Vickers microhardness of 200 HV and T64 had a Vickers microhardness of 330 HV. In terms of T12, which had a Vickers microhardness of $310.7 \pm 0.5316$ HV, signifying that it would perform similar to that of the currently approved T64 medical implant in relation to wear resistance. As

a result, T12 titanium alloy is a good mechanical compromise between high hardness and low Young's modulus, which enables its suitability for use in bone implants.

Energy-dispersive X-ray spectrometry (EDS) is a surface analytical technique commonly used for elemental analysis or chemical characterisation as well as the element distribution within a sample (Wang, 2016). EDS is used in conjunction with scanning electron microscope (SEM) that allows for the X-rays to be emitted from a sample during bombardment by an electron beam during element analysis within a sample (Kumar et al., 2016). In this study, EDS map for the elemental composition analysis revealed that on each titanium alloy substrate including CPT, T64 and T12, the elements were uniformly distributed. This would indicate that during cellular interaction, they are expected to respond similarly across the surface on each individual titanium alloy substrates since all the elements are uniformly distributed.

Furthermore, the topography of an implant has the ability to influence cellular response such as cell adhesion, morphology, proliferation, and differentiation that have been shown in previous research findings (Gordin et al., 2004). Surface preparation maybe critical for implant survival due to its great influence on cell responses. This will be addressed in the later chapters of this thesis.

## 2.5 Conclusion

Titanium and its alloys have been widely used in bone medical implants, mainly for the reconstruction of bone. The fabrication of the new AI generated biomimetic titanium alloy T12 is highly desirable for medical implant, due to its mechanical biocompatibility. This study has shown that T12 hardness in terms of surface deformation and wear resistance performance closely matches that of the current approved medical titanium alloy T64. Furthermore, we have shown that T12 has uniform distribution of elements across the surface that would allow cellular interaction to respond similarly throughout the entire surface during bone-implant integration.

# Chapter 3 - The Osteogenic cellular response to AI developed T12 titanium alloy

# Chapter 3 - The Osteogenic cellular response to AI developed T12 titanium alloy

This chapter will focus on bone cells response on different titanium alloy composition surfaces. It will start off with providing some background information into the different titanium alloys that will be evaluated under this project and will define the research questions for this study. It will continue onto the experimental methodology used to achieve results on cell morphology, cell viability, gene analysis and cytokines analysis. This chapter will then discuss these findings and what these results means in terms of which titanium alloy surface is more favourable to bone cells.

## 3.1 Introduction

Titanium and its alloys possess high strength, low weight and outstanding corrosion resistance properties, allowing greater suitability and demand for use in medical implants. More than 1000 tonnes of titanium are manufactured around the world for the purpose of medical implantation in patients each year (Veiga et al., 2012). Globally the life expectancy is ever increasing with an average life expectancy of 72 years (Roser et al., 2013). The demand for joint replacement surgery is continually growing due to the increase in life expectancy; where approximately 70-80% of all total hip joint replacement implants are manufactured from titanium alloys particularly Ti-6Al-4V (Tan et al., 2019). Titanium is one of the few materials that is able to match the requirements needed to be successfully implanted within the human body as it is light weight, strong, inert, non-magnetic, immune to corrosion and fully biocompatible. Due to these properties, titanium is able to integrate very well within the human bone and the surrounding tissue (Sidambe, 2014). The young's modulus for pure titanium and titanium alloys range between 103-120 gigapascals (GPa), whereas the stiffness of bone can range between 10-30 GPa (Elias et al., 2008; Liu et al., 2017). Henceforth, titanium and it's alloy such as Ti-6Al-4V is prone to the stress shielding effect due to the mismatch of stiffness to that of the adjacent bone, leading to greater bone resorption and bone cell death causing implant failure (Oldani & Dominguez, 2012; Tan et al.,

2019). To overcome this issue, cost-effective and biocompatible materials with low young's modulus are highly desirable to avoid stress shielding in bone implants (Wu et al., 2019).

The characteristic of Young's modulus describes the response of a material to stress and strain. This can be used to help with the understanding of mechanical biocompatibility. To achieve mechanical biocompatibility, metal used in various prostheses and orthopaedic implants must be mechanically harmonized with the surrounding bone tissue (Niinomi & Nakai, 2014). Due to the big differences between the current metal implants and natural bone's Young's modulus, the load transferred between implant to bone is non-homogeneous, leading to the reduction of stress stimulation of bone (Niinomi & Nakai, 2014; Oldani & Dominguez, 2012). This phenomenon is known as the stress shielding effect and under such conditions, bone is more likely to atrophy, leading to the loosening of the implant where it can easily re-fracture the cortical bone and damage the surrounding tissue (Niinomi & Nakai, 2014). With that said, it is believed that metals with Young's moduli that is equal to that of bone will be an ideal metal implant to for mitigate the stress shielding effect (Niinomi et al., 2012).

Apart from having a low Young's modulus, the material selected must be biocompatible, and non-toxic or harmful to the living tissue in the human body. The current approved titanium alloy Ti-6Al-4V for example consists of the elements aluminium and vanadium. Vanadium ions (Guan et al., 2017; Kawahara & Kato-Negishi, 2011; Siemers et al., 2016) contents from Ti-6Al-4V has been reported to cause toxicity in the body and aluminium is reported to be a neurotoxic element (Gomes et al., 2011; Gray et al., 2018; Khadija et al., 2018; Mravcová et al., 1993; Sommer et al., 2019). Henceforth, our group have developed a low Young's modulus titanium alloy that is composed of non-toxic and non-allergenic elements for biomedical applications. This novel titanium alloy with a composition of Ti-12Nb-12Zr-12Sn (T12) (in wt. %) was produced through AI machine learning approach called "βLow". The elements used within the titanium alloy composition are cost effective, and all elements are biocompatible. T12 has a Young's modulus closer to that of bone, less than 35 gigapascal (GPa). Therefore, a Young's modulus this low maybe effective in supressing the stress shielding effects in bone (Wu et al., 2019).

In this study, the cellular response to the titanium alloy substrate T12 was tested against commercialised pure titanium (CPT) and the titanium alloy Ti-6Al-4V (T64). Osteoblast and osteocyte cells are bone cells that are both involved in the bone remodelling cycle (bone formation and resorption) (Crockett et al., 2011; Prideaux et al., 2016), that were characterised on the different titanium alloy substrates to help evaluate the type of materials that these bone cells prefer best.

## 3.2 Methodology

### 3.2.1 Cell culture and maintenance

MC3T3-E1, osteoblast cells, were cultured in MEMα (Gibco, USA) supplemented with 10% FBS (Gibco, USA) and 1% penicillin/streptomycin (P/S) (Gibco, USA) at 37 °C with 5% $CO_2$. OCY454, osteocyte cells, were cultured and maintained in Minimum Essential Medium Alpha (MEMα) (Gibco, USA) supplemented with 10% foetal bovine serum (FBS) (Gibco, Australia) and 1% P/S (Gibco, USA) at 33 ºC with 5% $CO_2$. Osteocytes were allowed to reach confluence at 33 °C, then they were passaged and cultured at 37 ºC for an additional 2 weeks to differentiate to mature osteocytes. OCY454 cells expresses the green fluorescent protein (GFP) via fluorescence-activated cell sorting (FACS) directed by dentin matrix protein 1 (DMP1) promoter (DMP1-GFP) that fluoresces green under excitation and emission spectrum wavelength light of 495 nm/519 nm after 2 weeks to indicate matured osteocytes (Spatz et al., 2015). For all experiments, cells were seeded on individual titanium alloy substrates: CPT, T64 and T12 at a density of $2x10^4$ (OCY454) and $4x10^4$ (MC3T3-E1) cells/mL. Cells were incubated at 37 °C with 5% $CO_2$ for 48 hrs prior to experimentation. The experiment was repeated in triplicate.

### 3.2.2 Cell viability assay of osteoblast and osteocyte cells

MC3T3-E1 cells and OCY454 cells that were cultured independently on the 3 different titanium alloy substrates, were analysed in accordance to the manufacturer's instructions after day 1, 2, 4 and 7 with the PrestoBlue cell viability reagent (ThermoFisher Scientific, United States). PrestoBlue is a resazurin based solution that allows for live cells to be monitored over time and quantitatively measure cell proliferation. Briefly, the cells were incubated with the PrestoBlue solution for 10 minutes at 37 °C. The supernatant from the cells were collected and the fluorescence intensity at an excitation wavelength of 560 nm and emission wavelength of 590 nm were measured using the Infinite 200Pro microplate reader (Tecan, Switzerland). Furthermore, the total cell count was taken for both MC3T3-E1 cells and OCY454 cells after day 1, 2 and 3, to demonstrate cell proliferation and complement the

PrestoBlue cell viability reagent results. The cell count was done using a counting chamber neubauer improved double net ruling (Haemocytometer) by ProSciTech, Australia. The experiments were repeated in duplicate per each of the three biological replicates.

### 3.2.3 Immunostaining

To visualise the cytoskeleton of the MC3T3-E1 and OCY454 cells were first fixed and then stained. Cells were first washed 3 times with PBS to remove residual media and fixed using 4% paraformaldehyde (PFA) (w/v) (Sigma-Aldrich, USA) for 10 mins. Cells were then permeabilised following a 5 mins incubation with 0.3% Triton X-100 (v/v) (Sigma-Aldrich, USA), cells were co-stained with TRITC-conjugated phalloidin (Sigma-Aldrich, USA) (1:2000) and DAPI (Sigma-Aldrich, USA) (1:9000) for 20 mins. Cells were then washed 3 times with PBS to remove residual stain and stored at 4 °C until imaged.

### 3.2.4 Mouse cytokine antibody array membrane

OCY454 cells' cytokines signalling molecules on the different titanium alloy substrates including CPT, T12 and T64 were determined using the 'Mouse cytokine antibody array membrane' (Abcam, UK) to indicate which particular titanium alloy substrate is most favourable to osteocyte cells. Briefly, the OCY454 cells were seeded on the three different titanium alloy substrates at a density of $2x10^4$ for 48 hrs. After 48 hrs, the supernatant from each titanium alloy samples were collected and measured according to the manufacturer's instructions for the mouse cytokine antibody array membrane, which detects 22 cytokines simultaneously in one experiment. The chemiluminescence signals were read using the ChemiDoc MP imaging system (Bio-Rad, Australia), where the exposure time was set to rapid auto-exposure for all membranes. The relative expression levels of each cytokine were determined by normalising the array data, where one array membrane in this case the CPT or T64 sample was set to 'reference' to which the other array membranes (T12 sample) was normalised against. Henceforth, relative expression levels for each cytokine was calculated as per the instruction manual set out by the manufacturer, Abcam.

### 3.2.5 Microscopy

MC3T3-E1 and OCY454 cells' images were captured using the DeltaVision Elite Deconvolution Microscope equipped with the 40x (UApo/340) objective lens. Cells were imaged using the following settings: LED illumination for DAPI was set with emission wavelength of 435 nm and excitation wavelength of 390 nm, LED illumination for TRITC was set with emission wavelength of 597 nm and excitation wavelength of 542 nm, and the pixel size was set to 0.167 mm, 0.167 mm, 0.200 mm. A total of 10 images were acquired at random to ensure unbiased data collection from each of the three biological replicates.

### 3.2.6 Image analysis

All cells images were analysed using FIJI software. Cell morphology was evaluated following analysis of surface area, circularity and aspect ratio. Briefly, circularity was determined by the formula: $4\pi$ x [(Area)/([perimeter]$^2$)] where a value of one indicates a perfect circle and any value less than one indicates all other irregular shaped cells (Yuan, 2013). Aspect ratio (AR) is calculated using the equation AR = length of the longest chord/width of the longest chord, a value greater than 1 represents an elongated cell (Yuan, 2013). Solidity is calculated using the formula [Area]/[Convex area]; where a value less than 1 represents an irregular boundary of a cell actin filament that is protruding in multiple direction. To obtain the total live and dead *S. aureus* bacterial cell counts per image, the protocol 'Quantification of Live/Dead Staining Using Fiji Software' set out by BRTI Life Sciences was used for this study.

### 3.2.7 Digital Droplet PCR

RNA was collected from mammalian cells using a Qiagen AllPrep DNA/RNA Mini Kit (Cat no.: 80204, QIAGEN, Australia) as per manufacturer's protocol. Total RNA concentration was measured using a NanoDrop One/One$^C$ UV-Vis Spectrophotometer (ThermoFisher Scientific, United States) and samples were only used if the $A_{260/280}$ value ranged between a ratio of 1.9 to 2.1 Au. RNA was converted to cDNA using iScript reverse Transcription Supermix for RT-qPCR (Bio-Rad,

Australia). Oligo sequences (5' to 3') are outlined in Table 7 and 8 for osteoblast and osteocyte cell lines respectively. Samples were prepared for digital droplet PCR (ddPCR) following manufactures instructions for Qx200 ddPCR EvaGreen Supermix (Bio-Rad, Australia). The ddPCR reaction mix was placed into 'DG Cartridges for QX20/QX100' (Bio-Rad, Australia) with QX200 Droplet Generation Oil for EvaGreen (Bio-Rad, Australia) to generate the droplets using QX200 Droplet Generator (Bio-Rad, Australia). 40 µL of the generated droplets per gene were placed into a ddPCR 96-Well Plate (Bio-Rad, Australia), they were sealed using a heat sealer PX1 from Bio-Rad. Emulsion PCR was performed using C1000 Touch Thermal Cycler (Bio-Rad, Australia) following manufacturers recommended cycling protocol of 44 cycles with a fixed ramp rate of 2 °C/sec. The droplets were read using a BioRad droplet reader QX200 system.

### **3.2.8** Oligo sequences of osteocyte (OCY454) and osteoblast (MC3T3-E1) cells

**Table 7.** Oligo sequence for osteocyte (OCY454) cells.

| Oligo name | Forward or Reverse sequence | Oligo sequence (5' to 3') |
|---|---|---|
| GAPDH | Forward | AGGTCGGTGTGAACGGATTTG |
| GAPDH | Reverse | TGTAGACCATGTAGTTGAGGTCA |
| SOST | Forward | AGCCTTCAGGAATGATGCCAC |
| SOST | Reverse | CTTTGGCGTCATAGGGATGGT |
| DMP1 | Forward | AAGCTAGCCCAGAGGGACAGGCAA |
| DMP1 | Reverse | TTATCGGCGCCGGTCCCCGTAC |
| PHEX | Forward | GAAAGGGGACCAACCGAGG |
| PHEX | Reverse | AACTTAGGAGACCTTGACTCACT |
| OPG | Forward | AGAGCAAACCTTCCAGCTGC |
| OPG | Reverse | CTGCTCTGTGGTGAGGTTCG |
| RANKL | Forward | GCTGGGCCAAGATCTCTAAC |
| RANKL | Reverse | GTAGGTACGCTTCCCGATGT |

**Table 8.** Oligo sequence for osteoblast (MC3T3-E1) cells.

| Oligo name | Forward or Reverse sequence | Oligo sequence (5' to 3') |
|---|---|---|
| GAPDH | Forward | AATGTGTCCGTCGTGGATCTG |
| GAPDH | Reverse | CAACCTGGTCCTCAGTGTAGC |
| Col1α1 | Forward | ACGTCCTGGTGAAGTTGGTC |
| Col1α1 | Reverse | CCAGCAATACCCTGAGGTC |
| Runx2 | Forward | GCCCTCATCCTTCACTCCAAG |
| Runx2 | Reverse | GGTCAGTCAGTGCCTTTCCTC |
| OC | Forward | GAGGACCCTCTCTCTGCTCA |
| OC | Reverse | ACCTTATTGCCCTCCTGCTT |
| OPN | Forward | TCAGGACAACAACGGAAAGGG |
| OPN | Reverse | GGAACTTGCTTGACTATCGATCAC |
| ALP | Forward | ACAACCTGACTGACCCTTCG |
| ALP | Reverse | TCATGATGTCCGTGGTCAAT |

### 3.2.9 Statistical analysis

Statistical analysis was performed using GraphPad Prism 7 (GraphPad Software, CA, USA). All experiments were performed in biological triplicates (n=3). For cell morphological study, a total of 10 images were taken at random location from each of the tested substrates per biological replicate. All cells within the full view of the image were accounted for in the statistical analysis. Significance was determined using one-way ANOVA with a Tukey post-hoc analysis. All values are presented as mean ± SEM (standard error of the mean). P values less than 0.05 were considered statistically significant.

## 3.3 Results

### 3.3.1 Osteocytes adhere and spread on T12 surfaces comparable to medical titanium

Osteocytes are master regulators of both bone remodelling and regeneration, and it was therefore vital to determine the osteocyte response to the new class of titanium alloy substrate, T12. Osteocytes were seeded on the 3 different titanium substrates: commercially pure titanium (CPT), Ti-6Al-4V (T64) alloy, and Ti-12Nb-12Zr-12Sn (T12) alloy, to determine cell viability, morphology and gene expression of osteocytes in response to the different titanium alloy substrates.

Osteocytes seeded on the 3 different titanium alloy substrates, after day 1, 2, 4, and 7, showed an increased number of cells at each consecutive time point (Figure 23A). There was also no significant difference at each time point in terms of osteocytes cell viability that were seeded on the 3 different titanium alloy substrates, suggesting that the osteocytes are viable and are continuously proliferating. The osteocytes cell count that was taken after day 1, 2 and 3 as seen in Figure 23B, showed an increased number of cells at each consecutive time point. Again, there was no significant difference at each consecutive time point in terms of the total number of osteocytes that were seeded on the 3 different titanium alloy substrates. Overall, these results in Figure 23A and 23B indicate that none of the titanium alloy substrates have toxic effects on osteocytes as the cells on each titanium alloy substrate are viable and are continuously proliferating.

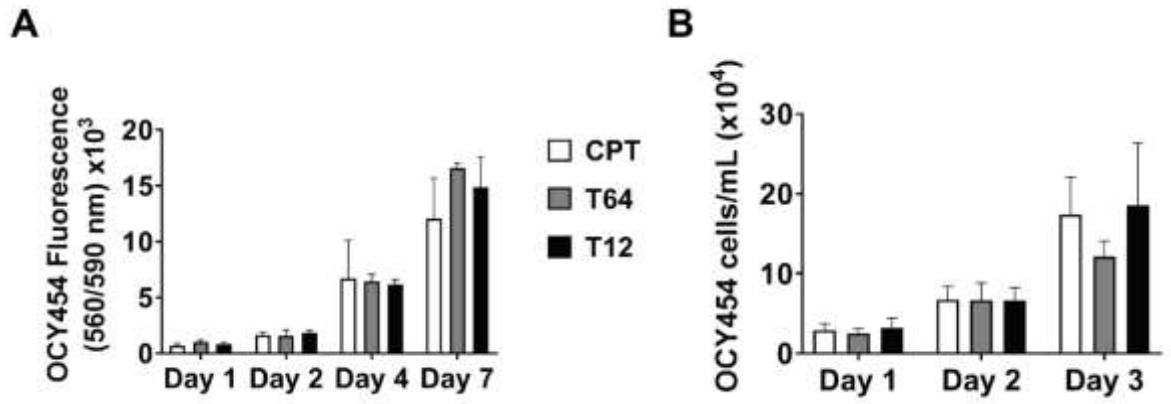


**Figure 23.** Analysis of OCY454 cells viability and proliferation following cell culture on the titanium substrates (CPT, T64 and T12). **A.** Live cells were monitored over time including at day 1, 2, 4 and 7 with PrestoBlue cell viability reagent. **B.** Live OCY454 cell count were examined at time points of day 1, 2 and 3, that were cultured on the three different titanium alloy substrates. n = 3 independent biological replicates. Data is presented as mean ± SEM. Statistical significance was determined using Two-Way ANOVA (with Turkey's post hoc analysis).

Following 48 hours of osteocytes culture on the different titanium alloy substrates, osteocytes were found to adhere and spread on all substrates tested (Figure 24A). The osteocytes actin cytoskeleton covers greater area per cell on CPT and T12 surfaces compared to T64 surface. T64 surface osteocytes' actin cytoskeleton also have a mixture of both circular and elongated cells compared to the other substrates. On the other hand, both CPT and T12 osteocyte cells morphology are similar in terms of area covered by the actin cytoskeleton per cell, that are irregularly shaped, with similar cell elongation (Figure 24A). Cell morphological analysis was undertaken to study the cellular organization and the physiological state of cells in response to all the different titanium substrates tested. Osteocytes seeded on titanium substrates CPT and T12 displayed a significant increased cell area when compared to the T64 (Figure 24B); suggesting slower osteocyte cell migration occurs on the surface of CPT and T12 compared to T64 (Refaaq et al., 2020). Interestingly, osteocytes seeded on either CPT or T12 were significantly larger when compared to those cells seeded on T64 alloy (Figure 24B) ($p < 0.0002$; one-way ANOVA with Tukey's post Hoc analysis), suggesting that the T12 alloy promote similar cell morphology, spreading and cellular response to that of the CPT surface. Circularity describes cells that

are circular to irregular shape where the actin cytoskeleton is branching out in multiple direction during cell spreading and migration, but it can't distinguish between how long different set of elongated cells are or which set of cells are protruding more or less on a particular substrate (Walters et al., 2017). Interestingly enough, there was significant difference in cellular circularity was determined for osteocytes seeded on the three titanium alloy substrates (Figure 24C), confirming that the titanium substrates did alter cell morphology ($p < 0.0001$; one-way ANOVA with Tukey's post Hoc analysis). It should be noted that a significant increase in cellular circularity was observed for osteocytes cultured on T64 substrates when compared to those cells cultured on the CPT and T12; suggesting that osteocytes seeded on T64 promotes increased osteocytes proliferation than CPT or T12, which can be observed by the mixture of both round to elongated osteocytes on T64 substrate that are also covering the least surface area per cell (Figure 24A). The aspect ratio focuses on the general shape of the cell in terms of elongation, whereas solidity determines how much the cell's actin cytoskeleton is protruding during cell spreading and migration. Osteocyte seeded on CPT substrates have a significantly increased aspect ratio compared to the osteocytes seeded on T12 (Figure 24D). On the other hand, the solidity of osteocytes on CPT is significantly reduced compared to both T64 and T12 (Figure 24E). Overall, T64 osteocytes covers the least surface area per actin cytoskeleton, produces a mixture of circular and elongated osteocytes, that have the least amount of protrusions occurring by the osteocytes actin cytoskeleton; suggesting that the osteocytes seeded on T64 substrate are undergoing faster migration, which occurs when cells are typically elongated. Whereas, branched out osteocytes actin cytoskeleton that are protruding in multiple direction would result in slower migration (Krause & Gautreau, 2014) as seen for the osteocytes seeded on CPT substrate in Figure 24A, this would mean that the osteocytes prefer T64 substrates best, whereas T12 performs similar to that of CPT. Furthermore, due to the significant increase in cell protrusions on both CPT and T12 substrates compared to T64, suggests that there is a significant increase in multi-dendrites structure on both CPT and T12 substrates than T64 substrate. The increased level of osteocytes' dendricity on CPT and T12 substrate compared to T64 substrate, denotes high level of connectivity between nearby osteocytes, leading to improved co-ordinated cellular response to mechanical stimuli during bone repair (Bonewald, 2008).

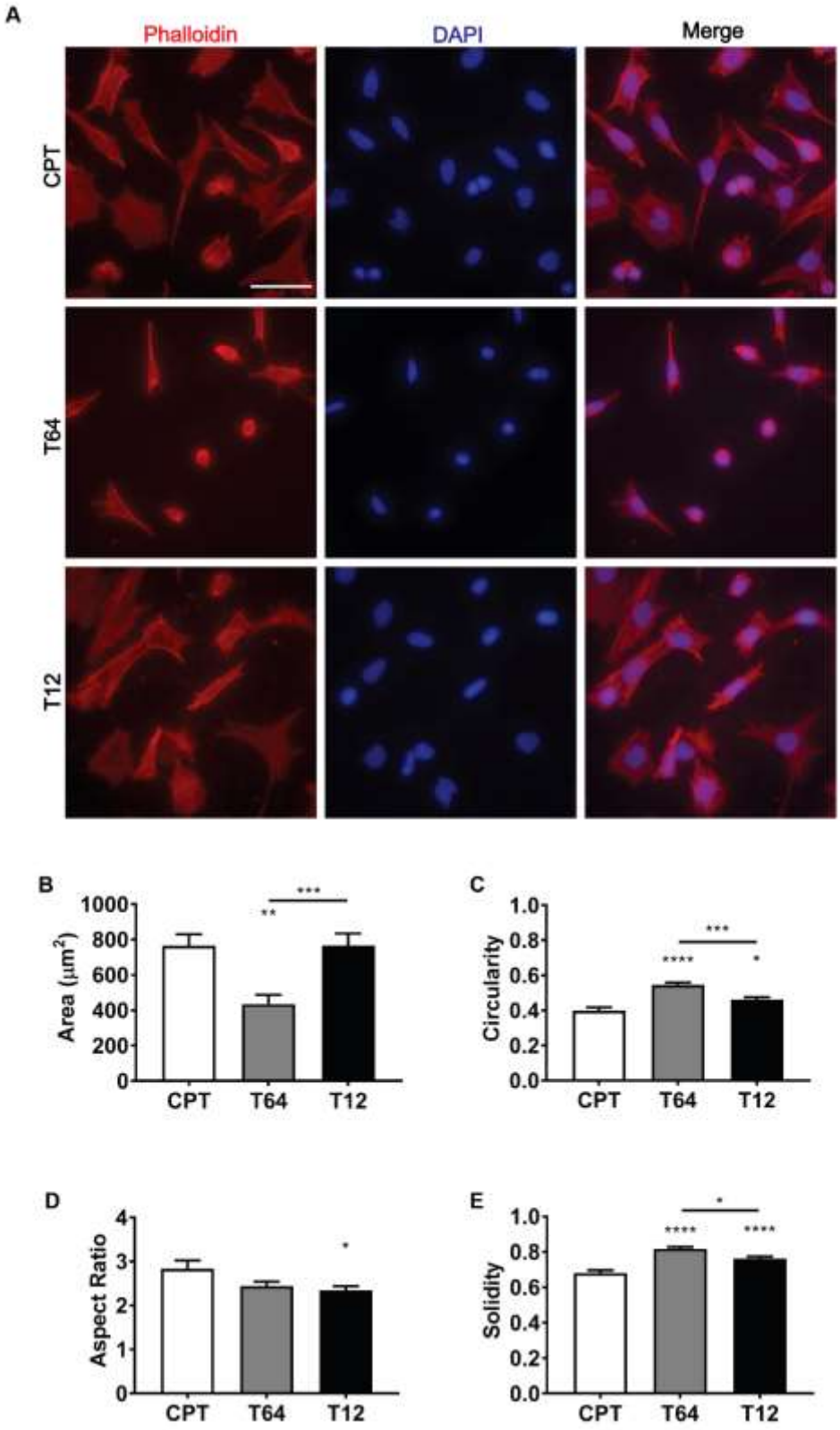


**Figure 24.** Analysis of OCY454 cells following 48 hours of culture on the titanium substrates (CPT, T64 and T12). A. Micrographs of OCY454 cells stained with phalloidin (red; first panel) to identify the actin cytoskeleton and with DAPI (blue; middle panel) to identify the nucleus. The last panel shows the merged images. Scale bar = 50 µm. B. Area of OCY454 cells cultured on indicated

substrates. C. Circularity of OCY454 cells cultured on indicated substrates. D. Aspect ratio of OCY454 cells cultured on indicated substrates. E. Solidity of OCY454 cells cultured on indicated substrates. n = 3 independent biological replicates. Data is presented as mean ± SEM. Statistical significance was determined using One-Way ANOVA (with Turkey's post hoc analysis). * $p < 0.05$, ** $p < 0.01$, *** $p < 0.001$, **** $p < 0.0001$.

### 3.3.2 Osteocyte gene expression on T12 in comparison to current approved medical implants

To compare osteocytes cellular response in terms of bone formation/resorption capabilities on T12 alloy against current approved medical implants (CPT and T64), key osteocyte genes including SOST, dentin matrix acidic phosphoprotein 1 (DMP1), phosphate regulating endopeptidase homolog X-linked (PHEX), osteoprotegerin (OPG) and receptor activator of nuclear factor kappa-B ligand (RANKL) were examined (Figure 25). Osteocytes seeded on the CPT substrate showed a significantly higher level of SOST gene expression compared with that of T64 and T12 substrate. On the other hand, T12 SOST gene expression (66.86 ± 6.63 copies/µL) were at similar level to T64 (56.46 ± 5.607 copies/µL, $P > 0.5390$), suggesting osteocytes favour bone formation over resorption on T12 compared to CPT as SOST is known to be a negative regulator of bone formation (Qin et al., 2013; Spatz et al., 2015). No significant differences in osteocyte DMP1 gene expression was found between those cells seeded on any of the substrates tested, suggesting that phosphate is regulated at a consistent rate by the osteocytes on all the tested substrates, which is required for proper mineralization of bone. Expression of DMP1 gene also denotes that osteocyte had reached maturity (Dallas et al., 2013; Econs et al., 1994). Statistically there is no significant difference in PHEX gene expression on the tested substrates; suggesting that osteocytes on all the tested substrates promote bone mineralisation at a similar rate. An indicator for bone formation OPG showed that T64 (105.5 ± 30.28 copies/µL) had statistically higher expression levels compared with CPT (30.13 ± 5.418 copies/µL, $p < 0.041$); whereas, T64 is statistically not significantly different to that of T12 (69.9 ± 7.262 copies/µL, $p > 0.3912$), which signifies T64 and T12 substrates has the capability to promote greater bone formation than CPT. RANKL expression which is an indicator of bone resorption, showed CPT is the only titanium substrate with a significantly higher expression levels than both T64 and T12 substrates ($p < 0.0002$; One-way ANOVA with Tukey's

post hoc analysis). Whereas the RANKL expression level between T64 and T12 is at a similar level, indicating CPT substrate to promote bone resorption mechanism. The OPG/ RANKL expression which indicates the balance between bone formation and resorption show a significantly reduced ratio by osteocytes on CPT ($0.5207 \pm 0.1218$) compared to T64 ($2.76 \pm 0.6724$, $p < 0.0101$). On the other hand, T64 OPG/ RANKL ratio is not significantly different to that of T12 ($2.113 \pm 0.2131$, $p > 0.5337$), suggesting CPT substrate favours bone resorption than bone formation; whereas, both T12 and T64 substrates OPG/ RANKL ratio indicates bone formation mechanism.

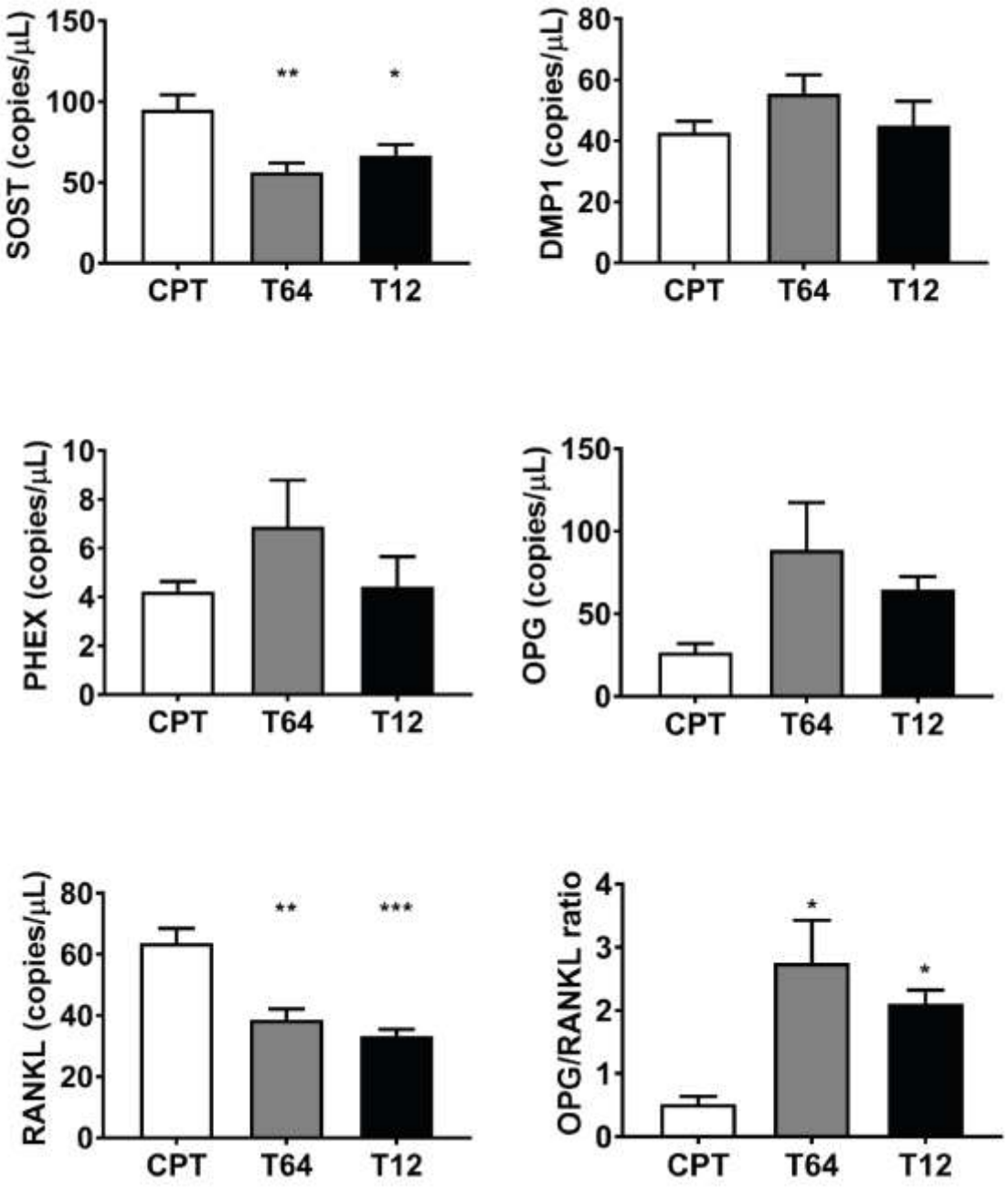


**Figure 25.** Analysis of OCY454 cells' gene expression following 48 hours of culture on the titanium substrates (CPT, T64 and T12). Indicated gene expression levels of OCY454 cells cultured on indicated substrates analysed following ddPCR. n = 3 independent biological replicates. Data is presented as mean ± SEM. Statistical significance was determined using One-Way ANOVA (with Turkey's post hoc analysis). * $p < 0.05$, ** $p < 0.01$, *** $p < 0.001$.

### 3.3.3 Osteoblasts shows significantly higher cell spreading on T12

Osteoblast cells are directly involved with synthesizing and mineralizing new bone, which are regulated by osteocytes during bone remodelling cycle to maintain bone mass. Similarly, to the osteocytes, osteoblasts cells were also cultured on the three different substrates to determine cell viability, cell morphology and gene expression of osteoblast in response to the different titanium alloy substrates. Osteoblast seeded on the 3 different titanium alloy substrates, after day 1, 2, 4, and 7, also showed an increased number of cells at each consecutive time point (Figure 26A). There was no significant difference at each time point in terms of osteoblasts cell viability that were seeded on the 3 different titanium alloy substrates except for day 7, where CPT had significantly lower amount of viable cells compared to both the titanium alloy substrates T64 and T12, suggesting that although the osteoblasts are viable, continuously proliferating at each tested time point, the cells inclusively prefer titanium alloy substrates as T64 and T12 best than CPT. These results were further complemented by the total osteoblast cell count at each consecutive time point after day 1, 2 and 3 (Figure 26B), to denote cell proliferation. The osteoblast cell count at each consecutive time point showed no significant between the three different titanium alloy substrates, suggesting that the cells are continuously proliferating on each titanium alloy substrate. Overall, these results in Figure 26A and 26B indicate that none of the titanium alloy substrates have toxic effects on osteoblast cells.

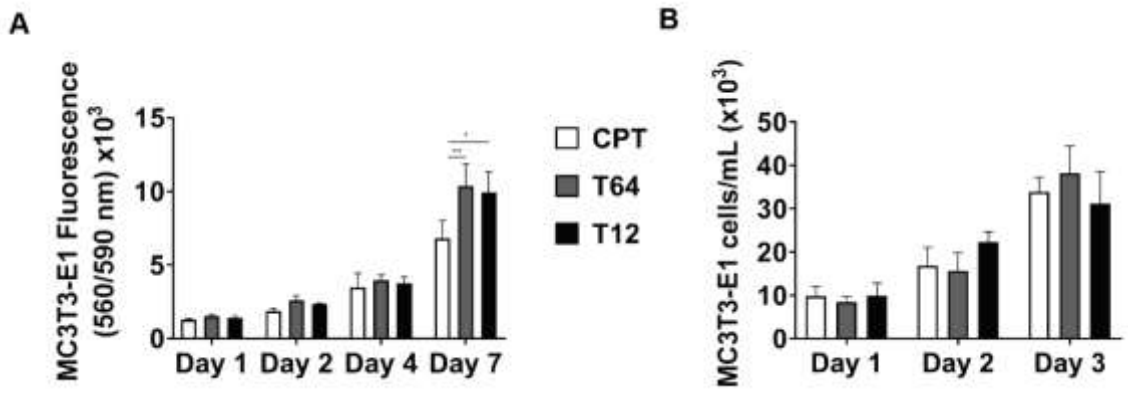


**Figure 26.** Analysis of MC3T3-E1 cells viability and proliferation following cell culture on plastic (CTRL), and the titanium substrates (CPT, T64 and T12). **A.** Live cells were monitored over time including at day 1, 2, 4 and 7 with PrestoBlue cell viability reagent. **B.** Live MC3T3-E1 cell count were examined at time points of day 1, 2 and 3, that were cultured on the four different substrates. n = 3 independent biological replicates. Data is presented as mean ± SEM. Statistical significance was determined using Two-Way ANOVA (with Turkey's post hoc analysis). * $p < 0.05$, ** $p < 0.01$.

After 48 hours of cell culture on the 3 different substrates, osteoblasts were found to adhere and spread on all the substrates tested (Figure 27A). The osteoblast cells on the 3 different substrates as seen in the micrographs in Figure 27A, shows the osteoblasts' actin cytoskeleton morphology on CPT covers greater surface area per cell during spreading compared to T64 and T12. T64 substrate produce very elongated osteoblast cells that are covering the least area by the actin cytoskeleton. T12 substrate promotes a mixture of both big and small osteoblast cells but with similar cell shape in terms of circularity and aspect ratio to that of CPT substrate (Figure 27A). On average, the area covered by osteoblast cell's actin cytoskeleton on both T64 and T12 titanium substrates had significantly lower area per cell compared to CPT ($p < 0.0001$; One-way ANOVA with Tukey's post hoc analysis). Furthermore, T64 ($1227 \pm 99.24$ $\mu m^2$) had a significantly lower osteoblast's actin cytoskeleton area compared with T12 ($1879 \pm 117.3$ $\mu m^2$, $P < 0.0031$) (Figure 27B); this would suggest that osteoblasts on T64 substrate are more active, spreading and migration faster compared to the titanium alloy substrates CPT and T12 (Refaaq et al., 2020). The cell's circularity had no significant difference between the three different substrates (Figure 27B) ($p > 0.0663$; one-way ANOVA with Tukey's post hoc analysis), which signifies that the osteoblast cells' cytoskeletons are all irregularly shaped and

branched out in multiple directions at a similar circularity ratio on all the substrates tested. Similarly observed in Figure 27A, the osteoblasts on T64 was the only titanium group which showed a significantly higher population of cell elongation compared to the other substrates (Figure 27D) ($p < 0.0001$; one-way ANOVA with Tukey's post hoc analysis). This would suggest that the osteoblast on T64 substrate are undergoing faster migration than on the other substrates tested (Krause & Gautreau, 2014) and would overall signify that cell morphology differs across the different titanium alloy substrates. Furthermore, in terms of solidity, T12 ($0.6615 \pm 0.01597$) substrate's osteoblast actin cytoskeleton is significantly reduced compared to CPT ($0.719 \pm 0.01106$, $p < 0.0056$) (Figure 27E), signifying that osteoblast cells on T12 substrates have greater amount of actin cytoskeleton protrusions than the osteoblast cells on CPT substrate; suggesting that slower osteoblast migration occurs (Krause & Gautreau, 2014) on T12 than on CPT substrate.

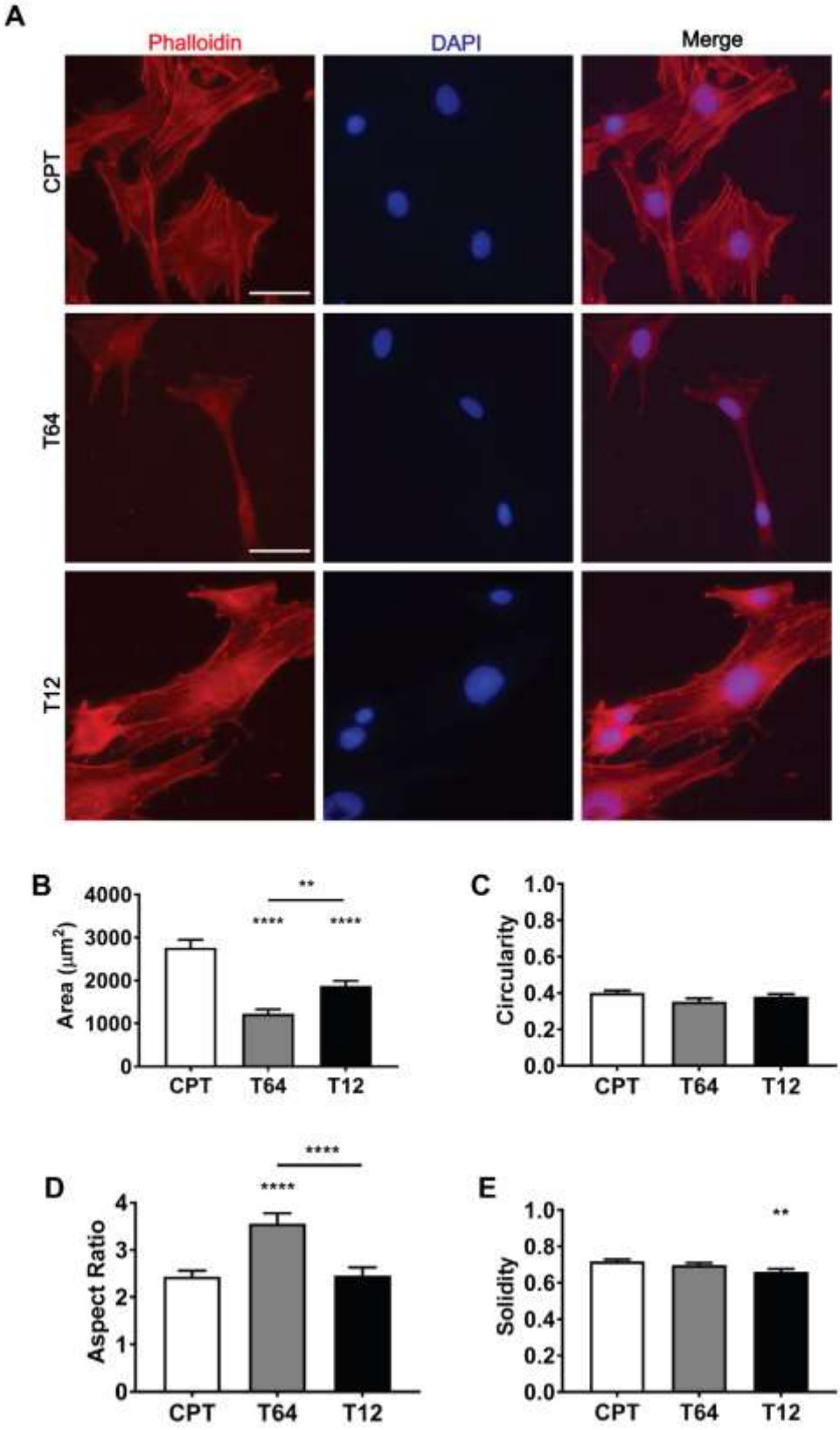


Figure 27**.** Analysis of MC3T3-E1 cells following 48 hours of culture on the titanium substrates (CPT, T64 and T12). **A.** Micrographs of MC3T3-E1 cells stained with phalloidin (red; first panel) to identify the actin cytoskeleton and with DAPI (blue; middle panel) to identify the nucleus. The last panel shows the merged images. Scale bar = 50 µm. **B.** Area of MC3T3-E1 cells cultured on indicated substrates.

**C.** Circularity of MC3T3-E1 cells cultured on indicated substrates. **D.** Aspect ratio of MC3T3-E1 cells cultured on indicated substrates. **E.** Solidity of MC3T3-E1 cells cultured on indicated substrates. n = 3 independent biological replicates. Data is presented as mean ± SEM. Statistical significance was determined using One-Way ANOVA (with Turkey's post hoc analysis). * $p < 0.05$, ** $p < 0.01$, **** $p < 0.0001$.

### 3.3.4 Osteoblasts on T12 express key bone formation genes

Osteoblasts play a crucial role in bone mineralization especially in the production of collagen type 1 (Col1α1). As such, key osteoblast bone regulatory gene markers were examined to determine the bone mineralization potential of osteoblast on T12. Col1α1 gene expression by osteoblasts showed similar levels of expression (Figure 28) ($p > 0.7437$; one-way ANOVA with Tukey's post hoc analysis). Runt related transcription factor 2 (RUNX2) gene expression also showed no significant differences between the titanium substrates, suggesting osteoblast cell proliferation occurs at a similar rate across the different substrates tested (Komori, 2019) ($p > 0.9509$; one-way ANOVA with Tukey's post hoc analysis). However, osteocalcin (OC) expression was significantly lower in T12 (16.2 ± 1.7 copies/µL) compared with T64 (42.67 ± 3.656 copies/µL, $P < 0.0222$), suggesting greater bone mineralisation occurs on T64 than T12 (Cundy et al., 2014; Sista et al., 2013) (Figure 28). The expression of osteopontin (OPN) by osteoblasts in T12 (1868 ± 41 copies/µL) was at the same level as T64 (2513 ± 303.3 copies/µL), whereas CPT (1243 ± 266 copies/µL) ($P < 0.0446$, one-way ANOVA) was significantly lower, suggesting bone mineralisation in terms of crystal growth occurs slower on CPT compared to osteoblast cells seeded on the other substrates. Furthermore, the expression of alkaline phosphatase 1 (ALP-1) was significantly higher in T64 (628.7 ± 81.08 copies/µL) compared with CPT (195 ± 71.6 copies/µL) and T12 (206.7 ± 41.6 copies/µL) ($p < 0.0059$, one-way ANOVA with Tukey's post hoc analysis), suggesting osseointegration occurs better on T64 than both CPT and T12. On the other hand, statistically ALP-1 gene expression on T12 substrate is not significantly different to that of CPT, which could suggest that osseointegration occurs at a similar rate to that of the CPT substrate.

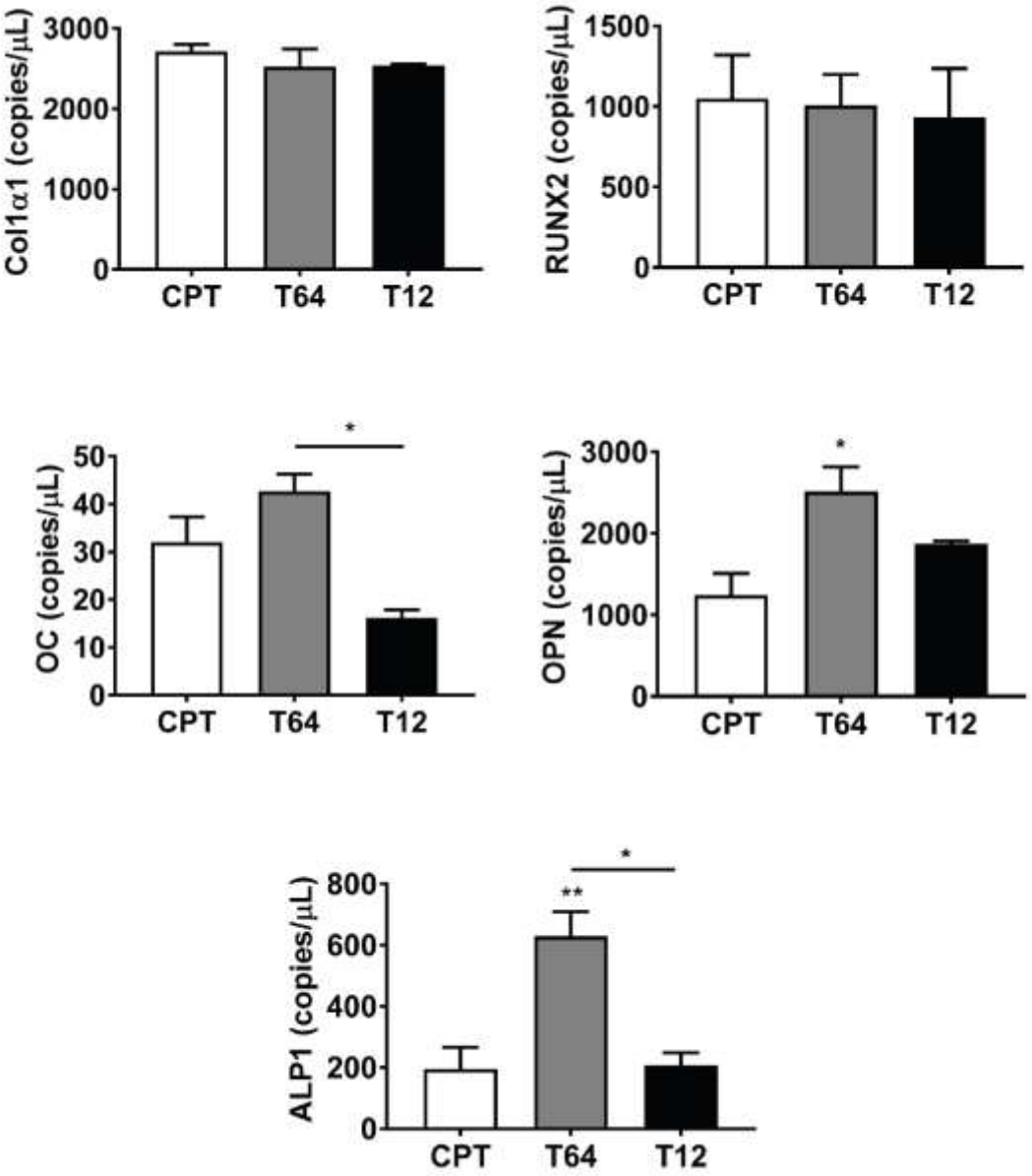


**Figure 28.** Analysis of MC3T3-E1 cells' gene expression following 48 hours of culture on the titanium substrates (CPT, T64 and T12). Indicated gene expression levels of MC3T3-E1 cells cultured on indicated substrates analysed following ddPCR. n = 3 independent biological replicates. Data is presented as mean ± SEM. Statistical significance was determined using One-Way ANOVA (with Turkey's post hoc analysis). * $p < 0.05$, ** $p < 0.01$, *** $p < 0.001$.

### 3.3.5 OCY454 cytokines secretion profile in response to the titanium alloy substrates

In order to determine cytokines' secretion profile from osteocytes cellular response on the different titanium alloy substrates, the mouse cytokines antibodies array membrane was performed on the collected supernatant from all the different titanium alloy substrates including CPT, T12 and T64 (Figure 29). Coincidently, all 22 cytokines were detected from the osteocytes (OCY454) cell line by the mouse cytokines antibodies array membrane.

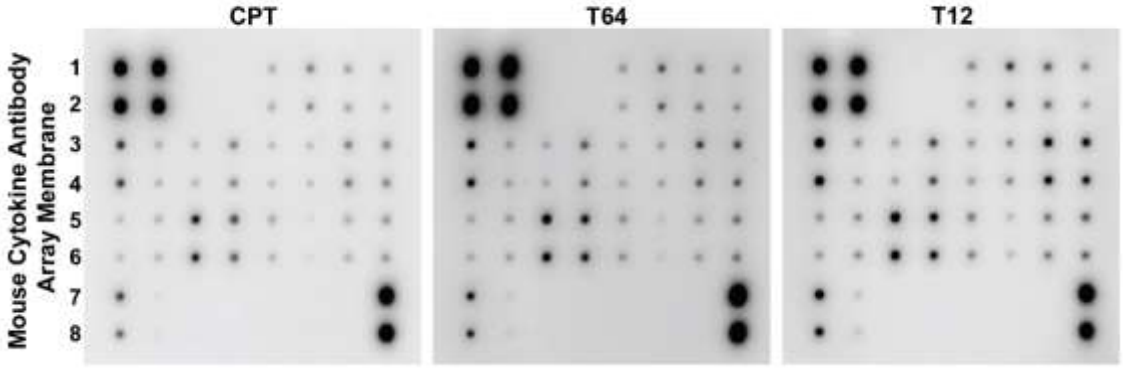


**Figure 29.** Visual representation of the mouse cytokine antibody array membrane that were used for the simultaneous detection of 22 mouse cytokine concentrations from OCY454 cell culture supernatant obtained from titanium alloy substrate CPT, T64 and T12. The supernatant was collected from each sample after 48 hours of OCY454 cell culture on each titanium alloy substrate.

Cytokines analysis of T12 substrate revealed that all 22 cytokines were similarly expressed to that of CPT substrate including: GCSF ($p = >0.9999$), GM-CSF ($p = >0.9999$), IL-2 ($p = >0.9999$), IL-3 ($p = >0.9999$), IL-4 ($p = >0.9999$), IL-5 ($p = >0.9999$), IL-6 ($p = >0.9999$), IL-9 ($p = >0.9999$), IL-10 ($p = >0.9999$), IL-12 ($p = >0.9999$), p40p70 ($p = >0.9999$), IL-12p70 ($p = >0.9999$), IL-13 ($p = >0.9999$), IL-17 ($p = >0.9999$), IFN-ϒ ($p = >0.9999$), MCP-1 ($p = >0.9988$), MCP-5 ($p = >0.9999$), RANTES ($p = >0.5246$), SCF ($p = >0.9999$), sTNFRI ($p = >0.9999$), TNF-α ($p = >0.9999$), Thrombopoietin ($p = >0.9999$), and VEGF ($p = >0.9999$) (Figure 30A, Table 9). Correspondingly, the level of all 22 cytokines expression on T12 substrate compared to T64 substrate were also similarly expressed, including: GCSF ($p = >0.9999$), GM-CSF ($p = >0.9999$), IL-2 ($p = >0.9999$), IL-3 ($p = >0.9999$), IL-4 ($p = 0.9888$), IL-5 ($p = >0.9999$), IL-6 ($p = >0.9999$), IL-9 ($p = >0.9999$), IL-10 ($p =$

>0.9999), IL-12 (p = >0.9999), p40p70 (p = >0.9999), IL-12p70 (p = 0.9993), IL-13 (p = >0.9999), IL-17 (p = >0.9999), IFN-ϒ (p = >0.9999), MCP-1 (p = >0.9999), MCP-5 (p = >0.9999), RANTES (p = 0.9980), SCF (p = >0.9999), sTNFRI (p = >0.9999), TNF-α (p = >0.9999), Thrombopoietin (p = 0.9944), and VEGF (p = >0.9999) (Figure 30B, Table 10). This overall signifies that osteocytes cellular response on T12 substrate is similar to that of both CPT and T64 substrates; indicating that numerous cytokines are secreted at the same rates by osteocytes, which collectively signifies similar rate of osseointegration on all the tested substrates.

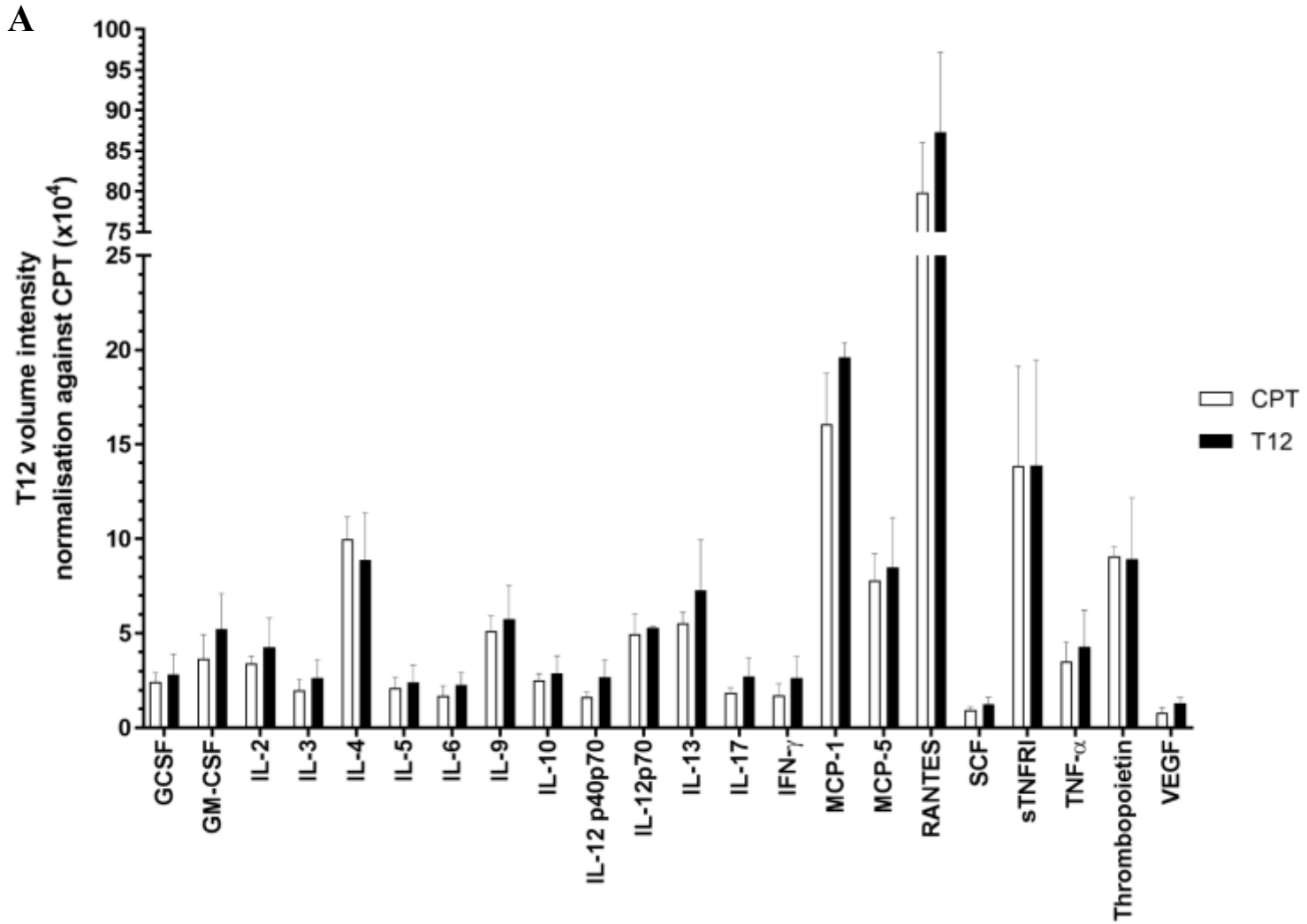
A
T12 volume intensity
normalisation against CPT (x10^4)
100
95
90
85
80
75
25
20
15
10
5
0
CPT
T12
GCSF
GM-CSF
IL-2
IL-3
IL-4
IL-5
IL-6
IL-9
IL-10
IL-12 p40p70
IL-12p70
IL-13
IL-17
IFN-γ
MCP-1
MCP-5
RANTES
SCF
sTNFRI
TNF-α
Thrombopoietin
VEGF

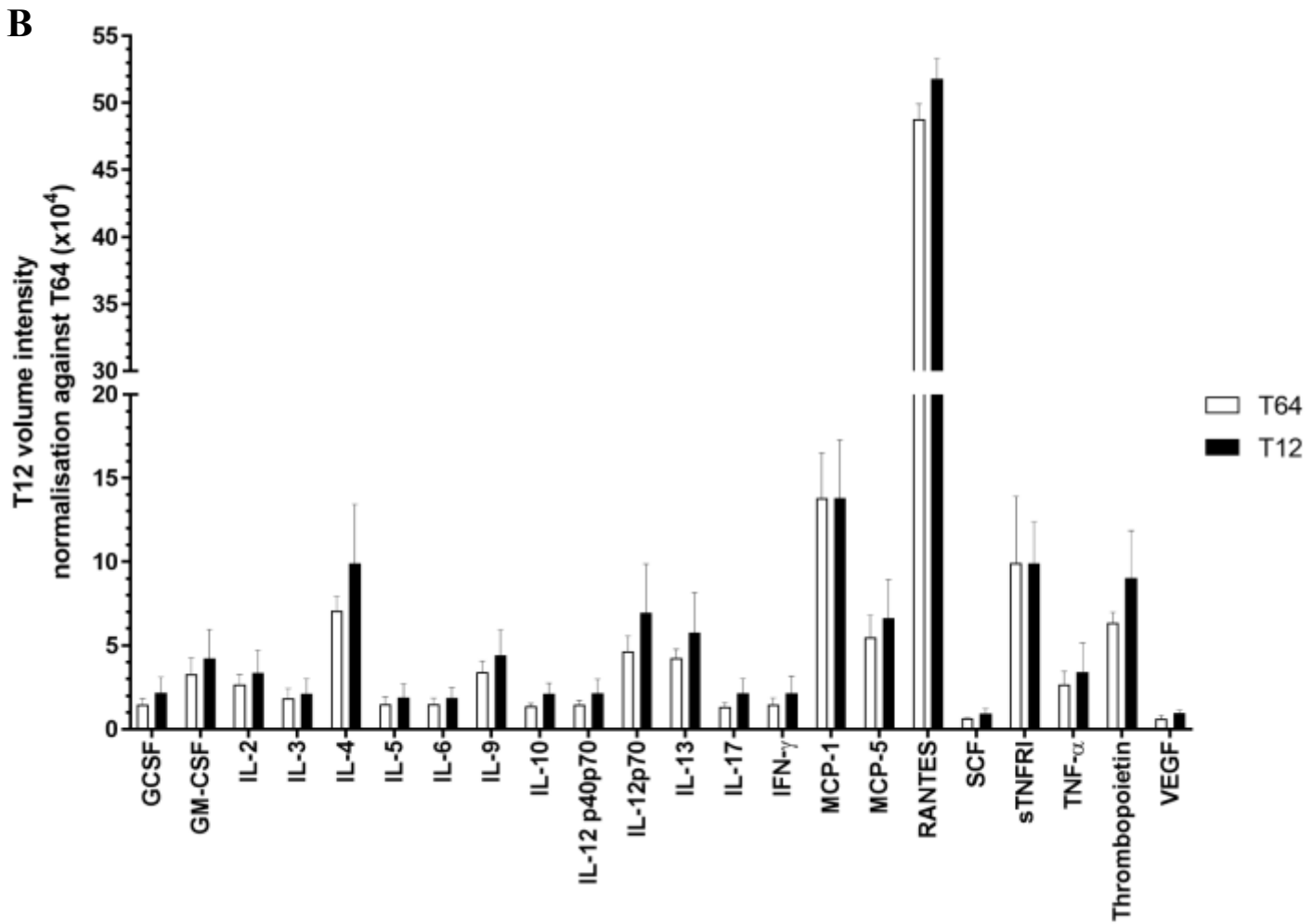


**Figure 30.** The relative cytokine levels expression of OCY454 cultured for 48 hours on the three different titanium alloy substrates including CPT, T64 and T12. **A.** The OCY454 cells' relative cytokine expression levels of T12 sample normalised against the 'reference' CPT sample. **B.** The OCY454 cells' relative cytokine expression levels of T12 sample normalised against the 'reference' T64 sample. Data is presented as mean ± SEM. Statistical significance was determined using Two-Way ANOVA (with Sidak post hoc analysis).

**Table 9.** Osteocytes (OCY454) response on T12 substrate against CPT substrate via cytokines expression in conditioned media.

| Cytokine | P-value | Significant | Fold Change | Change |
|---|---|---|---|---|
| sTNFRI | >0.9999 | No | 0.998915084 | ⇔ |
| IL-12p70 | >0.9999 | No | 0.935688923 | ⇔ |
| MCP-5 | >0.9999 | No | 0.917296875 | ⇔ |
| RANTES | 0.5246 | No | 0.914408444 | ⇔ |
| IL-9 | >0.9999 | No | 0.888571608 | ⇔ |
| IL-10 | >0.9999 | No | 0.880477898 | ⇔ |
| IL-5 | >0.9999 | No | 0.873922882 | ⇔ |
| GCSF | >0.9999 | No | 0.860283159 | ⇔ |
| TNF-α | >0.9999 | No | 0.823220099 | ⇔ |
| MCP-1 | 0.9988 | No | 0.819539766 | ⇔ |
| IL-2 | >0.9999 | No | 0.795953429 | ⇔ |
| SCF | >0.9999 | No | 0.761522754 | ⇔ |
| IL-13 | >0.9999 | No | 0.760980256 | ⇔ |
| IL-3 | >0.9999 | No | 0.757046511 | ⇔ |
| IL-6 | >0.9999 | No | 0.741273004 | ⇔ |
| GM-CSF | >0.9999 | No | 0.702382359 | ⇔ |
| IL-17 | >0.9999 | No | 0.689035232 | ⇔ |
| IFN-ϒ | >0.9999 | No | 0.649199209 | ⇔ |
| VEGF | >0.9999 | No | 0.634108321 | ⇔ |
| IL-12 p40p70 | >0.9999 | No | 0.614256721 | ⇔ |
| Thrombopoietin | >0.9999 | No | -1.01727639 | ⇔ |
| IL-4 | >0.9999 | No | -1.126670467 | ⇔ |

**Table 10.** Osteocytes (OCY454) response on T12 substrate against T64 substrate via cytokines expression in conditioned media.

| Cytokine | P-value | Significant | Fold Change | Change |
|---|---|---|---|---|
| MCP-1 | >0.9999 | No | 0.998634137 | ⇔ |
| RANTES | 0.998 | No | 0.941929237 | ⇔ |
| IL-3 | >0.9999 | No | 0.870942892 | ⇔ |
| MCP-5 | >0.9999 | No | 0.828276937 | ⇔ |
| IL-6 | >0.9999 | No | 0.80382607 | ⇔ |
| IL-2 | >0.9999 | No | 0.798926949 | ⇔ |
| IL-5 | >0.9999 | No | 0.784689137 | ⇔ |
| TNF-α | >0.9999 | No | 0.779983744 | ⇔ |
| GM-CSF | >0.9999 | No | 0.77786365 | ⇔ |
| IL-9 | >0.9999 | No | 0.775868124 | ⇔ |
| IL-13 | >0.9999 | No | 0.736671301 | ⇔ |
| IL-4 | 0.9888 | No | 0.715526037 | ⇔ |
| Thrombopoietin | 0.9944 | No | 0.705985499 | ⇔ |
| SCF | >0.9999 | No | 0.697401527 | ⇔ |
| IL-12 p40p70 | >0.9999 | No | 0.682658432 | ⇔ |
| IFN-ϒ | >0.9999 | No | 0.681573885 | ⇔ |
| GCSF | >0.9999 | No | 0.680214649 | ⇔ |
| IL-12p70 | 0.9993 | No | 0.672922198 | ⇔ |
| IL-10 | >0.9999 | No | 0.657864857 | ⇔ |
| VEGF | >0.9999 | No | 0.640809424 | ⇔ |
| IL-17 | >0.9999 | No | 0.632953874 | ⇔ |
| sTNFRI | >0.9999 | No | -1.004549029 | ⇔ |

## 3.4 Discussion

The integration between bone and implant is an intricate process with various challenges including the effects of stress shielding where implants' stiffness are mismatched in terms of Young's modulus to that of bone, causing bone to atrophy over time leading to implant failure (Niinomi & Nakai, 2014). To address this challenge, researchers have been developing titanium alloys that more closely mimic the stiffness of bone ~33GPa. Whilst there are potential titanium alloys developed, their introduction as mainstream implant materials have been limited by high costs, bulk manufacturing, and efficacy. The development of biomaterials with different compositional compounds have been limited by the scale and time it takes to develop and characterize these materials. As such, we have developed βLOW which is a machine learning platform to establish a high-throughput process in which biomaterials such as titanium alloys can be quickly assessed and produced and characterized. One of these new class of titanium alloy is Ti-12Nb-12Zr-12Sn (T12) which have been shown to display stiffness similar to bone ~35GPa. Previous study on the T12 material was focused on the development and physio-chemical characterization to determine its feasibility as a titanium alloy for biomedical applications and bulk production (Wu et al., 2019). The focus of this study is to determine the *in-vitro* biological efficacy of T12 for bone implant applications.

The importance of hardness testing is to help evaluate material's properties including strength, ductility and wear resistance as to ensure quality control and acceptance of materials to be suitable for its target application (Verdins et al., 2013). Hardness test is typically used to measure the metal's resistance to localized surface deformation (Alsaeedi & Ozdemir, 2018). Henceforth, in this study Vickers microhardness test was used to determine the hardness of the titanium alloy substrates. Poondla et al. (2009) used Vickers microhardness test to measure the hardness of CPT and T64, whereby on average CPT had a Vickers microhardness of 200 HV and T64 had a Vickers microhardness of 330 HV. In terms of T12, which had a Vickers microhardness of $310.7 \pm 0.5316$ HV, signifying that it would perform similar to that of the currently approved T64 medical implant in relation to wear resistance.

Energy-dispersive X-ray spectrometry (EDS) is a surface analytical technique commonly used for elemental analysis or chemical characterisation as well as the element distribution within a sample

(Wang, 2016). EDS is used in conjunction with scanning electron microscope (SEM) that allows for the X-rays to be emitted from a sample during bombardment by an electron beam in the course of element analysis within a sample (Kumar et al., 2016). In this study, EDS map for the elemental composition analysis revealed that on each titanium alloy substrate including CPT, T64 and T12, the elements were uniformly distributed. This would indicate that during cellular interaction, they are expected to respond similarly across the surface on each individual titanium alloy substrates since all the elements are uniformly distributed.

In the early stages of bone implant procedure is the integration between the host bone and the implant material lead by the invasion of bone cells. To mimic this interaction, osteoblasts as a model for bone formation (Caetano-Lopes et al., 2007; Katagiri & Takahashi, 2002) and osteocytes as a bone regulator (Caetano-Lopes et al., 2007), were studied to evaluate the response of T12. The response of osteocytes is of particular interest as these cells are recognized to be highly mechanosensitive to its environment and as such is a good demonstrator of responding to the changes in bulk material stiffness.

The first contact between any titanium material in a biological setting is the adherence of the native and surrounding cells and its response to the material. Once the cells adhere to the titanium material, the response is governed by the material surface structure (Casaletto et al., 2001) , stiffness (Bose et al., 2018), and chemical composition (Bruschi et al., 2015; Zareidoost et al., 2012). The cell's "first contact" lies in its ability to spread on the titanium surface that initiates downstream biological response (Boyan et al., 1996). Previous studies have observed that osteocytes that have rounded cell morphology are more mechanosensitive and thereby would favour bone resorption mechanism than elongated osteocytes (Florencio-Silva et al., 2015; Sasaki et al., 2015; van Oers et al., 2015; Wu et al., 2018; Zhang et al., 2020). In this study, the osteocytes on T12 have similar cell elongation to that of T64, which suggest that the osteocytes on T12 will function similar to T64. Furthermore, in terms of osteoblast cell morphology, Uggeri et al. (2010) has observed that elongated osteoblasts on the surface of different titanium alloy substrates promotes bone formation (Subramanian et al., 2012; Uggeri et al., 2010). In this study, T64 substrates osteoblast cells are significantly more elongated compared to CPT and T12, indicating that T64 substrate's osteoblasts will favour greater bone formation activity.

Direct seeding of osteocytes onto T12 showed that the cells were able to adhere and spread with cell morphological features similar to T64. This is an indication that the cells do not respond adversely to the stiffness of the material and by adhering and spreading normally would allow it to enter the next phase of cellular function and response. A series of key osteocyte gene markers including *SOST*, *DMP1*, *PHEX*, *OPG/RANKL* was evaluated to provide an indication of how the cell function on T12. One of the key osteocyte bone marker is the SOST gene which is a negative regulator of bone formation and is primarily responsive to mechanical stimulus (Qin et al., 2013; Spatz et al., 2015). In the case of T12, the osteocyte SOST gene expression was comparable with T64 and is significantly lower than CPT which would suggest that the cell favours bone formation. This result demonstrates the mechanosensitivity of osteocytes to different stiffness material and reinforce the importance of bulk stiffness in cellular response. To support that the osteocytes are in favour of bone formation, the cell OPG/RANKL gene expression ratio was measured and compared. A number of studies have demonstrated that lower levels of OPG gene expression and high levels of RANKL gene expression with a significantly lower OPG/ RANKL ratio resulted in lower bone mineral density (Fadda et al., 2015; Goldring, 2015; Imel et al., 2014; Naylor & Eastell, 2015; Xu et al., 2012; Zimmerman et al., 2018). Zhang et al. (2014) demonstrated titanium implants that were implanted into the rat tibiae and exposed to delayed mechanical loading, lead to an increase OPG/ RANKL ratio which resulted in an increased peri-implant bone density (Zhang et al., 2014). The OPG/ RANKL ratio of osteocytes in T12 suggests once again that the cells are favouring bone formation indicative by the increased OPG/ RANKL ratio compared with CPT. Furthermore, T12 OPG/ RANKL ratio was not significantly different compared with T64 indicating the cells function similarly in regards to bone formation activity. In terms of osteocyte bone mineralization and maturation, DMP1 and PHEX gene expression showed that the osteocytes on T12 were able to express both genes at a comparable level with T64 and CPT. These results overall supports the notion that the osteocytes on T12 can function similar to the other titanium substrates.

Cytokines are small extracellular proteins that are released by cells to initiate a specific interaction or communication between cells (Zhang & An, 2007). The importance of cytokines in bone

tissue is that they function as mediators for cell-to-cell and matrix-to-cell communication. Osteocytes make up over 90% of all bone cells, that resides within the bone matrix, which are involved in regulating bone formation and resorption (Kanaji et al., 2009). Henceforth, in this study, we evaluated osteocytes cellular response on the three different titanium alloy substrates through cytokines in cell culture supernatants, which were determined by the mouse cytokines antibody array membrane.

Upon investigation, we identified a large number of osteocytes' cytokines that were previously shown to have a role in directing the bone remodelling process. Cytokines such as IL-6 and TNFα were both expressed at a comparable levels on all titanium alloy substrates CPT, T64 and T12 in our study, that has been shown to influence osteolysis during elevated levels of both IL-6 and TNFα expression (Cheung et al., 2012; Ru & Wang, 2020). Previous study's findings have also linked both of these cytokines upon their elevated expression with aseptic loosening of medical implants (Goodman et al., 1998; Kanaji et al., 2009). Furthermore, soluble tumour necrosis factor receptor type I (sTNFRI) has been demonstrated to hinder the effects against TNFα apoptosis/biological activity (Selinsky & Howell, 2000; Wei et al., 2001). Due to the sTNFRI cytokine counteract effects on TNFα cytokine levels (Schett et al., 2005), this would suggest that bone remodelling activity, cell viability and proliferation occurs at a similar rate on all titanium alloy substrates CPT, T64 and T12. This is owing to the counterbalance and increased levels of sTNFRI secretion to that of TNFα secretion on T12 when compared to either CPT or T64 substrates.

Furthermore, the anti-inflammatory cytokines IL-4, IL-10 and IL-13 were also observed to be all expressed at a similar levels on CPT, T64 and T12 substrates. These three cytokines have been previously demonstrated to play a role in inhibiting osteoclasts by reducing RANKL production, and conversely increasing OPG gene expression to denote bone formation activity (Frost et al., 1998; Kanaji et al., 2009). Overall, IL-4, IL-10 and IL-13 expression suggest that the osteocytes' cellular response on T12 in terms of bone formation activity, is similar to that of CPT and T64 substrates.

Osteocytes have also been linked with controlling bone vascularisation through the expression of vascular endothelial growth factor (VEGF) cytokine. The upregulation of VEGF by osteocytes have been shown to be directly responsible for angiogenesis (Jilka et al., 2013; Prasadam et al., 2014; Wang

et al., 2007). Wang et al. (2007) study findings have shown that by increasing VEGF expression in knockout mice. The high level of VEGF overexpression led to the development of extremely dense, and heavily vascularized long bones in mice compared to the control group. In this study's findings, the level of VEGF secretion by osteocytes on T12 compared to either CPT or T64 is not significantly different, which could suggest that the bone development would be similarly dense and vascularized on all the tested substrates.

Since osteocytes has direct influence on bone formation and resorption process, our study findings have demonstrated that osteocytes cellular response is similar on all the tested titanium alloy substrates. This in effect would result in similar rate of osseointegration on CPT, T64 and T12 substrates. Collectively, our findings suggest that the osteocytes bone formation activity occurs at a comparable level on all the tested titanium alloy substrates including CPT, T64 and T12.

Osteocytes is a regulator of bone remodelling and so it is important to evaluate the actual bone forming osteoblasts as these would be the cells to be in direct contact with the material in forming bone. Osteoblasts plays a significant role in the bone formation process and is mediated by the response of osteocytes (Bonewald, 2011). This is especially critical in the bone-implant integration as the promotion of osteoblast function will improve bone formation (Gesty-Palmer et al., 2009). One of the key function of osteoblasts in bone mineralization is the production of collagen type 1 (Col1α1) (Saeed & Iqtedar, 2015). Approximately 90% of the bone matrix is made up of collagen, making it the most abundant protein in the body[17]. Coupled together with the RUNX2 expression which acts as a master switch that regulates the proliferation of osteoblast progenitors, allowing osteoblast cells to be committed to its lineage, whilst regulating a host of other bone matrix proteins (Komori, 2019). Similarly, osteocalcin (OC) is also another key osteoblast marker involved in bone mineralization (Cundy et al., 2014; Sista et al., 2013). Shapira et al. (2009) study's findings shows that osteoblasts OC gene expression is not significantly different and is consistently expressed on the tested surfaces of micro-rough Ti-$_6$Al-$_4$V and Ti-$_6$Al-$_7$Nb. In the present study, osteoblasts seeded on T12 showed Col1α1 and RUNX2 expression levels to be at similar levels amongst all the titanium experimental groups which indicates that the cells are able to function and express key bone formation markers. In addition, OPN gene is also involved in

the regulation of bone mineralisation and crystal growth by binding with OC and hydroxyapatite to form a complex with collagen (Barth et al., 1989; Guo et al., 2013). Henceforth, the increased level of OPN gene expression on both T12 and T64 would signify that the osteoblast cells prefer titanium alloy substrates best in terms of bone mineralisation activity than the unalloyed titanium CPT.

The Alkaline phosphatase 1 (ALP-1) protein is a by-product of bone formation and thereby the level of ALP-1 gene expression would signify the activeness of osseointegration (Subramanian et al., 2012). Guo et al. (2013) demonstrated that both titanium alloys (Ti-$_{6}$Al-$_{4}$V and Ti-$_{35}$NB-$_{2}$TA-$_{3}$Zr) showed enhanced ALP-1 gene expression by the osteoblasts compared to the commercially pure titanium surface at each tested time point. Our study's findings confirms the results achieved by Guo et al. (2013) where CPT ALP-1 gene expression is significantly lower than T64, except for T12, signifying greater bone mineralization on the titanium alloy T64 than both CPT and T12. Titanium alloys due to their higher surface energies are able to promote greater osteoblast cell adhesion and thereby enhance osseointegration compared to unalloyed titanium (Guo et al., 2013; Sista et al., 2013). These results taken together demonstrate that the osteoblasts on T12 can function at similar levels as the control groups in terms of osteoblast cells' bone formation activity.

Taken together these results suggest that T12 is able to promote bone formation through osteocytes and osteoblasts function. To date, this is the first reporting of a new class of biomedical titanium alloy produced as a result of machine learning that is able to develop and deliver a new generation of titanium alloy biomaterials for different biological and clinical applications. It should be noted that the machine learning algorithm (βlow) used to develop T12 concurrently generated another 70 alloy composition that possess bone-like stiffness that has yet to be investigated. This study serve as a clear demonstration the convergence of machine learning and biomaterial development and how we can leverage this technology to enhance bone regeneration. The results from this study also demonstrate the potential and importance of bone-like stiffness titanium alloy which would address current limitation of T64. Overall, the T12 titanium alloy is an effective material and holds significant clinical potential in future medical implants.

With the advancement of metal additive manufacturing, T12 can be manufactured with a bone-like porosity and developed into a personalised bone implant. To achieve this, future studies will examine the *in vivo* response of the T12 alloy to determine the clinical osseointegration and improve long-term implant response.

## 3.5 Conclusion

Titanium alloys at different compositions with the same surface topography effects cellular response to its surface both visually in terms of cell morphology and gene expression. Hence, the difference in cell morphology effects gene expression on the different titanium alloy composition surfaces. Out of the 5 genes expression analysed for osteocyte cells, titanium alloy T12 showed similar genes expression to that of the control T64 surface. For osteoblast cells, key bone forming genes such as ALP-1 were upregulated on T64 compared to both CPT and T12. Other genes indicative of bone resorption like SOST and RANKL were downregulated on T12 compared to CPT. In contrast to CPT, those same bone forming genes were significantly downregulated for both osteoblast and osteocytes cells. Therefore, in terms of *in vitro* studies, bone cells prefer the titanium alloy surface of T12 than CPT for optimum osseointegration.

# Chapter 4 - Implant on chip platform for in-vitro fluid shear stress evaluation of biomaterials

# Chapter 4 – Implant on chip platform for in-vitro fluid shear stress evaluation of biomaterials

This chapter will focus on osteocytes response on different titanium alloy composition surfaces while under the conditions of fluid shear stress for 24 hrs using an implant-on-chip device to expose cells to 0.5 dynes/cm$^2$ and 1 dynes/cm$^2$ of shear stress. It will start off with providing some background information of why bone cells like osteocytes require shear stress and how implant-on-chip device will help better understand osteocytes response to titanium alloy substrate in an *in vitro* condition. The background of this study will define the research questions for this study. It will continue onto the experimental methodology used to achieve results on the gene analysis of osteocytes that were exposed to fluid shear stress conditions using the custom-tailored implant-on-chip device. This chapter will then discuss these findings and what these results means in terms of which titanium alloy surface is more favourable to bone cells like osteocytes.

## 4. Introduction

Bone is a living, growing tissue that is composed of highly structured collagen mesh matrix in combination with mineral deposits. The mineral deposits consist of hydroxyapatite while the collagen's organisation plays a critical role in bone elasticity (Pendleton et al., 2020). The combination of collagen and hydroxyapatite thereby, provides bones with strength as well as flexibility, which is enough to withstand stress. Bones are maintained by the co-ordination of three main cell types including osteocytes, osteoblasts and osteoclast cells. Bones, muscles and joints work together to support the framework for mobility as well as to support and protect vital internal organs (Hazenberg et al., 2009). Bones are continuously going through the bone formation and resorption mechanism known as the bone remodelling process during mobility or as required by the body. With that said, bone is a dynamic tissue that is able to constantly adapt to the changing mechanical stress demands (Monteiro et al., 2021).

Osteocytes plays an integral role in regulating bone mechanoadaptation and in adjusting and maintaining bone mass, which has direct influence on both bone forming osteoblasts and bone resorbing

osteoclast cells' functionalities (Thi et al., 2013). Osteocytes make up 95% of all bone cells, whilst 4-6% are osteoblast cells and the remaining 1-2% are osteoclast cells (Javed et al., 2010). Osteoblasts differentiates into osteocyte cells during the bone formation activity where osteoblasts bury itself in the mineral matrix of bone deposits. Osteocytes resides within the lacuna of the mineralised bone matrix, where it starts developing the dendritic processes that extends out into spaces known as canaliculi. Osteocytes are able to utilise its dendritic processes to sense local and systemic environmental changes within the bone to then determine a co-ordinated response through the activation of osteoblast and osteoclast cells activity to help repair and maintain bone structural integrity (Metzger & Narayanan, 2019). Therefore, osteocytes are viewed as the main mechanosensing cells that has the capability to detect mechanical load due to their unique distribution throughout the mineralized bone matrix and their interconnectedness to neighbouring osteocytes as well as osteoblasts via gap junction. Henceforth, once mechanical stimuli are detected by osteocytes, they send signalling molecules to other effector cells (osteoblast and osteoclast) that help regulate bone formation and resorption (You et al., 2008).

Most cells and in particular osteocytes can simultaneously experience biochemical signals and mechanical stimulus that can establish a response and coordinate cellular behaviour by regulating critical signalling pathways (Monteiro et al., 2021). Mechanical force or stimulus in an in-vitro setting can be established through substrate stiffness, topography, compression, stretch or fluid shear stress among many other techniques that can help transduce cell surface mechanosensors to influence specific cellular decisions i.e. proliferation, migration, phenotype and differentiation (Kaarj & Yoon, 2019; Monteiro et al., 2021). These mechanical forces provide signals for morphogenesis in the course of organ development (Varner & Nelson, 2014), wound healing (Rosińczuk et al., 2018) and tissue homeostasis (Barnes et al., 2017) to name a few. Organ-on-a-chip technology has enabled new opportunities to study cell biology by replicating key features of an *in vivo* cellular microenvironment. Generally, it is of upmost importance to characterise mechanical forces in an *in vitro* settings, in order to better understand *in vivo* physiology (Kaarj & Yoon, 2019).

In this study, polydimethylsiloxane (PDMS) based microfluidic cell culture devices were used as they have been proven to be permeable to oxygen (Thomas et al., 2010) and thereby, generating

physiologically relevant oxygen environments. To test the efficacy of PDMS microfluidic cell culture device, osteocytes were used as a bone regulator (Caetano-Lopes et al., 2007) as these cells are recognised to be highly mechanosensitive; henceforth, osteocytes were characterised on titanium alloy T12, which were compared against CPT and T64 substrates. The cells on all three substrates were exposed to 0.5 dynes/cm$^2$ and 1 dynes/cm$^2$ of fluid shear stress for 24 hours using a custom tailored implant-on-chip microfluidic device to study the cellular response to titanium alloy substrates under fluid shear stress conditions. The implant-on-chip microfluidic device had to be custom tailored to accustom the different sizes of the titanium alloy substrates cultured with osteocytes. The two different pressure rates at 0.5 dynes/cm$^2$ and 1 dynes/cm$^2$ were used in this study as osteocytes cellular response varies in accordance to different pressure rates as demonstrated in a previous research findings conducted by Spatz et al. (2015). The 24 hours' FSS run time point for this study was chosen as previous study conducted by Li et al. (2013) indicated that osteocytes under fluid shear stress environment does not proliferate until after 24 hours. This would suggest that osteocytes would require at least 24 hours to adapt to the FSS environment and thereby properly respond to both the FSS as well as to the titanium alloy substrates.

## 4.1 Methodology

### 4.1.1 Production of implant-on-chip

The negative impression of an implant-on-chip mould was designed in a 3D CAD design software called SolidWorks (version 2020) (Massachusetts, USA). The mould was 3D printed using a resin 3D printer called Form 2 from formlabs (Massachusetts, USA). Once the mould was 3D printed, a liquid material of polydimethylsiloxane (PDMS) was poured into the cavity of the mould to help cast out an implant-on-chip. PDMS (Sylgard 184 silicone elastomer base) (element14, USA), was prepared at a ratio of 10:1 with elastomer curing agent (element14, USA). PDMS and the elastomer curing agent were mixed well, poured into the mould and degassed for 20 minutes to remove all the bubbles trapped within the PDMS mixture. The PDMS mould was then stored at 65°C to cure overnight. The cured PDMS implant-on-chip cast was taken out of the mould, where the inlet and outlets were cored with a 1.5 mm biopsy punch. PDMS implant-on-chip was sterilised with 80% ethanol and then followed by 30 minutes of UV sterilisation under the cell culture cabinet prior to placing titanium alloy substrates seeded with osteocytes for fluid shear stress test.

### 4.1.2 OCY454 cell culture and maintenance

Cell culture for osteocyte (OCY454) cells were maintained similar to as described in chapter 3. For all experiments, cells were seeded on individual titanium alloy substrates: CPT, T64 and T12 substrates at a density of $1x10^5$ (OCY454) cells/mL. Cells were incubated at 37 °C with 5% $CO_2$ for 24 hrs prior to experimentation. The experiment was repeated once for each of the three biological replicates.

### 4.1.3 OCY454 fluid shear stress experiment

The flow rate for both 0.5 dynes/$cm^2$ and 1 dynes/$cm^2$ were determined by using the 'flow simulation' tool built in SolidWorks. The liquid for this simulation was set to water in SolidWorks, since both water and cell culture media (MEMα, supplemented with 10% FBS and 1% P/S) has close

to similar viscosity(Michaels et al., 1995). The flow simulation in SolidWorks was able to calculate the 'flow velocity' of the liquid directed from the inlet, over the implant substrate placed in the middle of the chip and through towards the outlet. The flow rate for media to be pumped through the implant-on-chip was determined using the formula: Flow (Q) = flow velocity (V) multiply by the cross sectional area of the measurement location (A).

The flow rate for both 0.5 dynes/cm$^2$ and 1 dynes/cm$^2$ were calculated to be 0.317 mL/min and 0.466 mL/min respectively. The seeded OCY454 on each titanium alloy substrate were placed in the chip where the top cover was sealed tightly using microseal 'B' adhesive sealer (Bio-Rad, USA). Using a NE-4000 programmable 2 channel syringe pump (New Era Pump Systems, USA), with a 10 mL BD syringe (Becton, Dickinson (BD), USA), where 8 mL of cell culture media (MEMα, supplemented with 10% FBS and 1% P/S) was pumped through the inlet towards the outlet and then pulled continuously on repeat for 24 hours at a rate of the mentioned flow rates for each shear stress. Each tested titanium alloy substrate consisted of a static control sample (without applying fluid shear stress) and the other treated group was with the applied fluid shear stress; both set of samples were placed in the 37°C incubator with 5% $CO_2$ for 24 hrs. All experiments were repeated for 3 biological replicates.

### 4.1.4 Digital Droplet PCR

After 24 hours of fluid shear stress for both 0.5 dynes/cm$^2$ and 1 dynes/cm$^2$ applied independently on OCY454 seeded on the titanium alloy substrates CPT, T64 and T12, the RNA was collected and purified using a Qiagen AllPrep DNA/RNA Mini Kit (Cat no.: 80204, QIAGEN, Australia) as per manufacturer's protocol. The same protocol as described in chapter 3 was followed to analyse the osteocyte cells genes using the same 6 set of oligo sequences (5' to 3') that are outlined in table 7 but with the addition of two new genes DKK1 and SMAD1 as outlined in table 11 below.

**4.1.5** Oligo sequences of osteocyte (OCY454) for FSS conditions of 0.5 dynes/cm$^2$ and 1 dynes/cm$^2$.

**Table 11.** Oligo sequence for osteocyte (OCY454) cells.

| Oligo name | Forward or Reverse sequence | Oligo sequence (5' to 3') |
|---|---|---|
| DKK1 | Forward | CTCATCAATTCCAACGCGATCA |
| DKK1 | Reverse | GCCCTCATAGAGAACTCCCG |
| SMAD1 | Forward | GCTTCGTGAAGGGTTGGGG |
| SMAd1 | Reverse | CGGATGAAATAGGATTGTGGGG |

### 4.1.6 Statistical analysis

Statistical analysis was performed using GraphPad Prism 7 (GraphPad Software, CA, USA). All experiments were performed in biological triplicates (n=3). Significance was determined using one-way ANOVA with a Tukey post-hoc analysis. All values are presented as mean ± SEM (standard error of the mean). P values less than 0.05 were considered statistically significant.

## 4.2 Results

### 4.2.1 Fluid dynamics simulation in SolidWorks for Implant-on-chip

We developed and validated a PDMS microfluidic implant-on-chip cell culture system as seen in the schematic diagram in figure 31, to identify the mechanism by which fluid shear stress (FSS) regulates key osteocytes genes including *SOST, DMP1, PHEX, OPG, RANKL, SMAD1 and DKK1* that were characterised on the titanium alloy substrates (CPT, T12 and T64). SolidWorks 3D computer aided design software with the built-in flow simulation has the ability to precisely simulate and predict laminar flow as well as uniform FSS conditions throughout the designed channel within the flow chamber of the chip (Figure 32a and 32b). In this study, we subjected OCY454 cells to FSS conditions in two-dimensional culture conditions of 0.5 dynes/cm$^2$ and 1 dynes/cm$^2$ (Table 12) bi-directionally, while being seeded on titanium alloy substrates for 24 hrs to better understand the cellular response to implant surfaces in an *in vitro* environment by replicating *in vivo* cellular microenvironment. The 24 hrs time point was chosen as previous studies have pointed out that it takes 24 hrs for osteocytes to adapt to their FSS environment (Li et al., 2013).

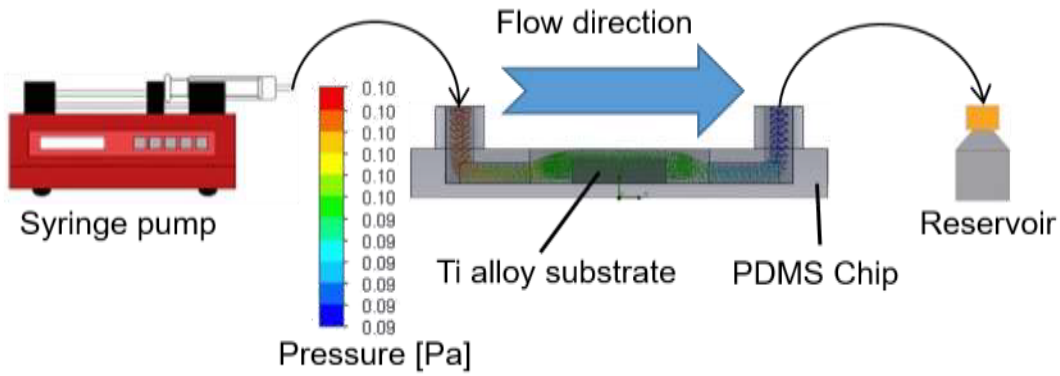


**Figure 31.** Microfluidic implant-on-chip, fluid shear stress stimulation schematic design. A PDMS flow chamber chip enclosed over a titanium alloy substrate and sealed tightly using microseal 'B' adhesive sealer (Bio-Rad, USA). The flow rate is controlled by a 'NE4000 programmable 2 channel syringe pump'.

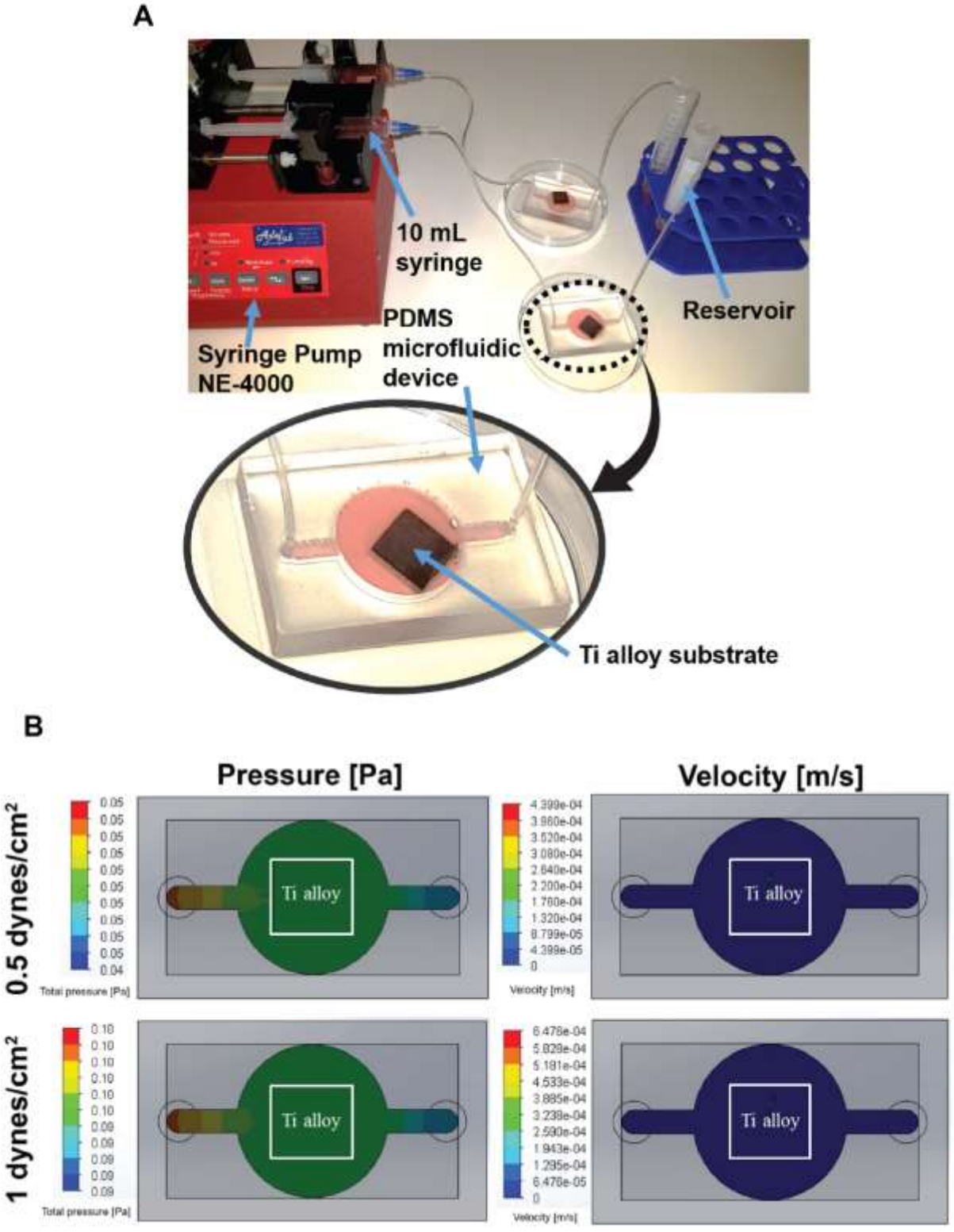


**Figure 32.** Simulation of Implant-on-chip with titanium alloy substrate (CPT, T12 and T64). A. Full assembly of implant-on-chip microfluidic device with the NE-4000 pump for FSS on osteocytes characterised on titanium alloy substrates (CPT, T12 and T64). B. FSS simulation on implant-on-chip modelled and simulated in SolidWorks.

**Table 12.** Fluid dynamic simulation results for Implant-on-chip.

| Fluid shear stress (dynes/cm^2) | Maximum Pressure (Pa) | Maximum Velocity (m/s) | Cross sectional area ($mm^2$) | Flow rate (mL/min) |
|---|---|---|---|---|
| 0.5 | 0.05 | 0.0004399 | 12 | 0.317 |
| 1 | 0.1 | 0.0006476 | 12 | 0.466 |

As seen in Figure 33, osteocyte cells were able to adhere and spread on all the substrates tested following static control and fluid shear stress condition for 24 hours. Under FSS conditions the osteocytes are less confluent compared to their static control counter parts for all the tested substrates, which would signify that under FSS bidirectional flow under both 0.5 dynes/$cm^2$ and 1 dynes/$cm^2$ would be forcing cells to detach from the surfaces of CPT, T64 and T12 titanium alloy substrates. The osteocytes seeded on CPT, T64 and T12 under FFS conditions consisting of osteocytes with rounded morphology compared to their static CTRL counterparts where majority of the osteocytes have elongated morphology (Figure 33). Osteocytes are mechanosensing cells that are able to detect FSS as low as 0.2 dynes/$cm^2$, initiating the release of important messenger molecules such as intracellular calcium, nitric oxide, prostaglandin E2 and adenosine triphosphate resulting in increased osteogenesis and increased osteocyte differentiation (Wang et al., 2019). Previous in vitro studies based on fluid shear stress on osteocytes focused on 0.5 dynes/$cm^2$ and 2 dynes/$cm^2$ (Sato et al., 2020; Spatz et al., 2015). However, the exact physiological FSS still remains unclear (Choi et al., 2022). Henceforth, in this study, 0.5 dynes/$cm^2$ and 1 dynes/$cm^2$ of fluid shear stress was used based on documented parameters.

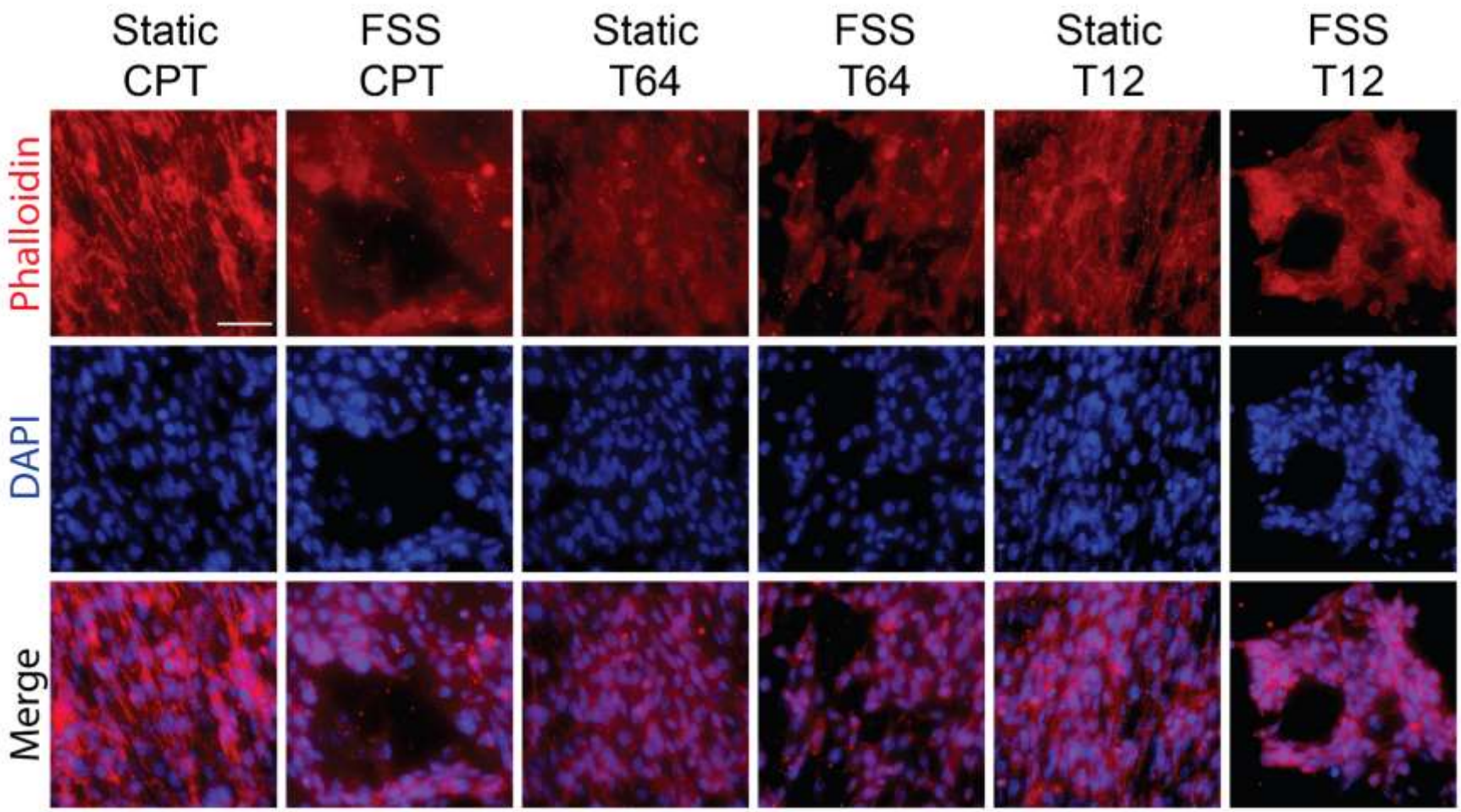


Figure 33**.** A representation of osteocyte cells' adhesion and spreading following 24 hours of culture on the titanium substrates (CPT, T64 and T12) under static control and FSS conditions. Micrographs of osteocyte cells stained with phalloidin (red; first row) to identify the actin cytoskeleton and with DAPI (blue; middle row) to identify the nucleus. The last row shows the merged images. Scale bar = 50 µm.

### 4.2.2 Osteocyte gene expression on T12 under fluid shear stress conditions in comparison to current approved medical implants

To compare osteocytes cellular response in terms of bone formation/resorption capabilities on T12 alloy against current approved medical implants (CPT and T64) under fluid shear stress conditions, key aforementioned osteocyte genes were examined (Figure 34). FSS conditions significantly suppressed SOST, RANKL and DKK1 gene expression at both 0.5 dynes/cm$^2$ and 1 dynes/cm$^2$ on all the tested substrates, for which all these three genes have been known to be negative regulators of bone formation. Similarly, DMP1 gene expression also has a gradual decrease on all the tested substrates, with a significant reduction particularly at 1 dynes/cm$^2$ FSS conditions compared to static control group, which could denote phosphate to be regulated at reduced levels under FSS on all the tested substrates as phosphate is required for proper mineralisation of bone. Statistically there is no significant difference in PHEX gene expression on the tested substrates between FSS and static control groups; suggesting that osteocytes on all the tested substrates for both FSS and static control groups promote bone mineralisation at a similar rate. On the other hand, FSS conditions at 1 dynes/cm$^2$ in particular caused a significant increase in SMAD1, and OPG gene expression that lead to the significant increase in OPG/RANKL gene expression, suggesting FSS conditions at 1 dynes/cm$^2$ leads to bone formation activity on all the tested substrates. These results overall demonstrated that OCY454 cells are intricately responsive to mechanical forces under distinct FSS conditions for genes in particular such as SOST, DMP1, OPG, RANKL, SMAD1, and DKK1.

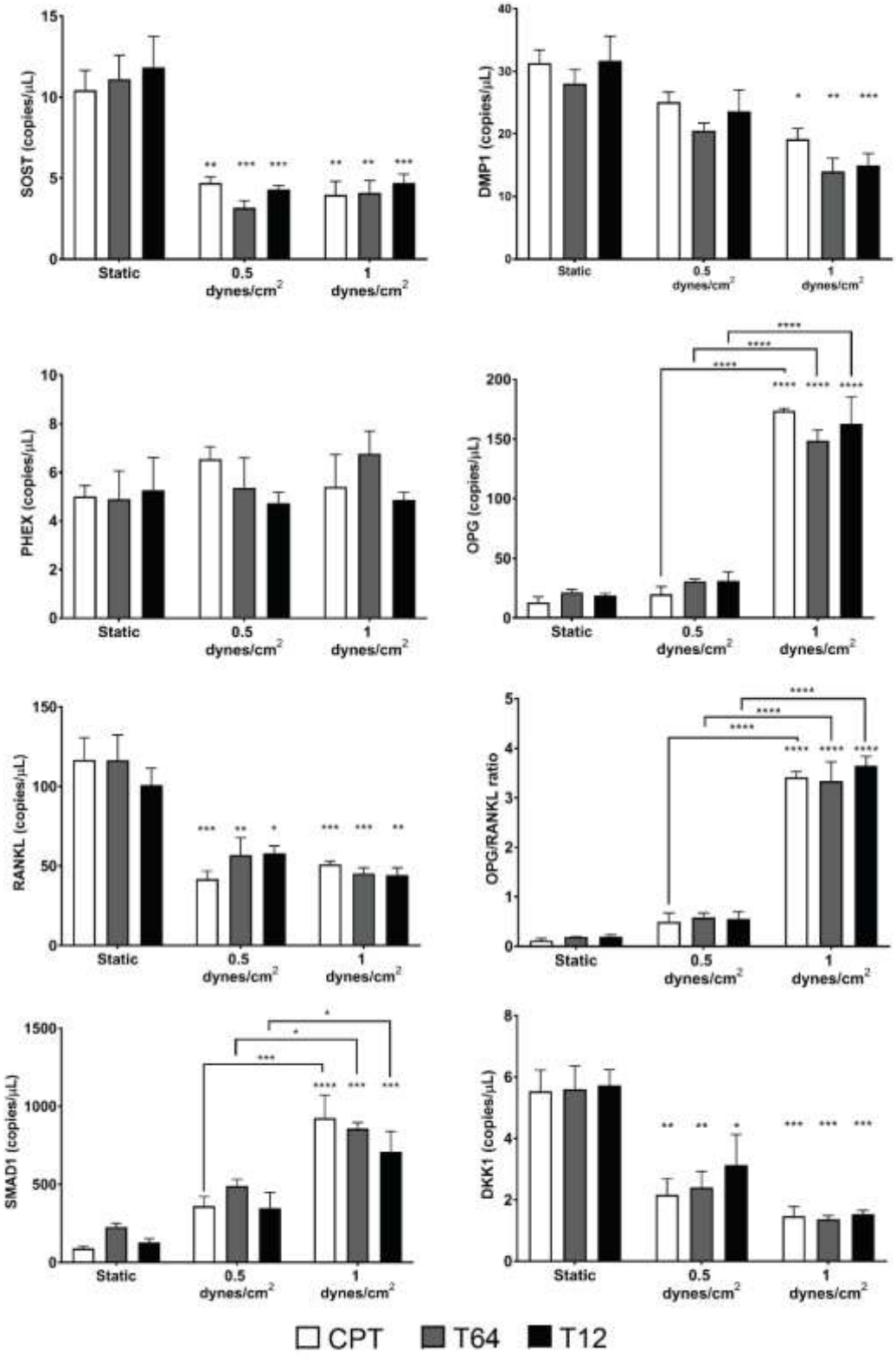


**Figure 34.** OCY454 cultured on titanium alloy substrates (CPT, T64 and T12) under fluid shear stress condition for 24 hours. Comparison of static control, fluid shear stress of 0.5 dynes/cm2 and 1 dynes/cm2 for the OCY454 gene expression (SOST, DMP1, PHEX, OPG, RANKL, OPG/RANKL ratio, SMAD1 and DKK1) cultured on titanium alloy substrates. n = 3 independent biological

replicates. Data is presented as mean ± SEM. Statistical significance was determined using Two-Way ANOVA (with Turkey's post hoc analysis). * $p < 0.05$, ** $p < 0.01$, *** $p < 0.001$, **** $p < 0.0001$.

## 4.3 Discussion

According to previous studies findings, osteocytes (OCY454) can be induced by FSS as low as 0.2 dynes/cm$^2$, which signifies that they play a significant role in the mechanosensing process (Wadhwa et al., 2002; Wood et al., 2017). Other studies have applied between 1-2 dynes/cm$^2$ of FFS, to study the mechanosensing genes and signalling pathways of OCY454 cells (Monteiro et al., 2021; Wood et al., 2017). As such we address how FSS effects osteocytes cellular response to three different titanium alloy substrates (CPT, T64 and T12) by developing our own implant-on-chip microfluidic device to accustom the overall titanium alloy substrate and expose osteocytes to FSS that are characterised on each titanium alloy substrate. In addition to chapter 3, the implant-on-chip microfluidic device will help replicate key features of an *in vivo* cellular microenvironment within an *in vitro* setting. FSS conditions will help provide a better understanding of *in vivo* physiology of how osteocytes respond to T12 substrate and determine the in-vitro biological efficacy under FSS conditions, for the potential use of T12 in bone implant applications.

As specified before in chapter 3, osteocytes are mechanosensing cells that are able to detect mechanical stimuli to then determine a response through the activation of bone forming osteoblast or bone resorbing osteoclast, which is to help repair and maintain bone structural integrity (Metzger & Narayanan, 2019). In this study, osteocytes were seeded at a higher density, which achieved confluent cells on each surface with similar elongated morphology on all tested titanium alloy substrates on both static control group and FSS group, denoting that the cells are able to adhere and spread on all the tested substrates for both static control group and FSS group. Under FSS conditions, some detachment of osteocytes can be observed on all the tested substrates, which could be due to the osteocytes experiencing constant agitation of the back and forth fluid shear stress for a continuous 24 hours' period and could also be caused during the transferring of titanium alloy substrates in and out from the PDMS implant-on-chip chamber.

Direct seeding of osteocytes at high density did allow cells to adhere and spread on all the tested substrates under both static control and FSS conditions; where a series of key osteocytes gene markers including *SOST*, *DMP1*, *PHEX*, *OPG/RANKL, SMAD1, and DKK1*were evaluated to provide an

indication of how the cell function on T12 substrate under FSS conditions. As mentioned in chapter 3, SOST gene is a negative regulator of bone formation and is directly responsive to mechanical stimulus (Qin et al., 2013; Spatz et al., 2015). In this study, SOST gene expression was significantly reduced at both 0.5 dynes/cm$^2$ and 1 dynes/cm$^2$ compared to the static control group on all the tested titanium alloy substrates, which would suggest that under FSS conditions between 0.5-1 dynes/cm$^2$, osteocytes would favour bone formation activity. Previous study's findings conducted by Spatz et al. (2015), demonstrates that SOST gene is suppressed under FSS for OCY454 under low FSS at 0.5 dynes/cm$^2$ to 2 dynes/cm$^2$ as well as under high FSS conditions at 8 dynes/cm$^2$ compared to static control group, which directly complements this study's findings.

DMP1 gene expression is indicative of osteocytes maturation as well as it is critical for proper mineralization of bone and dentin (Dallas et al., 2013). Similarly, PHEX gene expression is also directly involved in phosphate homeostasis and mineralization of bone matrix (Dallas et al., 2013; Shih et al., 2002). In this study, DMP1 gene expression is significantly reduced on all the tested substrates under 1 dynes/cm$^2$ compared to the static control group, indicating higher pressure results in reduced bone mineralization. On the other hand, PHEX gene expression is unaffected by FSS conditions compared to the control group on all the tested substrates, denoting proper mineralization of bone matrix where FSS conditions does not influence the expression of PHEX gene. In a previous study's findings that was conducted by Spatz et al. (2015), demonstrated that under low FSS conditions at 0.5 dynes/cm$^2$ and 2 dynes/cm$^2$, DMP1 gene expression levels were expressed at a consist rate similar to the static control group; but at high FSS conditions at 8 dynes/cm$^2$ resulted in a significant increase in DMP1 gene expression. This overall shows that depending on the amount of pressure applied on osteocytes, the osteocytes' response in terms of bone mineralisation output will also differ.

Furthermore, the mechanosensitivity of osteocytes response to the three different titanium alloy substrates is further demonstrated by OPG and RANKL gene expression. The OPG/RANKL gene expression ratio demonstrates bone formation or bone resorption activity. A number of studies have shown that lower OPG gene expression with high levels of RANKL gene expression that overall resulted in lower OPG/RANKL ratio led to decreased bone mineral density (Fadda et al., 2015;

Goldring, 2015; Imel et al., 2014; Naylor & Eastell, 2015; Xu et al., 2012; Zimmerman et al., 2018). A study conducted by Yan et al. (2018) shows the effects on FSS conditions on OPG/RANKL ratio, whereby FSS conditions at 10 dynes/cm$^2$ suppressed RANKL leading to the increase in OPG/RANKL ratio denoting bone formation activity. Yan et al. (2018) study findings complements this study's findings where FSS conditions both at 0.5 dynes/cm$^2$ and 1 dynes/cm$^2$, suppressed RANKL gene expression on all the tested substrates. Whereas, at 1 dynes/cm$^2$ significantly increased OPG gene expression on all the tested substrates resulting in a significant OPG/RANKL ratio; suggesting bone formation activity takes place under fluid shear stress conditions particularly at 1 dynes/cm$^2$. Spatz et al. (2015) study's findings suggests that RANKL gene expression is suppressed at low shear stress (0.5-2 dynes/cm$^2$) but increased significantly at high shear stress (8 dynes/cm$^2$). Overall these results suggest that the amount of FSS applied on osteocytes significantly deter how osteocytes respond in terms of bone formation and resorption activity.

In addition, SMAD1 is another gene that is involved in bone formation activity, where in a study conducted by Tasca et al. (2018) showed that SMAD1/5 knock out mice increased factors associated with osteoclast activity. Monteiro et al. (2021) showed that SMAD2/3 in OCY454 cells is highly responsive to FSS conditions. There was a significant increase in SMAD2/3 gene expression over time under 1 dynes/cm$^2$ of FSS (Monteiro et al., 2021), which shows that SMAD2/3 gene expression is regulated by shear stress stimulation in osteocytes. In this study, SMAD1 gene expression was significantly upregulated for osteocytes seeded on all the tested substrates under 1 dynes/cm$^2$, denoting bone formation activity and complementing the OPG/RANKL gene expression.

Moreover, the gene expression of DKK1 in osteocytes is known to be a critical negative regulator of Wnt/β-catenin pathway. Numerous *in vivo* studies have demonstrated that DKK1 gene expression was significantly supressed under mechanical loading that led to increased bone mass (Lara-Castillo et al., 2015; Pflanz et al., 2017). In this study, DKK1 gene expression was also significantly supressed under both 0.5 dynes/cm$^2$ and 1 dynes/cm$^2$ FSS conditions, signifying bone formation activity which again complements the results for SOST gene expression as well the OPG/RANKL gene expression ratio.

The study revealed that osteocytes cellular response on all the titanium alloy substrates are directly influenced by FSS stimulation. The results achieved in this study demonstrates that low level of FSS stimulation on bone medical implants might be beneficial as it influences increased bone formation activity. The amount of FSS applied on osteocytes can deter osteocytes response greatly, as demonstrated in this study as well as by Spatz et al. (2015) study's findings where RANKL gene expression is suppressed under low FSS conditions (0.5 dynes/cm$^2$ and 2 dynes/cm$^2$) but under high FSS of 8 dynes/cm$^2$, the RANKL gene expression was significantly increased denoting bone resorption activity. Future studies will need to focus on and examine both low pressure between 1-2 dynes/cm$^2$ and high pressure at 8-10 dynes/cm$^2$ to how osteocytes respond to implant surfaces, which will accurately demonstrate how osteocytes function and respond to implant surfaces by creating an *in vivo* microenvironment in an in-vitro setting. Furthermore, future studies on osteocytes response on medical implant substrates under FSS can be further confirmed by factors derived from osteocyte conditioned medium. The conditioned medium can be implemented in osteoblast and osteoclast either in co-culture models or independent models to see a similar targeted response triggered by osteocytes under FSS conditions. Overall, this study has demonstrated a novel approach in creating a PDMS implant-on-chip that mimics close to the native physiological conditions, where this chip allows for both long 24 hours' duration studies as well as it can be applied for short duration i.e. a couple of hours.

## 4.4 Conclusion

This study revealed that FSS stimulation on osteocytes cultured on three different titanium alloy substrates (CPT, T12, and T64), could improve biological activity by mimicking *in vivo* microenvironment under in-vitro setting using an implant-on-chip FSS device. This allows for better understanding of how bone cells like osteocytes respond to implant surfaces in their native artificial microenvironment. Our study's findings show that FSS (0.5-1 dynes/cm$^2$) rapidly suppresses SOST, RANKL, and DKK1; while promoting the expression of OPG and SMAD1, revealing a novel mechanism by which physical stimulation on osteocytes cultured on varying titanium alloy substrates could potentially lead to increased bone formation activity under low shear stress.

# Chapter 5 - Bacterial adhesion and survivability response on T12 titanium alloy

# Chapter 5 – Bacterial adhesion and survivability response on T12 titanium alloy

This chapter will focus on the bacteria S. *aureus* cells adhesion on the different titanium alloy composition surfaces. It will start off with providing some background information on S. *aureus* bacteria and how such bacteria cause chronic infections during medical implantation procedures. The background will end with defining the research questions for this study. It will continue onto the experimental methodology used to achieve results on the total alive and dead bacterial cell count on each titanium and titanium alloy substrates. This chapter will then discuss these findings and what these results means in terms of which titanium alloy surface is able to inhibit bacterial cells best.

## 5. Introduction

*Staphylococcus aureus* is a facultative, anaerobic, gram-positive bacterium. In humans, it is a member of the normal skin micro-flora as well as the nasal passages. S. *aureus* has a range of complex virulence factors and regulators that provides this bacterium with the ability to transition between commensalism to pathogenic state as it is able to escape from the host immune defences. Furthermore, this pathogen has the ability to overcome and acquire antibiotic resistance traits through various mechanisms that are often poorly understood (Missiakas & Schneewind, 2013). Hence, this is why S. *aureus* is responsible for significant morbidity and mortality worldwide (Grosz et al., 2014).

The infection incidence rate of S. *aureus* bacteraemia (SAB) ranges between 20 to 50 cases out of a population of a 100,000 per year. Approximately 10-30% of these patients die from SAB related infection. In comparison, this accounts for a greater number of deaths than patients dying from AIDS, tuberculosis, and viral hepatitis combined. The mortality age group is consistent within the older population as they are twice as likely to die from SAB infection (Van Hal et al., 2012).

S. *aureus* is known to cause bloodstream, skin and soft tissue infections as well as pneumonia. Currently, there is no vaccine for S. *aureus* infection (Parker, 2018). S. *aureus* is most often transmitted from patient to patient by the contaminated hands of health professionals and doctors (McBryde et al.,

2004). Normally the skin and mucous membranes are an effective barrier against bacterial infections. However, in circumstances where the skin is damaged due to trauma or the mucosal membrane is damaged via viral infection, then in such cases it can give access to S. *aureus* to gain entry into the underlying tissues or the bloodstream and cause infection (Flannagan et al., 2016). Furthermore, people that are immunocompromised or have invasive medical devices are predominantly vulnerable to bacterial infections (Flannagan et al., 2016; S. D. Kobayashi et al., 2015).

A hospital acquired infection, also known as nosocomial infection is where a patient is exposed to an infection within a hospital or a health care facility. Implant nosocomial infection poses significant complications that impacts patients' quality of life, requires long-term administration of antibiotics, multiple operations, and prolonged hospitalisation. The patient is further effected by the prolonged absence from work and the loss of significant income (Holinka et al., 2013). It has been noted that the incidence rate of implant-related infections is increasing with the increase rate of prosthetic joint replacement surgeries. Staphylococci, gram-positive, non-motile and non-spore forming bacteria are amongst the common pathogens involved in nosocomial infections in orthopaedic patients. S. *aureus* being a coagulase-positive is commonly responsible for early-onset infections, while coagulase-negative bacteria like staphylococcus epidermidis causes late-onset infections. Both of these bacteria has the ability to adhere to medical implants and devices that causes chronic infections (Holinka et al., 2013; Tsang & Simpson, 2020).

Titanium and titanium alloys are important biomaterials that are used in majority of medical implants due to their mechanical properties and good biocompatibility (Holinka et al., 2013). In order to inhibit bacterial adhesion and promote osseointegration, antibacterial coating on the implant's surfaces have been implemented, which has shown to be effectively preventing bacterial adhesion onto the implant's surfaces during *in vitro* studies (Barth et al., 1989; Holinka et al., 2013). However, the efficacy of antimicrobial coated medical implants needs to be demonstrated in randomised clinical trial to confirm the effectiveness during long-term implantation (Darouiche, 2003).

S. *aureus* is often linked with post-surgical implant infections. This is mainly due to their strong affinity to adhere to a wide variety of implant materials, which includes stainless steel, titanium, and

titanium alloys. Once bacterial adhesion occurs on to an implant surface, then it is extremely difficult to remove once it has been implanted as subsequent biofilm formation takes place at the implanted region. Bacteria like S. *aureus* forms biofilms on medical implants and devices, which presents major problems. These problems initiates with the bacterial communities within the implanted region provides a reservoir of bacteria that shed into the rest of the patient's body to cause chronic infection (Gu et al., 2016). Biofilm bacteria are highly resistant to antibiotics treatment and are extremely difficult to eliminate with conventional antimicrobial therapies. When both host responses and antibacterial therapies fails to eliminate the bacterial infection that are growing in a biofilm, then a chronic inflammatory response is initiated at the site of the bacterial biofilm infection. Chronic inflammation can linger for months or even years after the bacterial infection has been eliminated where it leaves the patient's body in a constant state of alert. This becomes a problem where the inflammation can become activated even when there is no apparent injury or disease and starts attacking nearby healthy tissues and organs (Barth et al., 1989; Gu et al., 2016; Landskron et al., 2014).

In circumstances where the bacterial adhesion occurs before tissue regeneration takes place, the patient immune defences is usually unable to prevent bacterial colonization for certain bacteria that are capable of forming a protective biofilm layer. Hence, inhibition of bacterial adhesion is vital to prevent implant-associated infection due the fact that biofilms are extremely resistant to both the host's immune system and antibiotics. To overcome this issue, orthopaedic implant's materials needs to be habitable by osteoblast cells (bone forming cells) and at the same time inhibit bacterial adhesion (Ribeiro et al., 2012).

In this study, the microbial test was conducted with S. *aureus* on titanium alloy Ti-12Nb-12Zr-12Sn (T12) against commercialised pure titanium (CPT) and the titanium alloy Ti-6Al-4V (T64). S. *aureus* cellular response on the different titanium alloy samples were examined using the cell viability and cytotoxicity assay for the bacteria live and dead cells on the implant samples' surfaces. The initial adhesion and the overall biofilm development of S. *aureus* was examined over a period of time intervals including at 0 hr, 4 hour and 24 hour time points, using crystal violet staining method.

# 5.1 Methodology

## 5.1.1 Titanium alloy substrates

The titanium and titanium alloy samples tested under this study includes commercially pure titanium (CPT), Ti-6Al-4V (T64), and Ti-12Nb-12Zr-12Sn (T12). The same titanium alloy substrates as described in chapter 2 and 3 are used in this study. This involved culturing Staphylococcus *aureus* cells on the 3 different titanium alloy substrates.

## 5.1.2 *S.* aureus growth and maintenance

Staphylococcus *aureus* (S. *aureus*, ATCC 25923) bacterial strain was used to examine the bacterial growth response on the different titanium alloy composition samples. S. *aureus* was first streaked on a brain heart infusion agar plate, which was incubated at 37 °C for 16-18 hrs. Bacterial tryptone soya broth (TSB) medium was prepared by transferring 2.5 grams of Tryptone Soy Broth (Dehydrated) powder (ThermoFisher Scientific, United States) into 100 mL of distilled water. The TSB medium was autoclaved to sterilize the medium. Three single S. *aureus* colonies were obtained from the brain heart infusion agar plate and were added to three different 30 mL sterile TSB medium flasks for 3 biological replicates. TSB medium with bacteria was grown overnight at 37 °C with orbital shaking at 100 RPM using Shaker (Bioline, Australia). The absorbance reading based on turbidity, was taken using Infinite 200Pro microplate reader (Tecan, Switzerland) from the overnight inoculum at an optical density (OD) 600nm, which were 0.138 nm (blank), and the 3 biological replicates 1.07 nm, 0.98 nm and 0.96 nm. The overnight inoculum was diluted into 1:100 TBS medium and was further grown for 2-hrs at 37 °C with orbital shaking at 100 RPM. Following the 2-hr growth period, the inoculum was again further diluted into 1:100 TSB medium. 2 mL of the TSB medium with S. *aureus* was added to sterile titanium alloy samples (CPT, T12 and T64). All samples were then incubated at 37 °C for 18 hrs. The experiment was repeated in duplicate per each of the three biological replicates.

### 5.1.3 Live/Dead analysis

To determine S. aureus cell viability, the 'Viability/Cytotoxicity Assay for Bacteria Live & Dead cells' (Biotium, California, USA) was used. The staining protocol was conducted following the manufacturer instructions. Briefly, the TSB medium was first removed and all the surfaces were washed twice with a 0.85% NaCl solution (w/v). The bacteria were then co-stained with DMAO (live cells) and EthD-III (dead cells) for 30 mins and then washed twice with 0.85% NaCl solution. Bacterial cells were then fixed with 4% PFA for 30 mins and washed twice with 0.85% NaCl solution to remove residual PFA. All samples were immersed in 0.85% NaCl solution prior to imaging.

### 5.1.4 Crystal violet staining to analyse initial adherence of viable S. *aureus* on T12 alloy

To determine the initial adherence and early stages of biofilm formation of S. *aureus*, the crystal violet assay (Sigma-Aldrich, USA) was used. The staining protocol was conducted following an optimised protocol for S. *aureus* staining set out by Merritt et al. (2011). Briefly, once 2 mL of the TSB medium with S. *aureus* that were seeded on to sterile titanium alloy samples (CPT, T12 and T64) for time points including 0 hr, 4 hrs and 24 hrs. All samples were then incubated at 37 °C for the mentioned time points. The experiment was repeated in duplicate per each of the three biological replicates. After each time point, the titanium alloy substrates were washed twice with 0.85% NaCl solution to help remove all the dead bacterial cells from each substrate and then the bacterial cells on each titanium alloy substrate were then stained with 0.2% crystal violet staining solution for 20 mins. The excess stain was washed twice with NaCl before each titanium alloy substrate was immersed in NaCl solution to be ultra-sonicated at 40 kHz for 5 min at 37°C to help detached all live bacteria. The stained cells were washed and centrifuged twice at 5000 rpm for 5 mins to remove excess stain without disrupting the pallet, which were then air dried for 1-2 hours until no liquid crystal violet remains. The dried crystal violet stained bacterial cells from each of the titanium alloy substrate was solubilised with 125 µL of 30% acetic acid, which were mixed well and incubated at room temperature for 10 mins. 125 µL of the solubilized crystal violet stain was transferred to a new flat bottomed microtiter plate where the absorbance was read at

550 nm using Infinite 200Pro microplate reader where 125 µL of 30% acetic acid was used as a blank to normalise each bacterial stained sample.

### 5.1.5 Microscopy

Bacterial cell images were captured using the Delta Vision Elite Deconvolution Microscope with plate reader using the 40x (UApo/340) objective. The live bacterial cell images were taken using the green florescent (FITC channel) and the dead bacterial cells images were taken using the red florescent (mCherry channel). Cells were imaged using the following settings: LED illumination for FITC was set at emission wavelength 525 nm and excitation wavelength at 475 nm and mCherry was set at emission wavelength 625 nm and excitation wavelength at 578 nm, the pixel size was set to 0.105, 0.105, 1.45. A total of 10 images were acquired at random from each sample to ensure unbiased data collection.

### 5.1.6 Image analysis

All cells images were analysed using FIJI software. To obtain the total live and dead S. *aureus* bacterial cell counts per image, the protocol 'Quantification of Live/Dead Staining Using Fiji Software' set out by BRTI Life Sciences was used for this study.

### 5.1.7 Statistical analysis

Statistical analysis was performed using GraphPad Prism 7 (GraphPad Software, CA, USA). All experiments were performed in biological triplicates (n=3). Again, for bacterial cell count, a total of 10 images were taken at random location from each of the tested substrates per biological replicate. All cells within the full view of the image were accounted for in the statistical analysis. Significance was determined using one-way ANOVA with a Tukey post-hoc analysis. All values are presented as mean ± SEM (standard error of the mean). P values less than 0.05 were considered statistically significant.

## 5.2 Results

### 5.2.1 T12 inhibits Staphylococcus *aureus* adhesion and viability

S. *aureus* is one of the leading bacterial infection that causes titanium implant failures. S. *aureus* is commonly found on the skin and can enter the body during implant surgeries and cause infection. In the present study, S. *aureus* ability to adhere to T12 was investigated. The S. *aureus* attachment on the titanium and the bacteria was stained for live (green) and dead (red) shown in Figure 35. It can be seen that S. *aureus* was able to adhere on all the titanium, but it is clear on T12 there is a significant reduction in the amount of alive and dead bacteria attached compared with the other experimental groups. The percentage of live S. *aureus* demonstrate T12 (38.54% ± 2.018%) to have statistically lower live bacteria as oppose to the other experimental substrates including CPT (49.09% ± 1.144%) and T64 (44.85% ± 1.458%) (Figure 36A) ($P < 0.0001$, one-way ANOVA with Tukey's post hoc analysis). Similarly, the percentage of dead S. *aureus* count on T12 substrate (61.46% ± 2.018%) was significantly higher compared to the other substrates including CPT (50.91% ± 1.144%) and T64 (55.15% ± 1.144%) (Figure 36B) ($P < 0.0001$, one-way ANOVA with Tukey's post hoc analysis). The S. *aureus* fold change on titanium alloy substrates (T64 and T12) was determined against the unalloyed titanium substrate CPT, where T12 (0.6024 ± 0.06961) showed a significantly reduced amount of live S. *aureus* on its surface compared to both CPT (1 ± 0) and T64 (1.316 ± 0.1675) (Figure 36C) ($P < 0.0001$, one-way ANOVA with Tukey's post hoc analysis). Similarly, the S. *aureus* dead cell's fold change on T12 (0.8341 ± 0.06342) was significantly reduced compared to CPT (1 ± 0) and T64 (1.55 ± 0.1899) (Figure 36D) ($P < 0.0001$, one-way ANOVA with Tukey's post hoc analysis). On the other hand, the fold change for both live and dead S. *aureus* cells on T64 substrate were significantly increased compared to CPT and T12 substrates; suggesting that T64 promotes S. *aureus* cells growth, whereas, T12 demonstrate statistically lower S. *aureus* cell attachment compared with the CPT and T64 substrates.

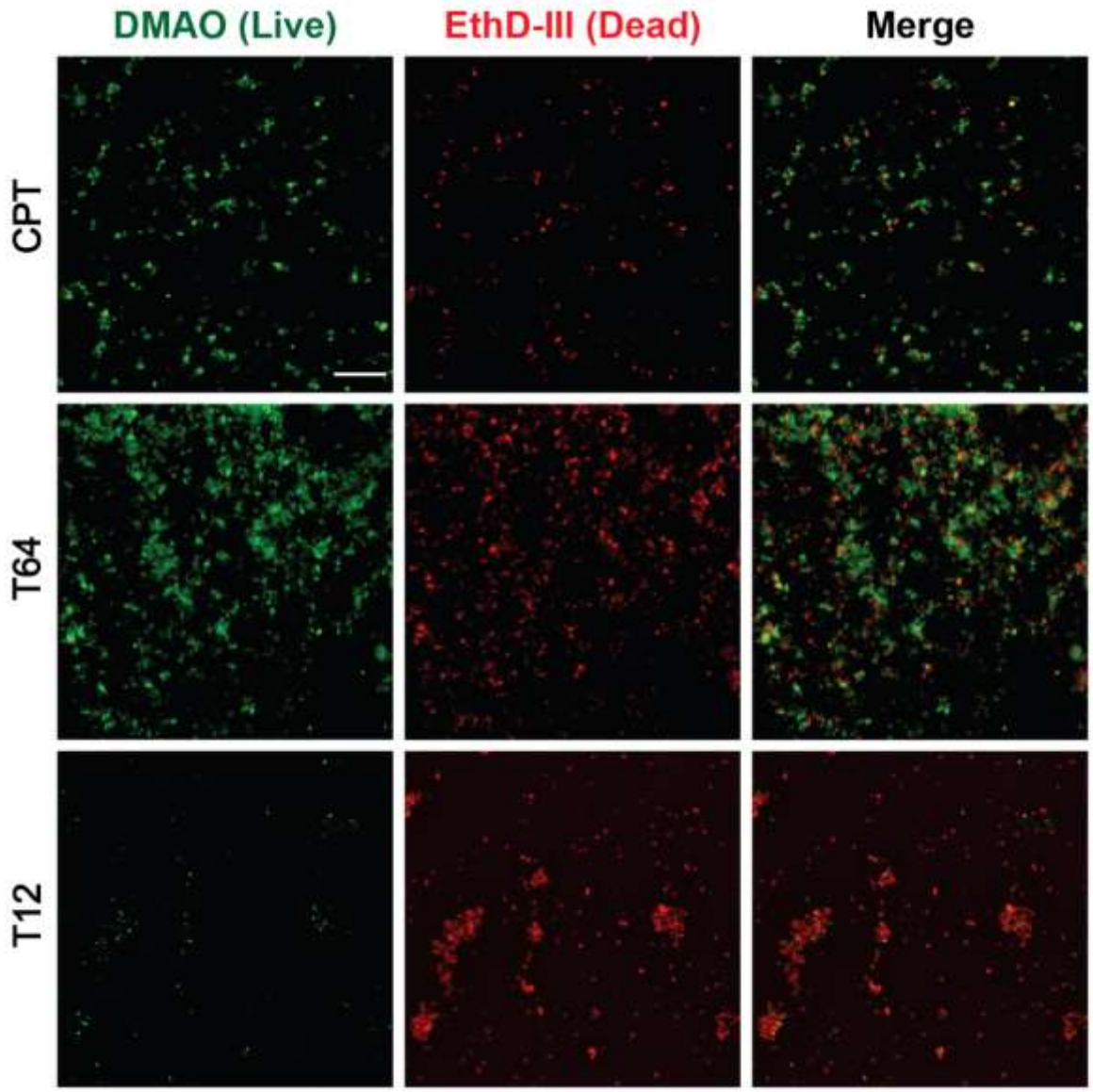


**Figure 35.** Micrographs of S. aureus (ATCC 25923) cells stained with DMAO (Green; first panel) to identify live cells and EthD-III (red; middle panel) to identify dead cells following 18 hours of culture on the titanium substrates (CPT, T64 and T12). The last panel shows the merged images. Scale bar = 25 µm.

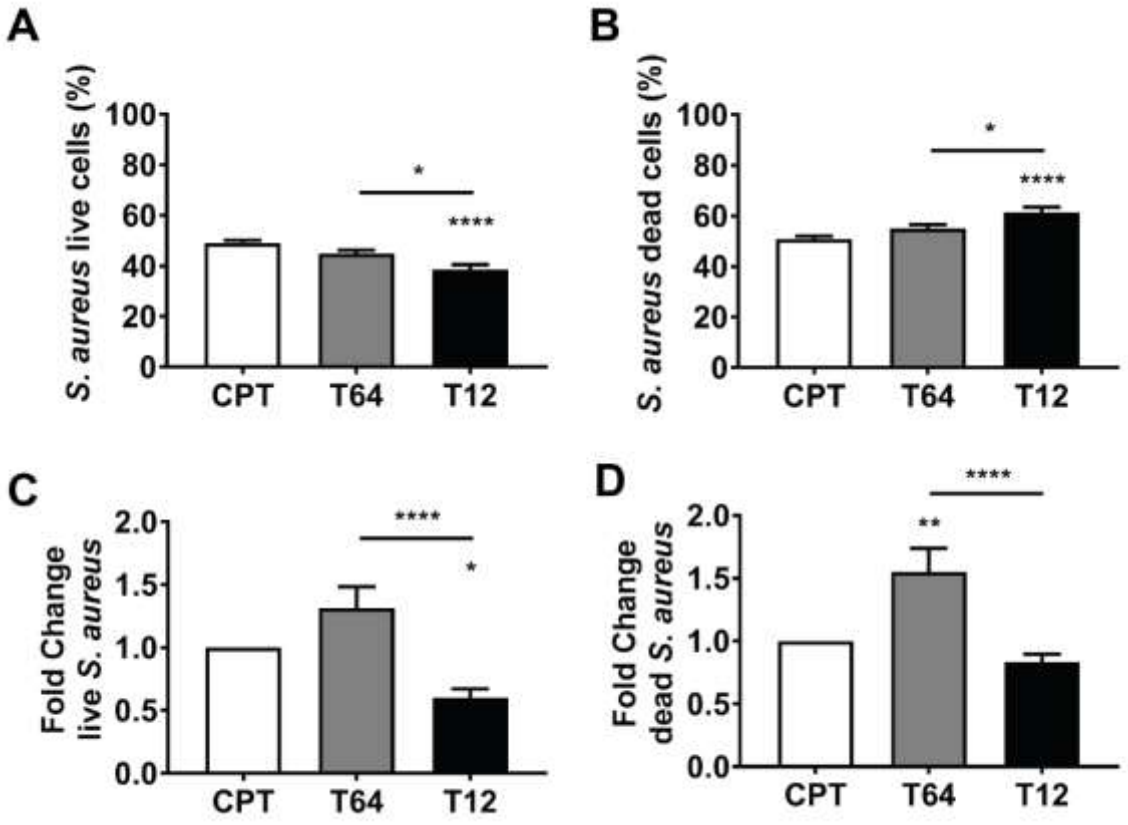


**Figure 36.** Analysis of S. aureus following 18 hours of culture on the titanium substrates (CPT, T64 and T12). **A.** S. aureus percentage live cell analysis on indicated substrates. **B.** S. aureus percentage dead cell analysis on indicated substrates. **C.** S. aureus fold change of live cells on titanium substrates normalised against CPT substrate. **D.** S. aureus fold change of dead cells on titanium substrates normalised against CPT substrate. n = 3 independent biological replicates. Data is presented as mean ± SEM. Statistical significance was determined using One-Way ANOVA (with Turkey's post hoc analysis). * $p < 0.05$, ** $p < 0.01$, **** $p < 0.0001$.

### 5.2.2 S. *aureus* initial adhesion and total biomass is significantly reduced on T12 alloy

S. *aureus* initial adhesion and biofilm development on implant surfaces was investigated in this study based on crystal violet staining. The initial bacterial adhesion after 4 hours was not significantly different (Figure 37A). On the other hand, the overall biomass after 24 hours was significantly reduced on T12 (2.983 Au ± 0.347 Au) and T64 (3.556 Au ± 0.316 Au) compared to CPT (4.794 Au ± 0.132 Au) ($P < 0.0003$, two-way ANOVA with Tukey's post hoc analysis); suggesting S. *aureus* proliferates on CPT a lot faster than both the titanium alloy substrates T12 and T64. Although, statistically there is no significant difference in the fold change as seen in Figure 37B, both T12 and T64 at 24 hours' time point shows the overall biomass on these 2 substrates reduced by 0.608 ± 0.051 and 0.741 ± 0.056 folds respectively.

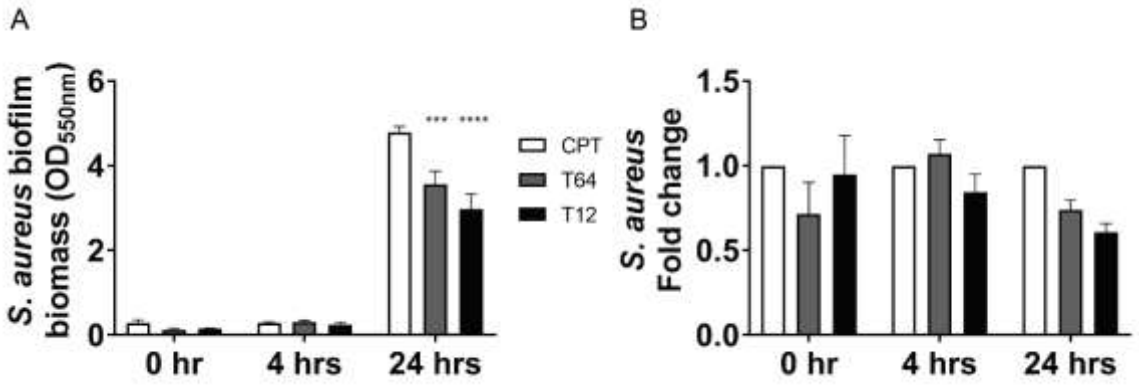


**Figure 37.** Initial bacterial adhesion and biofilm formation of S. aureus cultured on titanium alloy substrates (CPT, T64 and T12) at 0 hour, 4 hours, and 24 hours. **A.** Initial adhesion assay based on crystal violet staining ($OD_{550nm}$). **B.** S. aureus fold change of bacterial adhesion and biofilm formation over time at 0 hour, 4 hours and 24 hours on titanium alloy substrates normalised against CPT substrate. n = 3 independent biological replicates with 3 technical replicates. Data is presented as mean ± SEM. Statistical significance was determined using Two-Way ANOVA (with Turkey's post hoc analysis). *** $p < 0.001$, **** $p < 0.0001$.

## 5.3 Discussion

### 5.3.1 T12 exhibit antibacterial properties

One of the key leading factors in implant failure is the introduction of bacteria including S. *aureus* during implant surgeries. As such, it is important to determine the S. *aureus* response in bacterial adhesion and biofilm formation on T12 surface to examine the material's clinical applicability as a suitable bone implant material. The results showed that approximately 55.15% ± 1.458% of S. *aureus* cells autolysed on T64 indicating the initiation of biofilm formation. Interestingly, T12 which had 61.46 ± 2.018% of S. *aureus* autolysed on its surface after 18 hours, indicating that the S. *aureus* does not favour being on T12 surface compared to T64. Bacterial adhesion of S. *aureus* on T64 have shown in a study by Barth et al. (1989) the importance of the leaching of cations from metal alloys predominantly aluminium and vanadium ions from T64 seem to enhance S. *aureus* cell division and growth, which was also observed in our T64 samples where T12 had a significant 0.6694 ± 0.071 folds decrease of live bacteria that was present compared to T64.

One of the key advantage of the T12 production by AI machine learning development is the ability to insert known ions that possess beneficial properties to the material. The presence of niobium (NB) and Tantalum (Ta) have both been shown to inhibit bacterial cells including S. *aureus* and while not inducing any harmful effects on bone cells such as osteoblast (MC3T3-E1) cells on its surface (Shimabukuro et al., 2019). As demonstrated in the results, the bulk T12 material is shown to induce inhibitory effects on S. *aureus* cell adhesion and proliferation where a significant increase of 61.46 ± 2.018% dead cells was observed. Furthermore, S. *aureus* cell number on T12 substrate significantly decreased by 0.6694 ± 0.071 folds in the number of live cells and 0.7828 ± 0.06693 folds decrease in the number of dead cells compared to T64. This further demonstrates the reduced amount of S. *aureus* cells on the surface of T12 substrate compared to T64, which again alludes to the idea that T12 may have inhibitory effects on S. *aureus* bacterial cell adhesion and proliferation.

In order to examine the cellular behaviour of the pathogen like S. *aureus* on the different titanium alloy substrates including CPT, T64 and T12, crystal violet staining assay was used to determine initial adherence as well as biofilm accumulation amount (Merritt et al., 2011; Xu et al.,

2016). According to the crystal violet assay results, there is no significant difference during initial adherence of S. *aureus* cells on all tested titanium alloy substrates after 4 hours. After 24 hours, the total biomass of S. *aureus* on T12 titanium alloy substrate was significantly reduced compared to CPT, indicating that T12 titanium alloy substrate provides an unfavourable environment to S. *aureus* cellular adhesion, proliferation and growth. Verissimo et al. (2015) findings showed that S. *aureus* adhesion and proliferation was significantly reduced on Ti-35Nb-4Sn titanium alloy substrates compared to Ti-35Nb substrates; which has demonstrated that titanium alloys consisting of Nb and Sn shows promising results in improving medical implants where infections maybe of great concern. Verissimo et al. (2015) findings further complements the results of this study, where our novel titanium alloy T12 substrate uses both Nb and Sn in its composition which has demonstrated an effective response in reducing S. *aureus* proliferation.

One key strategy that has not being fully addressed in titanium based orthopaedic implants is decreasing infection. NB and Sn together has characteristics, which has been confirmed in previous studies findings by Verissimo et al. (2015) as well as in this study that has the ability to decrease bacteria attachment and thereby providing an unfavourable environment that decrease proliferation without the use of antibiotics. Future studies needs to be undertaken to determine the type of forces involved in Ti, Nb and Sn based alloys that influences the inhibition of bacterial functions. By understanding the type of forces involved during bacterial inhibition and proliferation from Nb-Sn based alloys, scientist can harness this mechanism in orthopaedic implants to further optimise antibacterial properties in NB and Sn based titanium alloys.

## 5.4 Conclusion

The titanium alloy substrates can affect bacterial adhesion like S. *aureus*. Titanium alloy CPT and T64 can enhance bacterial adhesion and growth. On the other hand, the titanium alloy T12 shows promising results to be used in medical implants. It has the ability to inhibit/supress the proliferation of bacteria like S. *aureus* as it has the least number of total alive and dead cells on its surface as well as reduced amount of total S. *aureus* biomass.

# Chapter 6 - Effects of geometric implant design on cellular response

# Chapter 6 – Effects of geometric implant design on cellular response

This chapter will focus on bone cells response on different 3D printed porous titanium alloy substrates. It will start off with providing some background information on current bone-implant integration success rate, which will define the research questions for this study. It will continue onto the experimental methodology used to achieve results on cell morphology and gene analysis. This chapter will then discuss these findings and what these results means in terms of which level of relative density of porous titanium alloy substrate is more favourable to bone cells.

## 6. Introduction

In 2014, the Australian healthcare system allocated an $11.8 billion budget to medical implants (*Industry Statistics - MTAA*, 2014). A significant proportion was attributed to bone fractures, as fractures are most common amongst the elderly population (28% of fractures occur in people over the age of 55) (CIA, 2018). This causes a significant socio-economic burden on patients and on the healthcare system. There is a need for innovative solutions in order to increase the efficiency and recovery of patients with medical bone implants. To achieve this, there is a requirement for better and improved osseointegration - the bonding between the implant and the surrounding bone tissue. The current challenge is that every patient is anatomically different and therefore recovery can substantially differ amongst the population. With the introduction of 3D metallic printing, personalized and optimised 3D printed implants allow for optimised fit and efficient recovery times. This project will focus on the development of personalized 3D printed bone implants in the hope of developing a paradigm for clinical translation of this promising technology in medical implant manufacturing.

Osseointegration failure can occur due to a number of factors that often result in the loosening of the implant. This includes low biocompatibility, poor surface composition and design of implants, bone quality, surgical technique, loading conditions and insufficient bone turnover (Apostu et al., 2018). Although lifespan for cementless titanium implants stands at 85% for a period of 10 years and decreases

to 70% at 15 years, the main concern for medical implants is aseptic loosening. As addressed previously in chapter 3 about the high stiffness of currently approved medical implants to that of bone, where stress shielding effect occurs due to the mismatch of implant's stiffness to that of bone; that leads to aseptic loosening of medical implant due to the increased bone resorption activity and bone cell death eventually causing implant failure (Oldani & Dominguez, 2012; Tan et al., 2019). Apart from decreasing the high stiffness by changing titanium alloy composition, another way to decrease the high stiffness is by reducing the relative density of medical implants that can be applied to current approved titanium alloys. By implementing porosity directly into the overall structure of medical implant design, it allows for the reduction of relative density of medical implants and thereby reducing the stiffness to overcome the stress shielding effect (Alloyed, 2021). An implant failing can then lead to revision surgery. This horrific complication produces pain and instability for the patient due to aggravated activity and the application of weight on to the loosened implant (Apostu et al., 2018). This impacts society through the loss of productivity, cost of treatment, and the physical rehabilitation of patients (Singaram & Naidoo, 2019).

The biological response to the titanium implant can be improved by applying various surface modification techniques as the tissue response to medical implants are influenced by the physicochemical properties of the implant's surface (Elias et al., 2008). 3D printing technology has the capability to fully control the 3D modelling features at a nano-level to help replicate the natural cellular environment that can influence and regulate molecular behaviour at a nanoscale level. Majority of the inorganic component of bone is hydroxyapatite, measured to be between 2 to 5nm in width and around 50 nm in length. The major organic component of bone is collagen I, measured to be around 300 nm in length and 0.5 nm in width. The surface roughness of natural bone ranges between 25-32 nm. This implies that the natural bone surface roughness holds nanometric features. This can be overcome by nanophase titanium surface roughness using 3D printing technology, to help replicate the surface roughness of bone (Rodriguez y Baena et al., 2017).

Moreover, research findings have shown that structural design, surface microstructural topography, surface chemistry or surface energy/wettability can affect the biological response, cell

behaviour, cell adhesion, cell proliferation and cell migration (Feller et al., 2015). These factors need constant regulation and optimisation for optimum bone-implant integration (Boyan et al., 2016). All adherent cells prefer micro to nano-rough topography. The conventional approach to fabrication of implants is done through traditional manufacturing methods utilising a top-down approach. Through this approach, the surface topographies are evaluated after the medical implant design is created. Therefore, the surface features cannot be customised or controlled as its fully depended on the synthesis process. Traditionally manufacturing medical implants have still not been fully evaluated in the direction towards finding out which type of surface topography and design is most optimal for host tissue-implant integration.

In this study, titanium alloy Ti-6Al-4V (T64) medical implant substrates are 3D printed at various level of porosity using a bottom-up approach with a Selective Laser Sintering (SLS) printer (supplied by Betatype Ltd, London, United Kingdom). This study investigates a novel approach into evaluating the cellular response of osteoblast (MC3T3-E1) and osteocyte (OCY454) cells on porous implant substrates, which will suggest the type of surface topography and porosity necessary for optimal osseointegration. The primary goal of this study is to propose another solution to the stress shielding effect as explained in chapter 3, which leads to aseptic loosening of medical implants. By reducing the stiffness of current approved medical implants through the application of porous designs on implant substrates similar to the stiffness of bone, which in theory will overcome the stress shielding effect and help promote long term bone-implant integration. The objective of this study is to design and fabricate different porous medical implants substrates based on previous studies and AI machine learning data, where cellular response from bone cells such as osteoblasts and osteocyte cells to the various porous titanium alloy substrates will help show the type of surface topography and porosity that bone cells prefer best.

# 6.1 Methodology

## 6.1.1 Porous titanium alloy substrates

The titanium alloy substrates tested in this project includes titanium alloy Ti-6Al-4V (T64) 'sandblasted with large-grit and acid-etched' (SLA) substrate (straumann, Switzerland), and the 3D printed porous titanium alloy substrates all made out of T64, which involved the following level of porosity in the form of percentage relative density (RD): 29%, 40%, 3.10%, 3.59%, 4.6%, 6.28%, 8.8%, 13.38%, core 1, core 2 and Gyroid (Betatype Ltd, United Kingdom). SLA surface implants are commercially approved process that are used in most orthopaedic implants. This involves sandblasting large-grit on to the surface of the implant and then it is followed by a cleaning process called acid etching to remove the remaining particles on the surface that had been left over during the sandblasting process. This process overall creates macro and micro rough surfaces(Park et al., 2018; Roehling et al., 2015).

In this study, the test group will involve titanium alloy Ti-6Al-4V (T64) medical implant substrates that are 3D printed at the listed level of porosity in the form of %RD where the substrates were 3D printed using the bottom-up approach with Selective Laser Sintering (SLS) 3D printer. The porous substrates were designed through AI machine learning which were both designed and supplied by Betatype Ltd, London, United Kingdom. Furthermore, SLA substrates will be used as a control substrate, which were manufactured and supplied by straumann, Switzerland.

## 6.1.2 Characterization of porous titanium alloys

Scanning Electron Microscope (SEM) was used to examine the surface topography of each of the porous titanium alloy substrates: SLA, porous substrates with a RD of 29% and 40%. Prior to imaging, the titanium alloy substrates were mounted on to carbon adhesive discs/tabs (ProSciTech, Australia). Each substrate was examined using the Zeiss SUPRA 55-VP SEM (Carl Zeiss, Germany). Images of low magnification at 100x and a high magnification at 1000x were taken from each substrate.

### 6.1.3 Cell culture and maintenance

Cell culture for both osteoblasts (MC3T3-E1) and osteocyte (OCY454) cells were maintained similar to as described in chapter 3. For all experiments, cells were seeded on individual porous titanium alloy substrates: SLA, RD of 29% and RD of 40% substrates, at a density of $1x10^5$ OCY454 and $1x10^5$ MC3T3-E1 cells/mL. Cells were incubated at 37 °C with 5% $CO_2$ for 48 hrs prior to experimentation. The experiment was repeated in triplicate.

### 6.1.4 Immunostaining

The immunostaining of MC3T3-E1 and OCY454 cells that were independently cultured on SLA, RD of 29% and RD of 40% porosity titanium alloy substrates, where after 48 hrs of cell culture, the cells were fixed and then stained. The procedure for immunostaining were followed exactly as described in chapter 3.

### 6.1.5 Microscopy

MC3T3-E1 and OCY454 cells' images were captured using the DeltaVision Elite Deconvolution Microscope equipped with the 40x (UApo/340) objective lens. Following exactly the same procedure as described in chapter 3. Again a total of 10 images were acquired at random from each substrate to ensure unbiased data collection.

### 6.1.6 Image analysis

All cells images were analysed using FIJI software. The cell morphology was evaluated following the exact same protocol procedures as described in chapter 3 to obtain data for area, circularity, aspect ratio and solidity for the titanium alloy substrates: SLA, RD of 29% and RD of 40%.

### 6.1.7 Digital Droplet PCR

After 48 hours of cell culture on the 3 different substrates (SLA, RD of 29% substrate and RD of 40% substrate), the RNA was collected and purified using a Qiagen AllPrep DNA/RNA Mini Kit (Cat no.: 80204, QIAGEN, Australia) as per manufacturer's instructions. The same protocol as described in chapter 3 was followed to analyse the osteoblasts and osteocyte cells genes using the same 6 set of oligo sequences (5' to 3') that are outlined in tables 7 and 8.

### 6.1.8 Designing bone-like medical implants based on 3D Voronoi lattice structure

A dental implant screw shape was designed in Solidworks 2020 (Massachusetts, USA). The 3D Voronoi lattice structure to create a porous dental implant was designed in a CAD software called Rhinoceros version 6 with the Grasshopper bundle (Washington, USA). Grasshopper is a visual programming language that runs alongside the 3D modelling Rhinoceros 6 application. The finalised bone-like Voronoi structured dental implant design was exported as a stl file for metal 3D printing using Selective Laser Sintering (SLS) printer.

### 6.1.9 Statistical analysis

Statistical analysis was performed using GraphPad Prism 7 (GraphPad Software, CA, USA). All experiments were performed in biological triplicates (n=3). Significance was determined using one-way ANOVA with a Tukey post-hoc analysis. All values are presented as mean ± SEM (standard error of the mean). P values less than 0.05 were considered statistically significant.

## 6.2 Results

### 6.2.1 Surface topography and relative density of porous 3D printed titanium alloy substrates

In this study we examined porous Ti-6Al-4V 3D printed substrates that were 3D printed and supplied by Betatype Ltd, United Kingdom, for potential use in medical implant, with the following % RD: 29%, 40%, 3.10%, 3.59%, 4.6%, 6.28%, 8.8%, 13.38% as well as other style of patterning 3D printed structure such as Core 1, Core 2 and Gyroid as seen in Figure 38. This overall demonstrates the fine accuracy and detail structures that can be 3D printed using the titanium alloy composition of Ti-6Al-4V, which is an already approved medical titanium alloy. During in-vitro studies, from the listed porous titanium alloy substrates, only RD of 29% and RD of 40% were good candidates for osteocytes and osteoblast cells to successfully adhere and spread on the compact porous surface compared to all the other substrates.

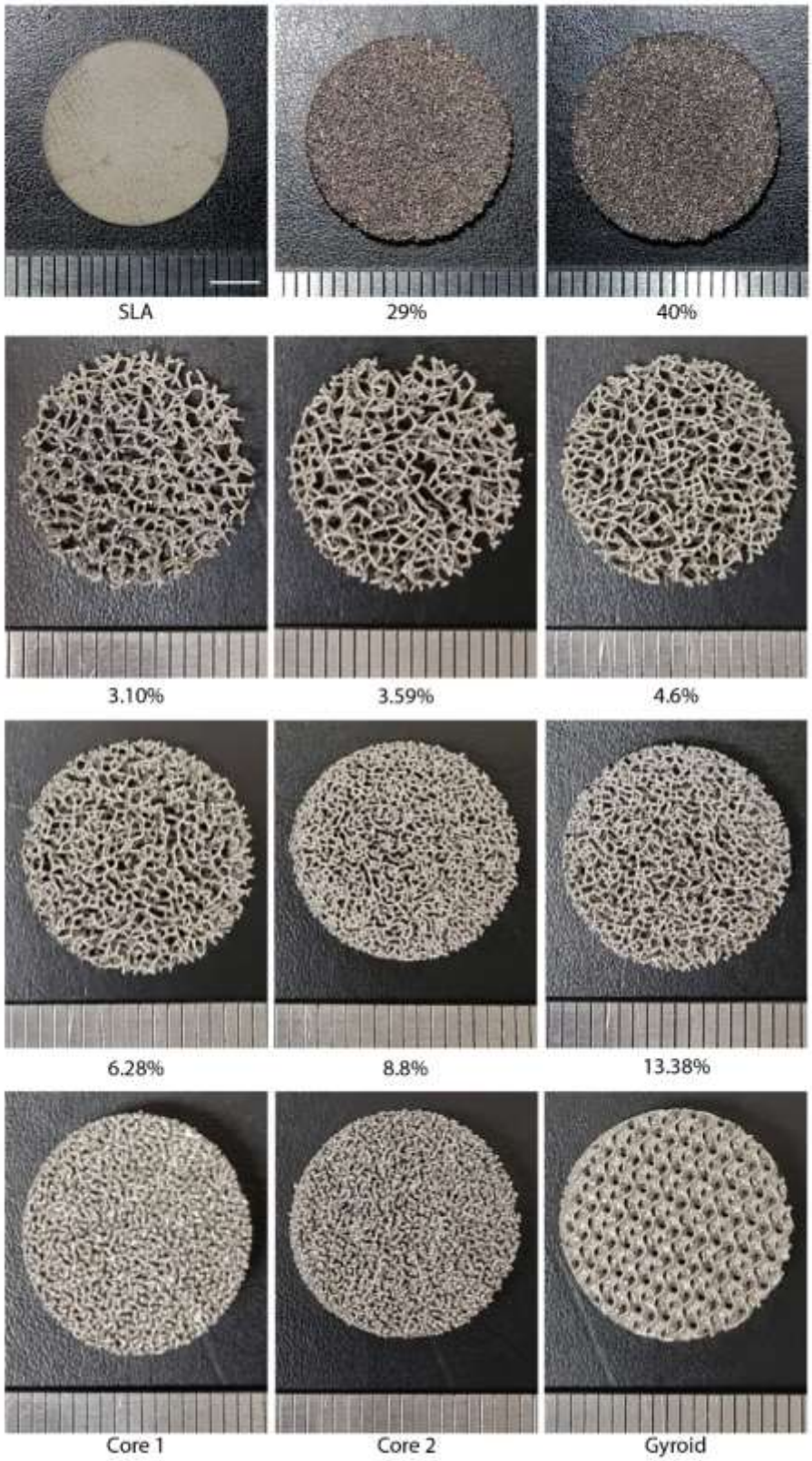


**Figure 38.** Surface topography of the overall porous titanium alloy substrates examined in this project: SLA, RD of 29%, RD of 40%, RD of 3.10%, RD of 3.59%, RD of 4.6%, RD of 6.28%, RD of

8.8%, 13.38%, Core 1, Core 2 and Gyroid, Images of porous titanium alloy substrates (scale bar = 4 mm).

Henceforth, the porous samples cellular response was compared against the control sample 'sandblasted with large-grit and acid-etched' (SLA) that was supplied by Straumann, Switzerland. SEM images of the porous titanium alloy substrates SLA, RD of 29% and RD of 40% for both low magnification (100x) and high magnification (1000x) are presented in figure 39 with their respective photographs; to show the micro-rough and porous topography of the three porous titanium alloy substrates, which overall possess very rough surfaces.

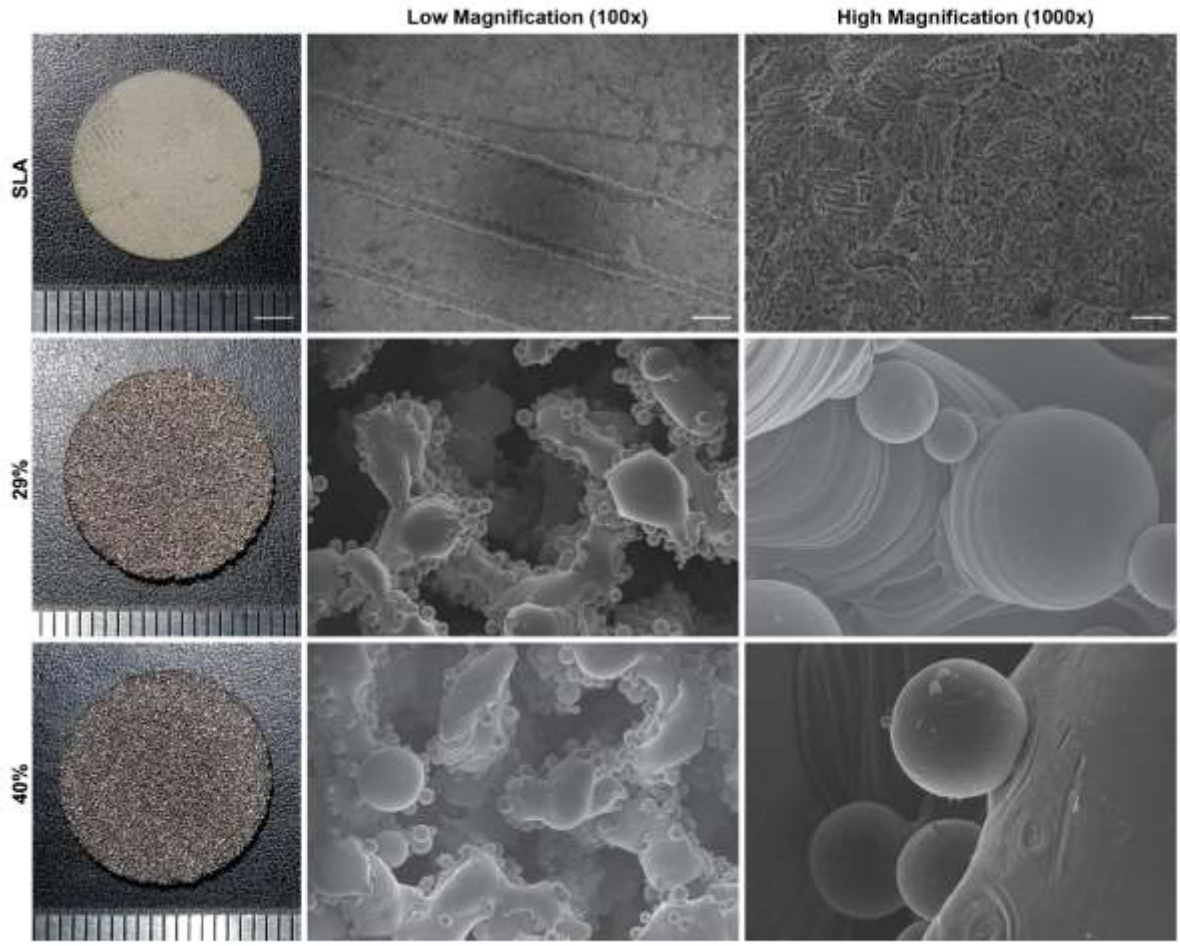


**Figure 39.** Surface topography of porous titanium alloy substrates: SLA, RD of 29% and RD of 40% porous titanium alloy substrates. Images of porous titanium alloy substrates (scale bar = 3 mm). Scanning electron microscope (SEM) images showing surface topography and porosity of porous Ti-6Al-4V substrates SLA, 29% and 40% at low magnification (100X) (Scale bar = 100 μm) and high magnification (1000X) (Scale bar = 10 μm).

### 6.2.2 OCY454 cells adhesion and cellular characteristics on RD of 29% and 40% porous substrates comparable to SLA

Considering recent evidence that suggest different surface topography effects all adherent type cell's morphology (Mangano et al., 2010; Rodriguez y Baena et al., 2017); and since osteocyte cells are master regulators of both bone remodelling and regeneration, they were seeded on titanium alloy samples with different level of porosity. Only SLA, RD of 29% and RD of 40% porous 3D printed titanium alloy substrates, were successful in acquiring cells to adhere and spread on these surfaces as seen in figure 40A, that were used to determine cell morphology and gene expression of osteocytes cellular response to the different level of porous titanium alloy substrates.

Following 48 hours of osteocytes culture on the different porous titanium alloy substrates, osteocytes were found to adhere and spread on all the three substrates tested (Figure 40A). Upon observation as depicted in figure 40A, osteocytes during cell spreading covers similar area per cell, as well as on all the three tested substrates consists of a mixture of both round to elongated cells. On the other hand, cell morphological analysis revealed that both RD of 29% (332.4 μm ± 19.28 μm) and RD of 40% (307.4 μm ± 20 μm) porous substrates had a significant increase in cell area when compared to SLA (244.1 μm ± 13.71 μm) ($p < 0.0351$; one-way ANOVA with Tukey's post Hoc analysis) (Figure 40B); suggesting slower osteocyte cell migration occurs on the RD surface of 29% and 40% porous substrates compared to SLA(Refaaq et al., 2020). Circularity refers to cells that are circular to irregular in shape where the cells' actin cytoskeleton shape are branched out in multiple direction during cell spreading and migration, although it can't define cells that are elongated to irregular shaped cells(Walters et al., 2017). With that said, there was a significant increase in circular circularity that was analysed on RD of 40% (0.7126 ± 0.01725) porous substrate compared to both SLA (0.6098 ± 0.01977) and RD of 29% (0.5831 ± 0.01831) porous substrates, ($p < 0.0001$; one-way ANOVA with Tukey's post Hoc analysis) (Figure 40C); the low circularity on both SLA and RD of 29% substrate could indicate greater osteocytes cell spreading(Walters et al., 2017) compared to the osteocytes on RD of 40% substrate. The aspect ratio defines the general shape of the cell in terms of elongation, whereas solidity examines the cell's actin cytoskeleton protrusion during cell spreading and migration(Krause

& Gautreau, 2014). The aspect ratio of the osteocytes seeded on RD of 29% porous substrate (2.628 ± 0.1378) is significantly increased compared to both SLA (2.136 ± 0.1329) and RD of 40% porous substrates (1.963 ± 0.08443, $p < 0.0003$; one-way ANOVA with Tukey's post Hoc analysis) (Figure 40D). On the other hand, the solidity of osteocytes on RD of 40% porous substrate (0.9317 ± 0.008529) is significantly increased compared to both SLA (0.8537 ± 0.01306) and RD of 29% porous substrates (0.8707 ± 0.01195, $p < 0.0001$; one-way ANOVA with Tukey's post Hoc analysis) (Figure 40E); suggesting that osteocytes undergo slower migration on RD of 40% porous substrate due to cells' actin cytoskeleton being more circular or branched out and protruding in multiple direction(Krause & Gautreau, 2014). Whereas, the osteocytes actin cytoskeleton on RD of 29% porous substrate would signify faster migration, which results from cells that are typically elongated(Krause & Gautreau, 2014). Overall, the osteocytes cellular response to that of different level of porous titanium alloy substrates did alter cell morphology.

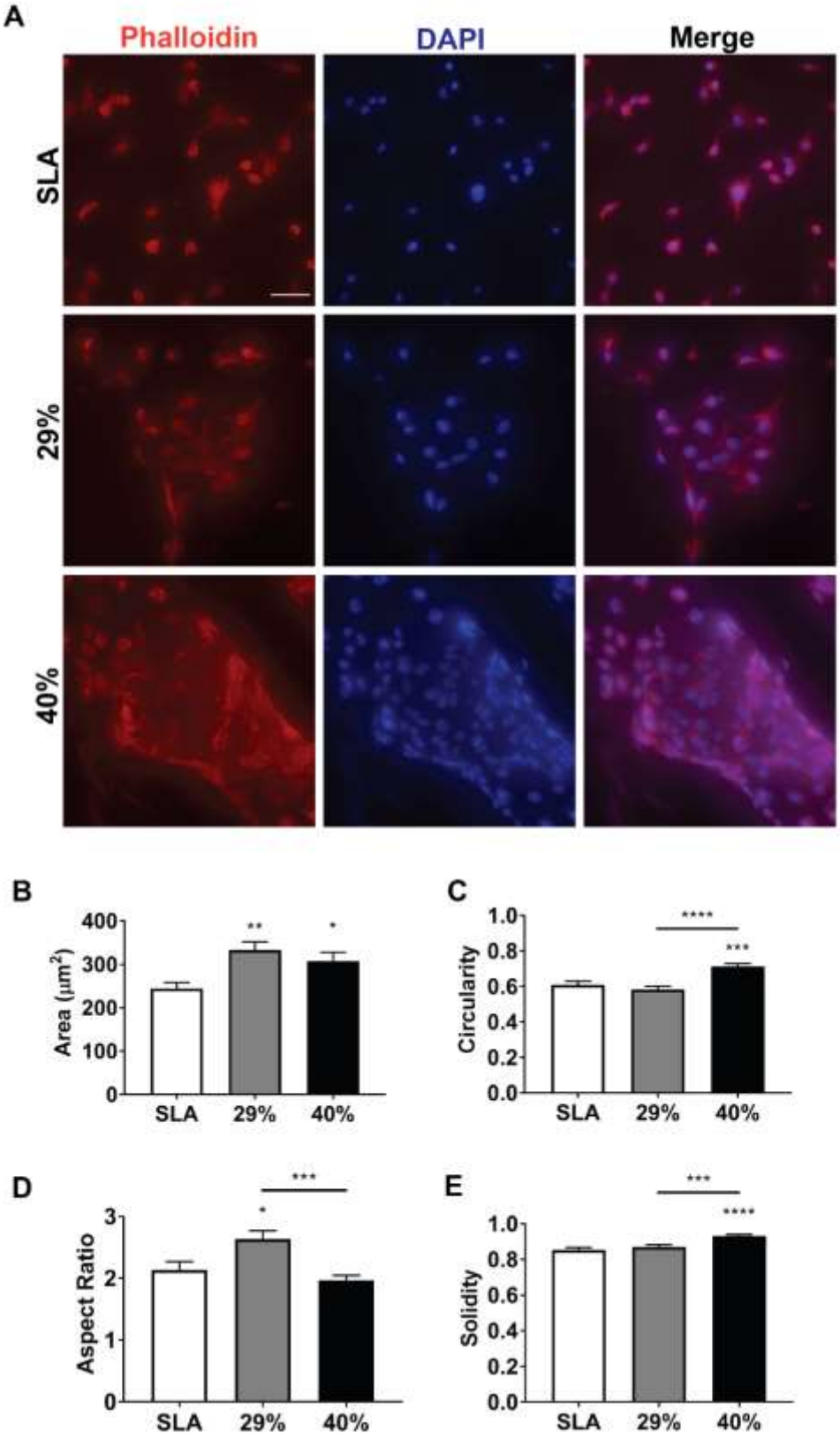


**Figure 40.** Analysis of OCY454 cells following 48 hours of culture on the porous titanium alloy substrates (SLA, RD of 29% and RD of 40% porous titanium alloy substrates). **A.** Micrographs of

OCY454 cells stained with phalloidin (red; first panel) to identify the actin cytoskeleton and with DAPI (blue; middle panel) to identify the nucleus. The last panel shows the merged images. Scale bar = 50 µm. **B.** Area of OCY454 cells cultured on indicated substrates. **C.** Circularity of OCY454 cells cultured on indicated substrates. **D.** Aspect ratio of OCY454 cells cultured on indicated substrates. **E.** Solidity of OCY454 cells cultured on indicated substrates. n = 3 independent biological replicates. Data is presented as mean ± SEM. Statistical significance was determined using One-Way ANOVA (with Turkey's post hoc analysis). * $p < 0.05$, ** $p < 0.01$, *** $p < 0.001$, **** $p < 0.0001$.

### 6.2.3 Osteocyte gene expression on RD of 29% and RD of 40% porous titanium alloy substrate in comparison to SLA

To compare osteocytes cellular response in terms of bone formation/resorption capabilities on RD of 29% and RD of 40% porous titanium alloy substrates against current approved technique SLA titanium alloy substrate, key osteocyte genes including SOST, DMP1, PHEX, OPG and RANKL were examined (Figure 41). Osteocytes cultured on RD of 29% substrate (27.6 ± 3.483 copies/µL) had a significant increase in SOST gene expression compared to RD of 40% substrate (7.067 ± 1.965 copies/µL) $p < 0.0047$; one-way ANOVA with Tukey's post Hoc analysis). Whereas, RD of 40% substrate had a significantly reduced SOST gene expression compared to both SLA (19.93 ± 2.392 copies/µL) and RD of 29% substrates; suggesting osteocytes favour bone formation over resorption on 40% porous substrate compared to both SLA and RD of 29% substrates as SOST is known to be a negative regulator of bone formation (Qin et al., 2013; Spatz et al., 2015). Furthermore, there was no significant difference in osteocytes DMP1 and PHEX gene expression on all the porous titanium alloy substrates tested, suggesting that phosphate which is required for proper mineralisation of bone is regulated at a constant rate by the osteocytes on all the porous titanium alloy substrates (Dallas et al., 2013; Econs et al., 1994). There was also no significant difference in OPG gene expression, which is an indicator for bone formation, on all the tested porous titanium alloy substrates. On the other hand, RANKL gene expression (indicator for bone resorption) was significantly downregulated on SLA substrate (23.3 ± 3.436 copies/µL) compared to both RD of 29% (74 ± 13.05 copies/µL) and RD of 40% (79 ± 9.504 copies/µL) substrates, indicating SLA substrate to promote bone formation mechanism. The OPG/ RANKL expression which indicates the balance between bone formation and resorption show a significantly reduced ratio by osteocytes on RD of 29% (0.9005 ± 0.2053) and RD of 40% substrate

(0.9239 ± 0.07019) compared to SLA (3.694 ± 0.789, $p < 0.0088$), which is indicative of SLA favouring greater bone formation activity than both RD of 29% and RD of 40% substrates.

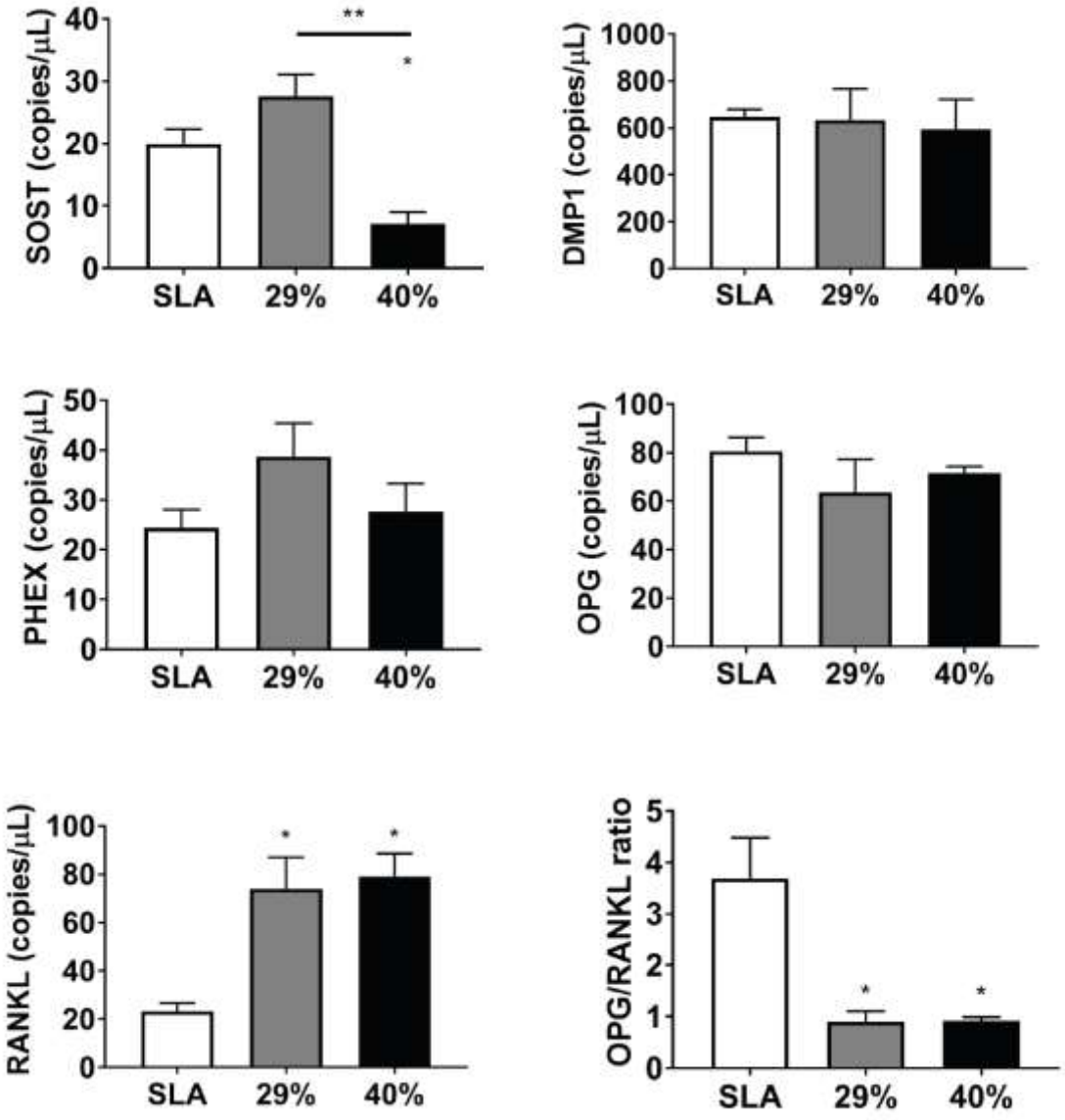


**Figure 41.** Indicated gene expression levels of OCY454 cells cultured on indicated substrates analysed following ddPCR. n = 3 independent biological replicates. Data is presented as mean ± SEM. Statistical significance was determined using One-Way ANOVA (with Turkey's post hoc analysis). * $p < 0.05$, ** $p < 0.01$.

### 6.2.4 Osteoblasts shows significantly higher cell spreading on RD of 29% and RD of 40% porous substrates

Osteoblast cells maintain bone mass by synthesizing and mineralizing new bone, that is directly regulated by osteocytes during the process of bone remodelling cycle. Henceforth, osteoblast cells were also cultured on the 3 different porous titanium alloy substrates (SLA, RD of 29% and RD of 40% porous titanium alloy substrates) to determine their cell morphology and gene expression of osteoblasts in response to the different level of porous titanium alloy substrates.

After 48 hours of cell culture on the 3 different porous titanium alloy substrates, osteoblasts were found to adhere and spread on all the substrates tested (Figure 42A). The osteoblast as seen in figure 42A displays osteoblasts actin cytoskeleton morphology on the 3 different porous substrates. The osteoblasts on the surface of SLA covers the least area per cell's actin cytoskeleton compared to RD of 29% and RD of 40% substrates. Whereas, the osteoblasts on the surface of RD of 29% and RD of 40% substrates has osteoblasts that covers greater area per cell's actin cytoskeleton compared to SLA. Furthermore, osteoblasts on all the porous titanium alloy substrates promotes a mixture of round to elongated cells during spreading (Figure 42A). On average, there was a significant increase in the area covered by osteoblasts' actin cytoskeleton on both RD of 29% ($535 \pm 31.33\ \mu m^2$) and RD of 40% ($527.3 \pm 33.71\ \mu m^2$) substrates compared to SLA ($236 \pm 13.02\ \mu m^2$) ($p < 0.0001$; One-way ANOVA with Tukey's post hoc analysis) (Figure 42B); this could possibly suggest that osteoblasts on SLA substrate are more active, spreading and migration faster compared to RD of 29% and RD of 40% substrates (Refaaq et al., 2020). There was also a significant reduction in circularity on both RD of 29% ($0.4755 \pm 0.02083$) and RD of 40% ($0.5632 \pm 0.02264$) porous substrates compared to SLA ($0.7 \pm 0.01888$) substrate ($p < 0.0001$; One-way ANOVA with Tukey's post hoc analysis) (Figure 42C); which signifies that the osteoblast's actin cytoskeleton during spreading on both RD of 29% and RD of 40% substrates are more irregularly shaped and branched out in multiple direction compared to SLA substrate. The cell's elongation determined by the aspect ratio of osteoblast's actin cytoskeleton on both RD of 29% ($2.413 \pm 0.1402$) and RD of 40% ($2.796 \pm 0.1586$) substrates were significantly increased compared to

SLA (1.957 ± 0.09808) substrate ($p < 0.0001$; One-way ANOVA with Tukey's post hoc analysis) (Figure 42D); suggesting that osteoblast on both RD of 29% and RD of 40% substrates are undergoing faster migration than the osteoblasts on SLA substrate (Krause & Gautreau, 2014). On the other hand, in terms of solidity, both RD of 29% (0.8158 ± 0.01413) and RD of 40% (0.7694 ± 0.01534) porosity titanium alloy substrates were significantly reduced compared to SLA (0.9071 ± 0.009378) substrate, signifying greater amount of protrusions to occur on both 29% and 40% porous titanium alloy substrates compared to SLA substrate ($p < 0.0001$; One-way ANOVA with Tukey's post hoc analysis) (Figure 42E). With respect to aspect ratio, solidity further confirm that SLA substrate to promote round osteoblast cell morphology, whereas, both RD of 29% and RD of 40% substrates to promote elongated morphology with multiple protrusion that suggest faster migration to occur (Krause & Gautreau, 2014) on both RD of 29% and RD of 40% substrates than the osteoblasts on SLA substrate.

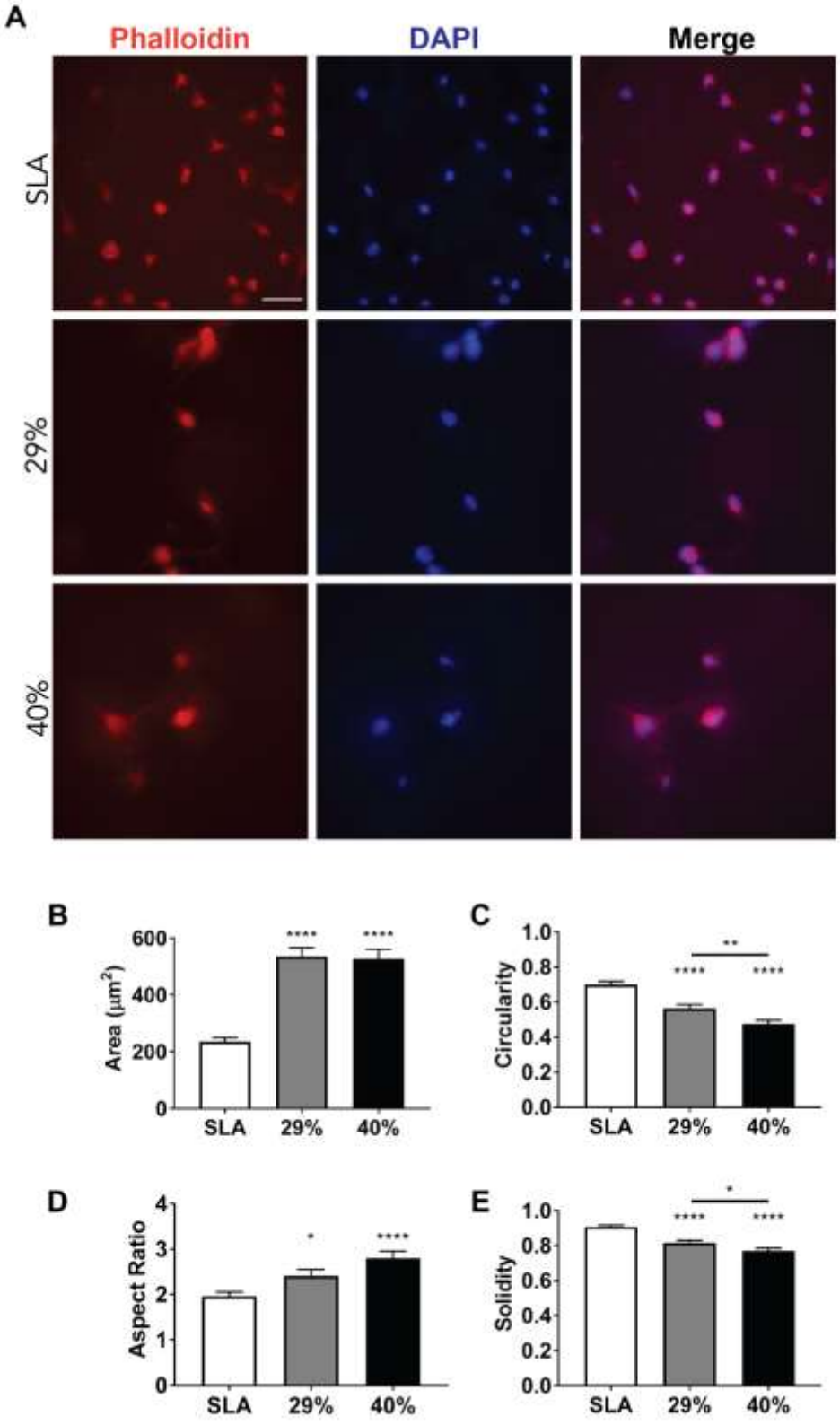


**Figure 42.** Analysis of MC3T3-E1 cells following 48 hours of culture on the porous titanium alloy substrates (SLA, 29% porosity and 40% porosity). **A.** Micrographs of OCY454 cells stained with phalloidin (red; first panel) to identify the actin cytoskeleton and with DAPI (blue; middle panel) to identify the nucleus. The last panel shows the merged images. Scale bar = 50 µm. **B.** Area of MC3T3-

E1 cells cultured on indicated substrates. **C.** Circularity of MC3T3-E1 cells cultured on indicated substrates. **D.** Aspect ratio of MC3T3-E1 cells cultured on indicated substrates. **E.** Solidity of MC3T3-E1 cells cultured on indicated substrates. n = 3 independent biological replicates. Data is presented as mean ± SEM. Statistical significance was determined using One-Way ANOVA (with Turkey's post hoc analysis). * $p < 0.05$, ** $p < 0.01$, **** $p < 0.0001$.

### 6.2.5 Osteoblasts on 3D printed titanium alloy substrates express key bone formation genes

Osteoblasts are directly involved in bone formation and mineralization to help maintain bone mass. As such, key osteoblast bone regulatory gene markers were examined to determine the bone mineralization potential of osteoblast on RD of 29% and RD of 40% porous titanium alloy substrates. Col1α1 gene expression by osteoblasts on RD of 40% (2614 ± 157.9 copies/µL) substrate was significantly increased compared to SLA (1367 ± 107.5 copies/µL) substrate ($p < 0.0101$; One-way ANOVA with Tukey's post hoc analysis) (Figure 43); suggesting that osteoblast bone mineralization activity(Saeed & Iqtedar, 2015) occurs at a greater level through the production of collagen on RD of 40% substrate than SLA substrate. While there is no significant difference in osteoblasts RUNX2 gene expression across the 3 different porous titanium alloy substrates, which indicates osteoblast cell proliferation to occur at a similar rate across the 3 different porous substrates tested(Komori, 2019) ($p > 0.2640$; one-way ANOVA with Tukey's post hoc analysis). Conversely, OC expression was significantly increased on RD of 40% (111 ± 8.327 copies/µL) substrate compared to both RD of 29% (53.9 ± 3.051 copies/µL) and SLA (56.9 ± 7.247 copies/µL) substrates ($p < 0.0014$; One-way ANOVA with Tukey's post hoc analysis), signifying that greater bone mineralisation occurs(Cundy et al., 2014; Sista et al., 2013) on RD of 40% substrate than both RD of 29% and SLA substrates. Whereas osteoblast OPN expression was found to be not significantly different on the 3 different porous substrates tested ($p > 0.5354$; one-way ANOVA with Tukey's post hoc analysis); suggesting that bone mineralisation in terms of crystal growth occurs at a similar rate on all the porous substrates tested. Coincidently, there was a significant increase in ALP-1 expression on RD of 29% (160.5 ± 11.5 copies/µL) substrate compared to both RD of 40% (38.65 ± 6.85 copies/µL) and SLA (75.7 ± 7.9 copies/µL) substrates ($p < 0.0052$; One-way

ANOVA with Tukey's post hoc analysis); suggesting that osseointegration occurs at a faster rate on RD of 29% substrate than both RD of 40% and SLA substrates.

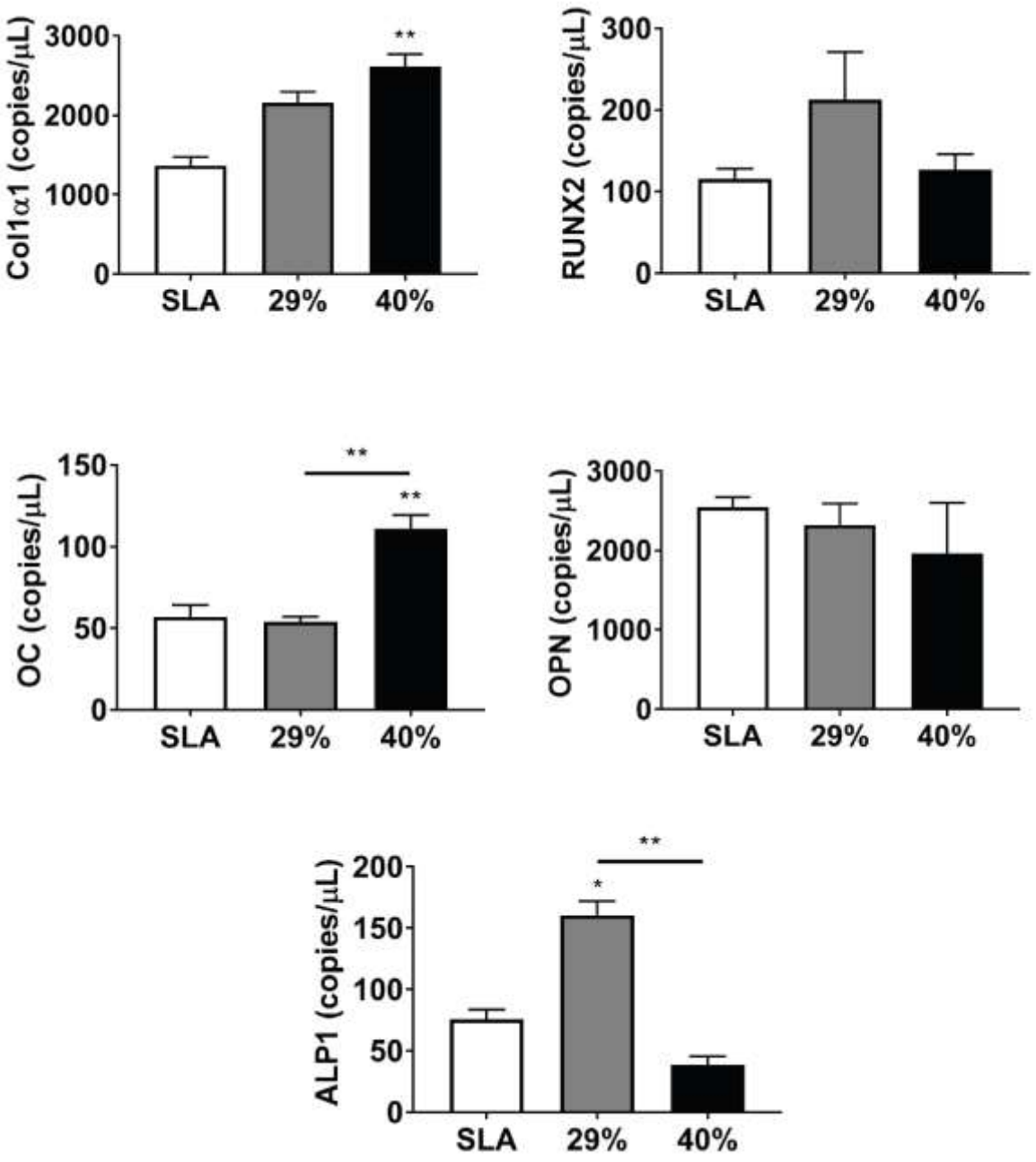


**Figure 43.** Indicated gene expression levels of MC3T3-E1 cells cultured on indicated substrates analysed following ddPCR. n = 3 independent biological replicates. Data is presented as mean ± SEM. Statistical significance was determined using One-Way ANOVA (with Turkey's post hoc analysis). * $p < 0.05$, ** $p < 0.01$.

### 6.2.6 Development of Voronoi lattice structured medical implants

3D Voronoi lattice structure has been mathematically proven that the porous interconnected microstructure of a 3D Voronoi shape, resembles that of the natural lattice structure of bone (Li et al., 2014). I set-up a coding algorithm based on a visual programming language using the Grasshopper addon as seen in figure 44, to design a porous bone-like Voronoi lattice structured dental implant. In this case, I can control the level of porosity, the thickness, and the thinness of the struts to design and develop with precision various medical implants for 3D printing. The output from the finalised 3D Voronoi dental implant as seen in figure 45 was exported as an stl file to be 3D printed using metal 3D printer with T12 powdered material.

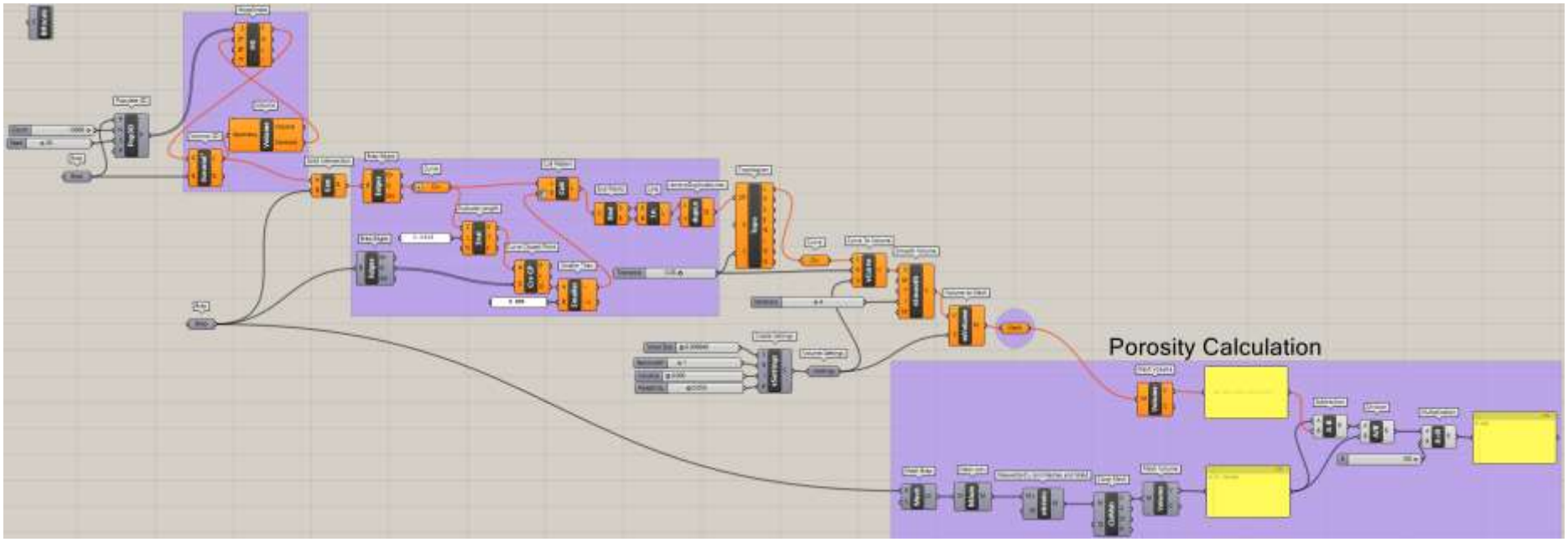


**Figure 44.** Grasshopper circuit workflow diagram to design and develop bone-like Voronoi lattice structured medical implant in Rhinoceros 6.

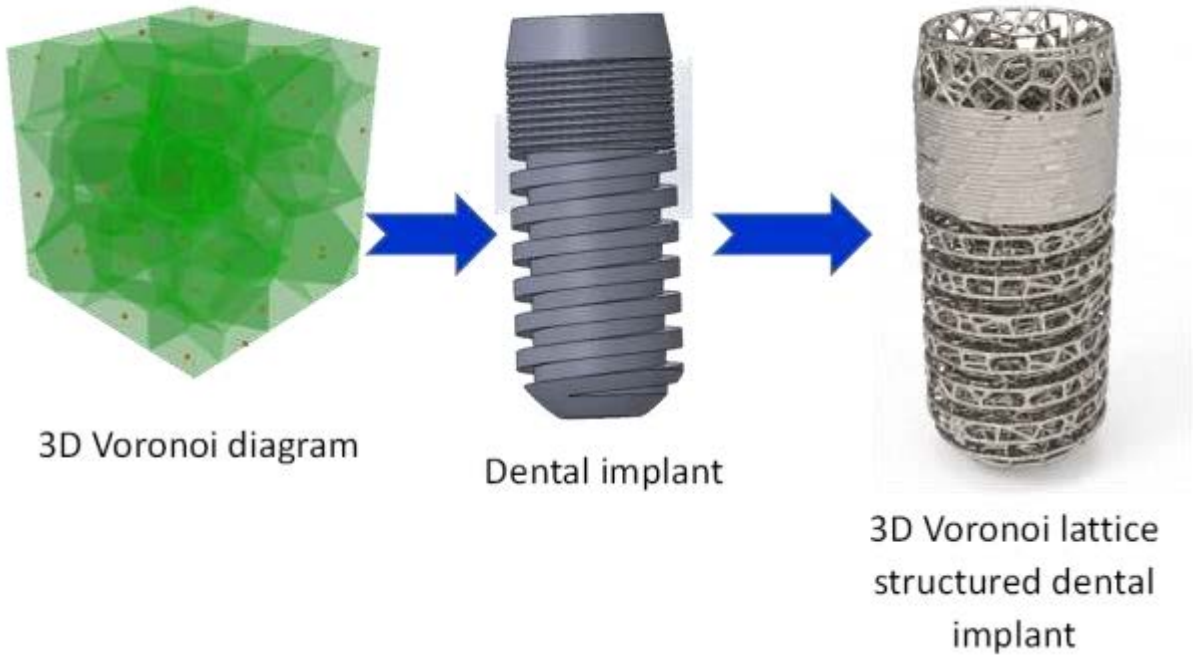


**Figure 45.** The 'Solid Intersection' component within Grasshopper was used between the '3D Voronoi' rectangular prism and the dental implant boundary to obtain a 3D Voronoi lattice structured dental implant.

## 6.3 Discussion

Despite bulk properties for medical implants are important factors due to their mechanical stability, it is ultimately the surface design in the end that contributes to osseointegration (Li et al., 2018). Although current 3D printing technology utilise the top-down approach, where the surface topographies are post-processed. In this case, the surface topographies are not controllable and are dependent primarily on the synthesis process. However, with the advancement in additive manufacturing, it has allowed 3D printers to fabricate medical implants using the bottom-up approach. In this case, the user has full control over the surface design and features such as surface topography and porosity, which cannot be achieved using the conventional 3D printer's top-down approach (Leukers et al., 2005). As such, we have designed and 3D printed titanium alloy (Ti-6Al-4V) at various levels of RD of porous titanium alloy substrates that are shown in figure 38, using the bottom-up approach with a SLS printer, which were manufactured and supplied by Betatype Ltd, United Kingdom; to determine its feasibility as a porous medical implant to enhance osseointegration. This study illustrates the accuracy, reliability and high resolution of SLS 3D printing technology of what it can achieve in terms of high quality porous titanium alloy medical implants' samples. The focus of this study is to determine the *in-vitro* biological efficacy of either RD of 29% or RD of 40% porous titanium alloy substrate for bone implant applications. The reduction of RD in porous medical implants is to help reduce the stiffness at a comparable level to that of bone, which in theory should overcome the complication associated with the stress shielding effect.

In the initial stages of bone implant procedures is the interaction between the host bone and bone cells to that of the medical implant material. To replicate this interaction, bone forming osteoblasts (Caetano-Lopes et al., 2007; Katagiri & Takahashi, 2002) were used as a model for bone formation activity and osteocytes were used as a model for bone regulation activity (Caetano-Lopes et al., 2007), which were studied to evaluate the cellular response on RD of 29% and RD of 40% porous titanium alloy substrates. Osteocytes being highly mechanosensitive are of particular interest in this study as their cellular response to the changes of the different level of porous substrates would govern the bone formation and resorption activity.

The initial contact between bone cells and titanium material is the adherence of cells from the surrounding bone tissue to govern its appropriate response to the material present within the implanted region. The cellular response is effected by factors relating to the material such as the surface structure (Casaletto et al., 2001), stiffness (Bose et al., 2018), and chemical composition (Bruschi et al., 2015; Zareidoost et al., 2012). Often it is the cells ability to spread on the titanium implant material that initiates downstream biological response (Boyan et al., 1996). Previous studies observation of osteocytes that have round cell morphology have been shown to be more mechanosensitive and thereby would influence bone resorption activity than osteocytes with elongated morphology (Florencio-Silva et al., 2015; Sasaki et al., 2015; van Oers et al., 2015; Wu et al., 2018; Zhang et al., 2020). In this study, osteocytes were more elongated on RD of 29% than both SLA and RD of 40% porous substrates. Also, RD of 40% promoted more circular osteocytes morphology than both SLA and RD of 29% porous substrates; suggesting that RD of 40% could influence osteocytes to be more mechanosensitive to trigger bone resorption activity than RD of 29% porous substrate. Furthermore, osteoblasts with elongated morphology observed on different titanium alloy substrates has been shown to promote bone formation activity in a study conducted by Uggeri et al. (2010). Osteoblast cells' morphology in this study were observed to be more elongated on RD of 40% porous substrate than both SLA and RD of 29% porous substrate; which could be indicative of greater osteoblast bone formation activity being promoted by RD of 40% porous substrate than both SLA and RD of 29% porous substrates.

Direct seeding of osteocytes on SLA, RD of 29% and RD of 40% porous titanium alloy substrates did alter cell morphology during cell adhesion and spreading. This indicates that the cellular response differs on varying levels of surface topography and porosity; governing how cells functions upon cell adhesion and in the way they spread on the surface. A series of key osteocyte gene markers including *SOST*, *DMP1*, *PHEX*, *OPG/RANKL* was evaluated to provide an indication of how the cell function on SLA, RD of 29% and RD of 40% porous titanium alloy substrates. SOST gene is known to be a negative regulator of bone formation and is primarily responsive to mechanical stimulus (Qin et al., 2013; Spatz et al., 2015). The SOST gene was significantly downregulated on RD of 40% compared to SLA and RD of 29% substrates, which could suggest that the cell favour bone formation activity on

40% porosity; demonstrating that osteocyte's mechanosensitivity to different level of surface topography and porosity is important to determine for favourable cellular response. OPG/RANKL gene expression ratio was determined and compared on the different level of porous substrates to denote the osteocytes are in favour of bone formation. Previous studies' findings have demonstrated that when OPG gene expression is downregulated and with a subsequent high upregulation of RANKL gene expression, leading to a significantly lower OPG/ RANKL ratio resulted in lower bone mineral density (Fadda et al., 2015; Goldring, 2015; Imel et al., 2014; Naylor & Eastell, 2015; Xu et al., 2012; Zimmerman et al., 2018). In this study, the osteocytes had a significant reduction in OPG/ RANKL ratio on both RD of 29% and RD of 40% porous substrates, which could suggest that the cells are favouring reduced amount of bone formation activity compared to SLA substrate's osteocytes. Also, there was no significant difference between RD of 29% and RD of 40% porous substrates for OPG/ RANKL ratio, indicating that the cells function similarly in regards to the bone formation/resorption activity. The osteocytes genes DMP1 and PHEX, which are involved in bone mineralization and maturation (Dallas et al., 2013; Shih et al., 2002) were expressed at a comparable level on all the porous substrates tested. These results overall suggest that osteocytes function and response can be effected by the different levels of topography and porosity of titanium alloy substrates.

Whilst osteocytes regulate bone remodelling, it is then of the upmost importance to evaluate the actual bone forming osteoblasts as these are the cells involved to be in direct contact with the porous materials in forming bone. Osteocytes governs osteoblast bone formation activity, which is critical in osseointegration as by the promotion of osteoblasts will improve bone formation (Bonewald, 2011; Gesty-Palmer et al., 2009). Osteoblasts key function in bone mineralization is the production of Col1α1 (Saeed & Iqtedar, 2015). Whereas, RUNX2 acts as a master switch that help regulates the proliferation of osteoblast progenitors to be committed to the osteoblast lineage (Komori, 2019). Similarly, OC is another osteoblast's gene involved in bone mineralization (Cundy et al., 2014; Sista et al., 2013). In this study, Col1α1 was highly upregulated on both RD of 29% and RD of 40% porous substrates compared to the control SLA substrate. Whereas, RUNX2 gene expression levels were at similar levels on all porous experimental groups; which indicates that although the osteoblast proliferation rate is similar on

all the substrates, the bone mineralization activity is more favoured on both RD of 29% and RD of 40% porous substrates than SLA. The osteoblast gene OPN, which binds strongly with OC and hydroxyapatite to form a complex with collagen that takes place during bone mineralisation and crystal growth (Barth et al., 1989; Guo et al., 2013). In this study, we observed increased levels of OC gene expression on RD of 40% compared to both SLA and RD of 29% porous substrates, while OPN gene expression is at similar level on all the porous substrates tested; which could be indicative that osteoblast's bone mineralisation and crystal growth activity is most favourable on RD of 40% than SLA and RD of 29% porous substrates. Osteoblasts expression of ALP-1 gene is a clinical marker for bone formation activity (Parvizi & Kim, 2010) and thereby the level of ALP-1 gene expression would indicate the activeness of osseointegration (Subramanian et al., 2012). In this study, ALP-1 gene expression was observed to be highly upregulated on RD of 29% than both SLA and RD of 40% porous substrates; which could signify that greater level of bone formation and mineralization is favoured on RD of 29% porous substrate than both SLA and RD of 40% porous substrates. These results taken together demonstrate that the osteoblasts on 3D printed RD of 29% and RD of 40% porous substrates function similar to if not better than the control group SLA substrate in terms of osteoblasts' bone formation activity.

Taken together these results suggests that 3D printed RD of 29% and RD of 40% porous titanium alloy substrates are able to promote bone formation activity through osteocytes and osteoblasts function. The fundamental concept of this study shows that smaller and more compact pores in 3D printed medical implant substrates with thin struts provides better biological properties in terms of cell adhesion and spreading. This study serve as a potential use for custom tailored 3D printed medical implant for patients and how to incorporate this promising technology to manufacture medical implants to further enhance bone-implant integration. The results for this study also demonstrate that bone cells can be incorporated in porous medical implants for bone ingrowth and thereby, potentially further enhancing bone-implant integration. With the advancement of metal additive manufacturing, medical implants can be manufactured with bone-like porosity and developed into a personalised bone implant. To achieve this, future studies will need to examine the *in vivo* response of these 3D printed porous

medical implants to determine the efficacy and reliability of osseointegration and to improve long-term fixation. Future studies will also need to address the mechanical biocompatibility of these 3D printed porous medical implant to withstand stress and strains under load for long term implantation. Furthermore, future studies, will also need to optimise the mechanical properties to mimic the stiffness of bone as well as the pore size that could potentially provide better cell adhesion, improve osseointegration and overcome the stress shielding effect with the use of currently approved titanium alloys.

3D Voronoi lattice structure has been chosen for this project because it has been mathematically proven to resemble the natural lattice structure of bone (Li et al., 2014). Many previous research findings showed that optimum porous design scaffolds should copy natural bone properties (Fantini & Curto, 2018; Fantini et al., 2016, 2017; Li et al., 2014). Voronoi is one of the most similar designs for bone at present. Whether the Voronoi structure is one of the best designs can only be known through mechanical and biological experiments. Henceforth, in this study the plan was to first know the most optimised lattice structure that bone cells prefer best and then translate that level of lattice structure as well as pore size and thickness of the struts to a Voronoi structured medical implant. But due to the whole COVID situation, we couldn't find a 3D printing manufacturing company that can utilise the new T12 material as well as we couldn't conduct *in vivo* animal studies due to COVID restrictions. Future studies can implement porous Voronoi medical implant *in vivo* as the listed level of porous AI generated relative density as seen figure 38. Once the most optimum level of porous Voronoi lattice structured medical implant is known *in vivo*, then human trial can be conducted.

## 6.4 Conclusion

The porous titanium alloy with a composition of Ti-6Al-4V that were 3D printed with different level of porosity (RD of 29% and RD of 40%) effects cellular response to its structure both visually in terms of cell morphology and gene expression. Hence, the differences in cell morphology across the different porous substrates, also effects gene expression for both osteoblast and osteocyte cells. Out of all genes analysed for osteocytes, RD of 40% porous titanium alloy substrate showed low expression for SOST gene. Whilst both 29% porosity and 40% porosity substrate demonstrating high expression for RANKL gene expression leading to low OPG/ RANKL ratio, signifying bone resorption activity. In addition, osteoblast cells cultured on 40% porous titanium alloy sample showed high gene expression for Col1α1 and OC; although ALP1 gene expression was low, it was still expressed at a similar rate to that of the control SLA substrate. These results overall demonstrate that both RD of 29% and RD of 40% porous titanium alloy substrates promotes bone formation activity at a comparable rate to that of the control SLA substrate and shows promising results to incorporate custom-tailored 3D printed porous medical implants for clinical application to further enhance osseointegration.

# 7. Conclusion

# 7. Conclusion

The AI developed T12 titanium alloy resulted in a very inexpensive process and enhanced progression in advancement in material science by accurately predicting a titanium alloy with bone-like Young's modulus in a span of a few months through the AI machine learning approach 'βlow'. This would otherwise be impossible to achieve using the conventional approach to develop new materials through the 'trial and error' process, which could easily drag on for years resulting in a very expensive R&D process. Henceforth, in this project I reported the *in vitro* biocompatibility assessment on T12 titanium alloy, which was my supervisor's recent breakthrough in constructing a titanium alloy that can be manufactured in bulk at an affordable cost, with a Young's modulus of 35 GPa; closely matching the natural bone's Young's modulus (20-30 GPa). To date, this is the first reporting to produce a new class of biomedical titanium alloy as a result of AI machine learning 'βlow' for the sole purpose of biological and clinical applications.

This is significant because current bone implants are non-homogeneous due to the big difference between the bone and the current metal implants' Young's modulus. Bone is more likely to atrophy, leading to the loosening of the implant where it can easily re-fracture the cortical bone and damage the surrounding tissue. This causes a significant socio-economic burden on patients and on the healthcare system. There is a need for innovative solutions in order to increase the efficiency and recovery of patients with medical bone implants. To overcome this issue, metal implants needs to be closer to the Young's modulus of bone such as our titanium alloy T12. In this project, I was able to show bone cells (osteoblast and osteocyte cells) prefer the surface of T12 equally to T64 but far better than CPT substrate. Furthermore, this study shows T12 was capable of inhibiting/supressing bacteria such as S. *aureus* proliferation, whilst causing no harm to both osteoblast and osteocyte cells on its surface.

In this project, the AI developed T12 titanium alloy was found to be biocompatible, nontoxic to bone cells such as osteoblast and osteocytes cells. T12 has the ability to inhibit/supress bacteria like S. *aureus* while simultaneously causing no negative effects to bone cells. T12 has the potential to be used in future medical implants especially due to its low Young's modulus, which will overcome

complications associated with the stress shielding effect that causes aseptic loosening. This would mean the implant would survive for longer within the implanted region as well as benefitting patients in saving costs associated with revision surgeries due to poor osseointegration. This project serve as a clear demonstration of combining machine learning with biomaterial development and how this technology can be leveraged to enhance bone-implant integration. Overall, this project results have shown that T12 titanium alloy is an effective material and holds significant clinical potential in future medical implants.

Cells within the human body are exposed to various forms of fluid shear stress and pressures. It has been well recognized that mechanical loading is fundamental for the normal development and maintenance of the muscles and bones. It has also been well established from previous studies that osteocytes have been known to regulate bone formation and resorption in response to fluid shear stress. Therefore, bone cells especially osteocytes that are examined during *in vitro* studies should also be evaluated under physiological FSS conditions. Currently there are no *in vitro* model to replicate physiological fluid shear stress for large biomaterials. So, in this case, I designed and developed a new platform to help replicate physiological conditions in an *in vitro* model. The significance of this platform is that it will allow myself and other people to examine the effect of FSS on osteocytes in different biomaterials. By utilising the implant on chip FSS device will allow us to better understand the cellular response during *in vitro* studies before undertaking *in vivo* studies. With that said, the implant on chip fluid shear stress device can improve biological activity by mimicking *in vivo* microenvironment in an in-vitro setting. This allows for better understanding of how bone cells like osteocytes respond to implant surfaces in their native artificial microenvironment. In this study, FSS of 0.5-1 dynes/cm$^2$ rapidly suppresses SOST, DKK1 and RANKL; while promoting the expression of OPG and SMAD1, signifying bone formation activity occurs at 1 dynes/cm$^2$.

Another solution to aseptic loosening is through the fabrication of porous 3D printed medical implants, which helps by reducing the stiffness of currently approved titanium alloy materials as T64 at a comparable level to that of bone. Since there are numerous geometric shapes and designs, and all these features effect the rate of osseointegration. To help speed up the R&D process, the AI machine learning approach was utilised again with the help from Betatype a 3D manufacturing company based

in the United Kingdom, that designed and manufactured all the porous structured medical implant samples based on the AI machine learning recommendations. The AI machine learning approach helped narrow down the best surface features and design to use for bone-implant integration. The AI recommended porous implants substrates were evaluated for the biological response *in vitro*. During *in vitro* studies, osteoblast and osteocyte cellular adhesion and spreading is best preferred on small, compacted pore structure with thin struts, which resulted from high relative density (29%-40%). The differences in cell morphology across the different porous substrates, also effects gene expression for both osteoblast and osteocyte cells. These results overall demonstrate that both RD of 29% and RD of 40% porous titanium alloy substrates promotes bone formation activity at a comparable rate to that of the control SLA substrate. The limitation of this study was that during *in vitro* study cell seeding on the porous substrates would not be consistent, as each technical replicate or biological replicate majority of the cells would penetrate right through the porous structure of the substrate and different amounts of cells would be captured. This in return would not produce consistent results for cell viability assessment and that is why cell viability assay was not examined for the porous substrates. *In vivo* studies on porous medical implants will better showcase the level of porosity and design that bone cells prefer best. The significance of this is that by implementing porous designs in medical implants will improve initial fixation as well as overcome aseptic loosening complications during long-term implantation, where the surrounding bone tissue integrates in and around the medical implant, holding the implant strongly in place compared to a non-porous medical implant. Porous medical implants will also help with the reduction of Young's modulus/stiffness in current bone medical implant's materials and thereby has the potential to overcome the stress shielding effect and improve osseointegration.

# Chapter 8 - Future direction: Development of new biomaterial implants for bone regeneration

# Chapter 8 - Future direction: Development of new biomaterial implants for bone regeneration

## 8. Future work

Overall, these research findings opens a new era into personalised 3D printed medical implants. This area of personalised 3D printed medical implants is heavily regulated by TGA in Australia where they expect custom 3D printed medical implants to be used as the last option given to patients if no other suitable device is available (TGA, 2021). To improve long-term implantation, research and development needs to continue to allow for new suitable materials to be discovered and implemented. So this project's results may break the ground for new research development within material science in particular to produce T12 fine powder for 3D metal printers that utilises the bottom-up approach to construct complex structures. The change in policies from TGA in Australia to allow for custom 3D printed medical implants for patients that chooses that option will allow for medical implants to fit perfectly in position, thereby reducing complications and risk factors associated with implant failure due to poor bone-implant integration. This project results will also influence researchers to implement AI machine learning process to design custom made medical implants from patient's medical image data such as X-rays; which will speed up the design and development process for custom made implants.

Furthermore, software development would be another area that could be influenced by this project's results to develop lattice designs for custom and standard medical implants more efficiently. Currently, 3D modelled complex lattice design architecture comes with lots of errors. Correcting these errors especially for custom made medical implants requires time and it overloads the manufacturing process. If these errors are not corrected, then it can lead to failed production. Henceforth, software that allows for lattice designs to be implemented into custom medical implants without errors is key to the advancement and progression in 3D printed custom tailored medical implants. Developers of software technology can take advantage of intellectual property by providing licence contracts to manufacturers that want to use their software to apply lattice designs to medical implants.

This project results can also impact advancement in metal 3D printing technology. Where complex 3D models can only be achieved through 3D metal printers utilising the bottom-up approach. It uses metal powder that is micro-welded layer by layer, where a user can control surface topography and porosity at each layer to form very complex structure that conventional manufacturing methods wouldn't be able to achieve. Advancement in additive manufacturing, T12 material can be produced with bone-like porosity as well as custom tailored medical implants. This can be only achieved when future studies examine T12 alloy *in vivo* to determine the clinical bone-implant integration and improve long-term implant response. Also by using this new T12 alloy material with a Voronoi lattice structure to 3D print a new class of medical implants to then evaluate the 3D printed lattice structured medical implant in an in vivo model before human trials; this can help advance medical bone implants and improve long-term fixation.

The results achieved in this project for the newly created titanium alloy T12 that has the capability to promote osseointegration and at the same time inhibit and supress S. *aureus* adhesion and proliferation without the use of antibiotics. This is significant because future studies will need to focus on the forces that are involved in Ti, NB and Sn based alloys that creates an unfavourable environment by suppressing bacterial cell proliferation and adhesion. That way such intermolecular forces can give better understanding to scientists to help heighten this mechanism in orthopaedic implants in suppressing bacterial cell's adhesion and proliferation, whilst at the same time does not cause any negative effects to host tissues such as bone cells (osteoblasts, osteocytes and osteoclast cells). This will help reduce the risk factors of patients from being infected by medical implantation surgical procedure. Since bacteria like S. *aureus* is part of the normal skin micro-flora where it has the ability to transition between commensalism to pathogenic state, when it is able to finds its way into the blood stream of the patient during a cut/injury or in this case during medical implant procedure. The newly created titanium alloy has the capability to enhance osseointegration due to its low Young's modulus and at the same time inhibit bacterial adhesion. Overall, these research findings will influence researchers and industries to start implementing this new titanium alloy T12 to be used in various medical implants.

In terms of implant-on-a-chip that allows for cell biology to be studied by replicating key features of an *in vivo* cellular microenvironment in an *in vitro* setting. Generally, it is of upmost importance to characterise mechanical forces in an *in vitro* settings, in order to better understand *in vivo* physiology (Kaarj & Yoon, 2019). The limitations of this project revolves around time constraints, where longer time points for up till a month of cellular response would have shown clear indication of the type of substrates that bone cells prefer best. Thereby, future studies based on cellular response to implant surfaces will need to evaluate bone cells at pressure between 0.5-1 dynes/cm$^2$ for longer periods of time such as for 14 to 28 days and taking cell viability and evaluating bone mineralization using alizarin red staining; which will accurately depict how osteocytes and osteoblast respond to implant surfaces through the creation of an artificial *in vivo* microenvironment. Furthermore, future studies can further confirm the osteocytes cellular response to titanium alloy substrates under FSS conditions for 14-28 days by factors derived from osteocytes within the conditioned medium, where this conditioned medium is to then be implemented in osteoblast and osteoclast either in co-culture models or independent models. This will help evaluate if osteocytes cellular response triggers similar targeted response within osteoblasts and osteoclasts cells, as osteocytes are master regulators of both osteoblast and osteoclast cells (Crockett et al., 2011; Prideaux et al., 2016). The longer time periods of 14-28 days will accurately demonstrate the rate of bone mineralisation activity on all the titanium alloy substrate and show which titanium alloy is best preferred by bone cells.

For future studies, personal advice on using PDMS material as depicted in this study instead of 3D printed resin-based materials since PDMS allows for oxygen diffusion to occur to help cells survive for longer study durations. A lot of time was wasted on selecting the correct material as the cells would die completely under 24 hrs of FSS conditions when using resin-based 3D printed material. Once we started using PDMS material for our implant on chip device, the osteocyte cells were all adherent and spreading instead of being detached and washed away since the cells would suffocate when no gas diffusion would occur under the resin-based material.

# 9. References


Ackerman, I. N., Bohensky, M. A., Zomer, E., Tacey, M., Gorelik, A., Brand, C. A., & De Steiger, R. (2019). The projected burden of primary total knee and hip replacement for osteoarthritis in Australia to the year 2030. *BMC musculoskeletal disorders, 20*(1), 1-10.

Alloyed. (2021). *Improving Orthopaedic Implant Materials & Structure*. alloyed. Retrieved 7 April 2022, from https://alloyed.com/alloys-case-study/improving-orthopaedic-implant-materials-structure/?fbclid=IwAR3PSMgcv3ngYb1pAisI0TpqZ3pNoLglWWE4eRBIT2BndnT-HsKZR81oUgM

Alsaeedi, R., & Ozdemir, Z. (2018). Evaluation of chemical mechanical polishing-based surface modification on 3D dental implants compared to alternative methods. *Materials, 11*(11), 2286.

Anitua, E., Sanchez, M., Orive, G., & Andía, I. (2007). The potential impact of the preparation rich in growth factors (PRGF) in different medical fields. *Biomaterials, 28*(31), 4551-4560.

Apos E, C. J., Ahern S, Truong T, Hansen J, Johnson MA. . (2019). *The Australian Spine Registry Annual Report* (2). Monash University.

Apostu, D., Lucaciu, O., Berce, C., Lucaciu, D., & Cosma, D. (2018). Current methods of preventing aseptic loosening and improving osseointegration of titanium implants in cementless total hip arthroplasty: a review. *Journal of International Medical Research, 46*(6), 2104-2119.

Barnes, J. M., Przybyla, L., & Weaver, V. M. (2017). Tissue mechanics regulate brain development, homeostasis and disease. *Journal of cell science, 130*(1), 71-82.

Barth, E., Myrvik, Q. M., Wagner, W., & Gristina, A. G. (1989). In vitro and in vivo comparative colonization of Staphylococcus aureus and Staphylococcus epidermidis on orthopaedic implant materials. *Biomaterials, 10*(5), 325-328.

Bianco, P., & Robey, P. G. (2015). Skeletal stem cells. *Development, 142*(6), 1023-1027.

Bogue, R. (2013). 3D printing: the dawn of a new era in manufacturing? *Assembly Automation, 33*(4), 307-311.

Bonewald, L. F. (2008). CHAPTER 8 - Osteocytes. In R. Marcus, D. Feldman, D. A. Nelson, & C. J. Rosen (Eds.), *Osteoporosis (Third Edition)* (pp. 169-189). Academic Press. https://doi.org/10.1016/B978-012370544-0.50010-0

Bonewald, L. F. (2011). The amazing osteocyte. *Journal of Bone and Mineral Research, 26*(2), 229-238.

Bose, S., Banerjee, D., Shivaram, A., Tarafder, S., & Bandyopadhyay, A. (2018). Calcium phosphate coated 3D printed porous titanium with nanoscale surface modification for orthopedic and dental applications. *Materials & Design, 151*, 102-112.

Boyan, B., Cheng, A., Olivares-Navarrete, R., & Schwartz, Z. (2016). Implant surface design regulates mesenchymal stem cell differentiation and maturation. *Advances in dental research, 28*(1), 10-17.

Boyan, B. D., Hummert, T. W., Dean, D. D., & Schwartz, Z. (1996). Role of material surfaces in regulating bone and cartilage cell response. *Biomaterials, 17*(2), 137-146.

Britannica, T. E. o. E. (2016). Osteoblast *Encyclopædia Britannica*. Encyclopædia Britannica, inc. https://www.britannica.com/science/osteoblast

Bruschi, M., Steinmüller-Nethl, D., Goriwoda, W., & Rasse, M. (2015). Composition and modifications of dental implant surfaces. *Journal of oral implants, 2015*.

Caetano-Lopes, J., Canhao, H., & Fonseca, J. E. (2007). Osteoblasts and bone formation. *Acta reumatológica portuguesa, 32*(2), 103-110.

Cansizoglu, O., Harrysson, O., Cormier, D., West, H., & Mahale, T. (2008). Properties of Ti–6Al–4V non-stochastic lattice structures fabricated via electron beam melting. *Materials Science and Engineering: A, 492*(1-2), 468-474.

Casaletto, M., Ingo, G., Kaciulis, S., Mattogno, G., Pandolfi, L., & Scavia, G. (2001). Surface studies of in vitro biocompatibility of titanium oxide coatings. *Applied surface science, 172*(1-2), 167-177.

Cheung, W.-Y., Simmons, C. A., & You, L. (2012). Osteocyte apoptosis regulates osteoclast precursor adhesion via osteocytic IL-6 secretion and endothelial ICAM-1 expression. *Bone, 50*(1), 104-110.
Choi, J. U. A., Kijas, A. W., Lauko, J., & Rowan, A. E. (2022). The mechanosensory role of osteocytes and implications for bone health and disease states. *Frontiers in Cell and Developmental Biology, 9*, 770143.
CIA. (2018). *The World Factbook - Central Intelligence Agency*. Central Intelligence Agency. Retrieved 1 November 2018, from https://www.cia.gov/library/publications/resources/the-world-factbook/geos/as.html
Cook, D., & Genever, P. (2013). Regulation of mesenchymal stem cell differentiation. *Transcriptional and Translational Regulation of Stem Cells*, 213-229.
Cortizo, A. M. a., Bruzzone, L., Molinuevo, S., & Etcheverry, S. B. (2000). A possible role of oxidative stress in the vanadium-induced cytotoxicity in the MC3T3E1 osteoblast and UMR106 osteosarcoma cell lines. *Toxicology, 147*(2), 89-99. https://doi.org/10.1016/S0300-483X(00)00181-5
Crockett, J. C., Rogers, M. J., Coxon, F. P., Hocking, L. J., & Helfrich, M. H. (2011). Bone remodelling at a glance. *Journal of cell science, 124*(7), 991-998.
Cundy, T., Reid, I. R., & Grey, A. (2014). CHAPTER 31 - Metabolic bone disease. In W. J. Marshall, M. Lapsley, A. P. Day, & R. M. Ayling (Eds.), *Clinical Biochemistry: Metabolic and Clinical Aspects (Third Edition)* (pp. 604-635). Churchill Livingstone. https://doi.org/10.1016/B978-0-7020-5140-1.00031-6
Dalby, M. J., Gadegaard, N., & Oreffo, R. O. (2014). Harnessing nanotopography and integrin–matrix interactions to influence stem cell fate. *Nature materials, 13*(6), 558.
Dallas, S. L., Prideaux, M., & Bonewald, L. F. (2013). The osteocyte: an endocrine cell… and more. *Endocrine reviews, 34*(5), 658-690.
Darouiche, R. O. (2003). Antimicrobial approaches for preventing infections associated with surgical implants. *Clinical infectious diseases, 36*(10), 1284-1289.
Davidson, J. A., & Tuneberg, L. H. (2001). Niobium-titanium-zirconium-molybdenum (nbtizrmo) alloys for dental and other medical device applications. Google Patents.
de Viteri, V. S., & Fuentes, E. (2013). Titanium and titanium alloys as biomaterials. In *Tribology-Fundamentals and advancements*. InTech.
Ducy, P., Zhang, R., Geoffroy, V., Ridall, A. L., & Karsenty, G. (1997). Osf2/Cbfa1: a transcriptional activator of osteoblast differentiation. *cell, 89*(5), 747-754.
Ďurišin, M., Ďurišin, J., Milkovič, O., Pietriková, A., & Saksl, K. (2019). Development and Characterisation of New Biocompatible Sn-Mg Lead-Free Solder. Journal of Metastable and Nanocrystalline Materials.
Econs, M. J., Samsa, G. P., Monger, M., Drezner, M. K., & Feussner, J. R. (1994). X-Linked hypophosphatemic rickets: a disease often unknown to affected patients. *Bone and Mineral, 24*(1), 17-24. https://doi.org/10.1016/S0169-6009(08)80127-4
Elias, C. N., Lima, J. H. C., Valiev, R., & Meyers, M. A. (2008). Biomedical applications of titanium and its alloys. *JOM, 60*(3), 46-49. 10.1007/s11837-008-0031-1
Fadda, S., Hamdy, A., Abulkhair, E., Elsify, H. M., & Mostafa, A. (2015). Serum levels of osteoprotegerin and RANKL in patients with rheumatoid arthritis and their relation to bone mineral density and disease activity. *The Egyptian Rheumatologist, 37*(1), 1-6.
Fakhry, M., Hamade, E., Badran, B., Buchet, R., & Magne, D. (2013). Molecular mechanisms of mesenchymal stem cell differentiation towards osteoblasts. *World journal of stem cells, 5*(4), 136-148.
Fantini, M., & Curto, M. (2018). Interactive design and manufacturing of a Voronoi-based biomimetic bone scaffold for morphological characterization. *International Journal on Interactive Design and Manufacturing (IJIDeM), 12*(2), 585-596.
Fantini, M., Curto, M., & De Crescenzio, F. (2016). A method to design biomimetic scaffolds for bone tissue engineering based on Voronoi lattices. *Virtual and Physical Prototyping, 11*(2), 77-90.

Fantini, M., Curto, M., & De Crescenzio, F. (2017). TPMS for interactive modelling of trabecular scaffolds for bone tissue engineering. In *Advances on Mechanics, Design Engineering and Manufacturing* (pp. 425-435). Springer.
Feller, L., Jadwat, Y., Khammissa, R. A., Meyerov, R., Schechter, I., & Lemmer, J. (2015). Cellular responses evoked by different surface characteristics of intraosseous titanium implants. *BioMed Research International, 2015*.
Feng, H., Jiang, B., Xing, W., Sun, J., Greenblatt, M. B., & Zou, W. (2022). Skeletal Stem Cells: Origins, definitions, and functions in bone development and disease. *Life Medicine, 1*(3), 276-293.
Feng, J. Q., Ward, L. M., Liu, S., Lu, Y., Xie, Y., Yuan, B., Yu, X., Rauch, F., Davis, S. I., & Zhang, S. (2006). Loss of DMP1 causes rickets and osteomalacia and identifies a role for osteocytes in mineral metabolism. *Nature genetics, 38*(11), 1310.
Flannagan, R. S., Heit, B., & Heinrichs, D. E. (2016). Intracellular replication of Staphylococcus aureus in mature phagolysosomes in macrophages precedes host cell death, and bacterial escape and dissemination. *Cellular microbiology, 18*(4), 514-535.
Florencio-Silva, R., Sasso, G. R. d. S., Sasso-Cerri, E., Simões, M. J., & Cerri, P. S. (2015). Biology of bone tissue: structure, function, and factors that influence bone cells. *BioMed Research International, 2015*.
Frost, A., Jonsson, K. B., Bränd strö m, H., Ohlsson, C., Ljunghall, S., & Ljunggren, O. s. (1998). Interleukin-13 inhibits cell proliferation and stimulates interleukin-6 formation in isolated human osteoblasts. *The Journal of Clinical Endocrinology & Metabolism, 83*(9), 3285-3289.
Frost, H. M. (2004). A 2003 update of bone physiology and Wolff's Law for clinicians. *The Angle Orthodontist, 74*(1), 3-15.
Gardner, M. W., & Dorling, S. (1998). Artificial neural networks (the multilayer perceptron)—a review of applications in the atmospheric sciences. *Atmospheric environment, 32*(14-15), 2627-2636.
Gesty-Palmer, D., Flannery, P., Yuan, L., Corsino, L., Spurney, R., Lefkowitz, R. J., & Luttrell, L. M. (2009). A β-arrestin–biased agonist of the parathyroid hormone receptor (PTH1R) promotes bone formation independent of G protein activation. *Science translational medicine, 1*(1), 1ra1-1ra1.
Ghiasi, M. S., Chen, J., Vaziri, A., Rodriguez, E. K., & Nazarian, A. (2017). Bone fracture healing in mechanobiological modeling: A review of principles and methods. *Bone reports, 6*, 87-100.
Goldring, S. R. (2015). The osteocyte: key player in regulating bone turnover. *RMD Open, 1*(Suppl 1), e000049. 10.1136/rmdopen-2015-000049
Gomes, C. C., Moreira, L. M., Santos, V. J. S. V., Ramos, A. S., Lyon, J. P., Soares, C. P., & Santos, F. V. (2011). Assessment of the genetic risks of a metallic alloy used in medical implants. *Genetics and molecular biology, 34*(1), 116-121. 10.1590/S1415-47572010005000118
Goodman, S., Huie, P., Song, Y., Schurman, D., Maloney, W., Woolson, S., & Sibley, R. (1998). Cellular profile and cytokine production at prosthetic interfaces: study of tissues retrieved from revised hip and knee replacements. *The Journal of bone and joint surgery. British volume, 80*(3), 531-539.
Gordin, D., Gloriant, T., Texier, G., Thibon, I., Ansel, D., Duval, J., & Nagel, M. (2004). Development of a β-type Ti–12Mo–5Ta alloy for biomedical applications: cytocompatibility and metallurgical aspects. *Journal of Materials Science: Materials in Medicine, 15*(8), 885-891.
Gray, J. P., Amacher, N., Ford, C., & Ray, S. D. (2018). Chapter 22 - Metal Antagonists and Metals. In S. D. Ray (Ed.), *Side Effects of Drugs Annual* (Vol. 40, pp. 279-288). Elsevier. https://doi.org/10.1016/bs.seda.2018.08.013
Grosz, M., Kolter, J., Paprotka, K., Winkler, A. C., Schäfer, D., Chatterjee, S. S., Geiger, T., Wolz, C., Ohlsen, K., & Otto, M. (2014). Cytoplasmic replication of S taphylococcus aureus upon phagosomal escape triggered by phenol-soluble modulin α. *Cellular microbiology, 16*(4), 451-465.
Grundei, H., & Gerdesmeyer, L. (2009). Set for creating an offset-resurfacing hip-joint implant. Google Patents.

Gu, J., Chen, P. Z., Seo, B. B., Jardin, J. M., Verma, M. S., Jahed, Z., Mofrad, M. R., Gu, F. X., & Tsui, T. Y. (2016). Adhesion characteristics of Staphylococcus aureus bacterial cells on funnel-shaped palladium–cobalt alloy nanostructures. *Journal of Experimental Nanoscience, 11*(7), 480-489.

Guan, C., Dang, R., Cui, Y., Liu, L., Chen, X., Wang, X., Zhu, J., Li, D., Li, J., & Wang, D. (2017). Characterization of plasma metal profiles in Alzheimer's disease using multivariate statistical analysis. *PloS one, 12*(7).

Guo, Y., Chen, D., Cheng, M., Lu, W., Wang, L., & Zhang, X. (2013). The bone tissue compatibility of a new Ti35Nb2Ta3Zr alloy with a low Young's modulus. *International journal of molecular medicine, 31*(3), 689-697.

Guvendiren, M., Molde, J., Soares, R. M., & Kohn, J. (2016). Designing biomaterials for 3D printing. *ACS Biomaterials Science & Engineering, 2*(10), 1679-1693.

Hanawa, T. (2021). Metals and medicine. *Materials transactions, 62*(2), 139-148.

Haykin, S. S., Haykin, S. S., Haykin, S. S., & Haykin, S. S. (2009). *Neural networks and learning machines* (Vol. 3). Pearson Upper Saddle River.

Hazenberg, J. G., Hentunen, T. A., Heino, T. J., Kurata, K., Lee, T. C., & Taylor, D. (2009). Microdamage detection and repair in bone: fracture mechanics, histology, cell biology. *Technology and Health Care, 17*(1), 67-75.

Holinka, J., Pilz, M., Kubista, B., Presterl, E., & Windhager, R. (2013). Effects of selenium coating of orthopaedic implant surfaces on bacterial adherence and osteoblastic cell growth. *The bone & joint journal, 95*(5), 678-682.

Hosny, H. A., El-Bakoury, A., Srinivasan, S. C., Yarlagadda, R., & Keenan, J. (2018). Tritanium Acetabular Cup in Revision Hip Replacement: A Six to Ten Years of Follow-Up Study. *The Journal of arthroplasty*.

Imel, E. A., DiMeglio, L. A., & Burr, D. B. (2014). Chapter 16 - Metabolic Bone Diseases. In D. B. Burr & M. R. Allen (Eds.), *Basic and Applied Bone Biology* (pp. 317-344). Academic Press. https://doi.org/10.1016/B978-0-12-416015-6.00016-2

*Industry Statistics - MTAA*. (2014). Medical Technology Association of Australia. Retrieved 1 November 2018, from https://www.mtaa.org.au/industry-statistics

Javed, A., Chen, H., & Ghori, F. Y. (2010). Genetic and transcriptional control of bone formation. *Oral and Maxillofacial Surgery Clinics, 22*(3), 283-293.

Jilka, R. L., Noble, B., & Weinstein, R. S. (2013). Osteocyte apoptosis. *Bone, 54*(2), 264-271.

Kaarj, K., & Yoon, J.-Y. (2019). Methods of delivering mechanical stimuli to organ-on-a-chip. *Micromachines, 10*(10), 700.

Kanaji, A., Caicedo, M. S., Virdi, A. S., Sumner, D. R., Hallab, N. J., & Sena, K. (2009). Co–Cr–Mo alloy particles induce tumor necrosis factor alpha production in MLO-Y4 osteocytes: a role for osteocytes in particle-induced inflammation. *Bone, 45*(3), 528-533.

Katagiri, T., & Takahashi, N. (2002). Regulatory mechanisms of osteoblast and osteoclast differentiation. *Oral diseases, 8*(3), 147-159.

Kawahara, M., & Kato-Negishi, M. (2011). Link between aluminum and the pathogenesis of Alzheimer's disease: the integration of the aluminum and amyloid cascade hypotheses. *International journal of Alzheimer's disease, 2011*.

Khadija, G., Saleem, A., Akhtar, Z., Naqvi, Z., Gull, M., Masood, M., Mukhtar, S., Batool, M., Saleem, N., & Rasheed, T. (2018). Short term exposure to titanium, aluminum and vanadium (Ti 6Al 4V) alloy powder drastically affects behavior and antioxidant metabolites in vital organs of male albino mice. *Toxicology reports, 5*, 765-770.

Kobayashi, S. D., Malachowa, N., & DeLeo, F. R. (2015). Pathogenesis of Staphylococcus aureus abscesses. *The American journal of pathology, 185*(6), 1518-1527.

Kobayashi, Y., Uehara, S., Koide, M., & Takahashi, N. (2015). The regulation of osteoclast differentiation by Wnt signals [Review]. *BoneKEy Rep, 4*. 10.1038/bonekey.2015.82

Kohli, N., Ho, S., Brown, S. J., Sawadkar, P., Sharma, V., Snow, M., & García-Gareta, E. (2018). Bone remodelling in vitro: Where are we headed?:-A review on the current understanding of physiological bone remodelling and inflammation and the strategies for testing biomaterials in vitro. *Bone, 110*, 38-46.

Komori, T. (2019). Regulation of proliferation, differentiation and functions of osteoblasts by Runx2. *International Journal of Molecular Sciences, 20*(7), 1694.
Krause, M., & Gautreau, A. (2014). Steering cell migration: lamellipodium dynamics and the regulation of directional persistence. *Nature reviews Molecular cell biology, 15*(9), 577-590.
Kumar, C. G., Pombala, S., Poornachandra, Y., & Agarwal, S. V. (2016). Synthesis, characterization, and applications of nanobiomaterials for antimicrobial therapy. In *Nanobiomaterials in Antimicrobial Therapy* (pp. 103-152). Elsevier.
Landskron, G., De la Fuente, M., Thuwajit, P., Thuwajit, C., & Hermoso, M. A. (2014). Chronic inflammation and cytokines in the tumor microenvironment. *Journal of immunology research, 2014*.
Lara-Castillo, N., Kim-Weroha, N., Kamel, M., Javaheri, B., Ellies, D., Krumlauf, R., Thiagarajan, G., & Johnson, M. (2015). In vivo mechanical loading rapidly activates β-catenin signaling in osteocytes through a prostaglandin mediated mechanism. *Bone, 76*, 58-66.
Le Guéhennec, L., Soueidan, A., Layrolle, P., & Amouriq, Y. (2007). Surface treatments of titanium dental implants for rapid osseointegration. *Dental materials, 23*(7), 844-854.
Lee, S., Porter, M., Wasko, S., Lau, G., Chen, P.-Y., Novitskaya, E. E., Tomsia, A. P., Almutairi, A., Meyers, M. A., & McKittrick, J. (2012). Potential bone replacement materials prepared by two methods. *MRS Online Proceedings Library Archive, 1418*.
Lei, P., Qian, H., Zhang, T., Lei, T., Hu, Y., Chen, C., & Zhou, K. (2022). Porous tantalum structure integrated on Ti6Al4V base by Laser Powder Bed Fusion for enhanced bony-ingrowth implants: In vitro and in vivo validation. *Bioactive Materials, 7*, 3-13.
Leukers, B., Gülkan, H., Irsen, S. H., Milz, S., Tille, C., Schieker, M., & Seitz, H. (2005). Hydroxyapatite scaffolds for bone tissue engineering made by 3D printing. *Journal of Materials Science: Materials in Medicine, 16*(12), 1121-1124.
Lewiecki, E. M. (2014). Role of sclerostin in bone and cartilage and its potential as a therapeutic target in bone diseases. *Therapeutic advances in musculoskeletal disease, 6*(2), 48-57.
Li, H., Zhang, A., Bone, L., Buyea, C., & Ramanathan, M. (2014). A network modeling approach for the spatial distribution and structure of bone mineral content. *The AAPS journal, 16*(3), 478-487. 10.1208/s12248-014-9585-8
Li, X., Liu, C., Li, P., Li, S., Zhao, Z., Chen, Y., Huo, B., & Zhang, D. (2013). Connexin 43 is a potential regulator in fluid shear stress-induced signal transduction in osteocytes. *Journal of Orthopaedic Research, 31*(12), 1959-1965.
Li, Z., Liu, C., Wang, B., Wang, C., Wang, Z., Yang, F., Gao, C., Liu, H., Qin, Y., & Wang, J. (2018). Heat treatment effect on the mechanical properties, roughness and bone ingrowth capacity of 3D printing porous titanium alloy. *RSC Advances, 8*(22), 12471-12483.
Lisowska, B., Kosson, D., & Domaracka, K. (2018). Lights and shadows of NSAIDs in bone healing: the role of prostaglandins in bone metabolism. *Drug design, development and therapy, 12*, 1753.
Liu, X., Chen, S., Tsoi, J. K. H., & Matinlinna, J. P. (2017). Binary titanium alloys as dental implant materials-a review. *Regenerative biomaterials, 4*(5), 315-323. 10.1093/rb/rbx027
López, M. F., Gutiérrez, A., & Jiménez, J. A. (2001). Surface characterization of new non-toxic titanium alloys for use as biomaterials. *Surface Science, 482-485*, 300-305. https://doi.org/10.1016/S0039-6028(00)01005-0
Mangano, C., De Rosa, A., Desiderio, V., d'Aquino, R., Piattelli, A., De Francesco, F., Tirino, V., Mangano, F., & Papaccio, G. (2010). The osteoblastic differentiation of dental pulp stem cells and bone formation on different titanium surface textures. *Biomaterials, 31*(13), 3543-3551.
McBryde, E., Bradley, L., Whitby, M., & McElwain, D. (2004). An investigation of contact transmission of methicillin-resistant Staphylococcus aureus. *Journal of Hospital Infection, 58*(2), 104-108.
Meltzer, A., Baumgarten, H., Testori, T., & Trisi, P. (2009). Pressure necrosis and osseointegration. *restoration, 4*, 7.
Merritt, J. H., Kadouri, D. E., & O'Toole, G. A. (2011). Growing and analyzing static biofilms. *Current protocols in microbiology, 22*(1), 1B. 1.1-1B. 1.18.

Metzger, C. E., & Narayanan, S. A. (2019). The role of osteocytes in inflammatory bone loss. *Frontiers in endocrinology, 10*, 285.
Michaels, J. D., Nowak, J. E., Mallik, A. K., Koczo, K., Wasan, D. T., & Papoutsakis, E. T. (1995). Interfacial properties of cell culture media with cell-protecting additives. *Biotechnology and bioengineering, 47*(4), 420-430.
Missiakas, D. M., & Schneewind, O. (2013). Growth and laboratory maintenance of Staphylococcus aureus. *Current protocols in microbiology, 28*(1), 9C. 1.1-9C. 1.9.
Moharrami, N., Langton, D. J., Sayginer, O., & Bull, S. J. (2013). Why does titanium alloy wear cobalt chrome alloy despite lower bulk hardness: A nanoindentation study? *Thin Solid Films, 549*, 79-86. https://doi.org/10.1016/j.tsf.2013.06.020
Monteiro, D. A., Dole, N. S., Campos, J. L., Kaya, S., Schurman, C. A., Belair, C. D., & Alliston, T. (2021). Fluid shear stress generates a unique signaling response by activating multiple TGFβ family type I receptors in osteocytes. *The FASEB Journal, 35*(3), e21263.
Morrell, A. E., Brown, G. N., Robinson, S. T., Sattler, R. L., Baik, A. D., Zhen, G., Cao, X., Bonewald, L. F., Jin, W., & Kam, L. C. (2018). Mechanically induced Ca 2+ oscillations in osteocytes release extracellular vesicles and enhance bone formation. *Bone research, 6*(1), 1-11.
Mravcová, A., Jírová, D., Jančí, H., & Lener, J. (1993). Effects of orally administered vanadium on the immune system and bone metabolism in experimental animals. *Science of the total environment, 134*, 663-669.
*Nasal Nose Prosthetics*. (2018). Genesis Prosthetic Arts. Retrieved 2 November 2018, from http://www.premiumprosthetics.com/nasal-prosthetics/
Naylor, K. E., & Eastell, R. (2015). Biochemical markers in bone disease. In *Rheumatology* (pp. 1656-1662). Elsevier.
Neumann, A., & Kevenhoerster, K. (2009). Biomaterials for craniofacial reconstruction. *GMS current topics in otorhinolaryngology, head and neck surgery, 8*.
Niinomi, M., & Nakai, M. (2014). Biomedical implant devices fabricated from low Young's modulus titanium alloys demonstrating high mechanical biocompatibility. *Mater Matters, 9*, 39-46.
Niinomi, M., Nakai, M., & Hieda, J. (2012). Development of new metallic alloys for biomedical applications. *Acta biomaterialia, 8*(11), 3888-3903.
Oldani, C., & Dominguez, A. (2012). Titanium as a Biomaterial for Implants. *Recent advances in arthroplasty, 218*, 149-162.
Olden, J. D., Joy, M. K., & Death, R. G. (2004). An accurate comparison of methods for quantifying variable importance in artificial neural networks using simulated data. *Ecological Modelling, 178*(3-4), 389-397.
Park, K.-S., Awamleh, A., Ibrahim, A. G., & Cho, S.-A. (2018). Comparison of removal torques between laser-etched and modified sandblasted acid-etched Ti implant surfaces in rabbit tibias. *The journal of advanced prosthodontics, 10*(1), 73-78.
Parker, D. (2018). A live vaccine to Staphylococcus aureus infection. Taylor & Francis.
Parvizi, J., & Kim, G. K. (2010). Chapter 160 - Osteoblasts. In J. Parvizi & G. K. Kim (Eds.), *High Yield Orthopaedics* (pp. 331-332). W.B. Saunders. https://doi.org/10.1016/B978-1-4160-0236-9.00171-1
Patel, S., Keshavarz, M., & Vlasea, M. (2021). Challenges during laser powder bed fusion of a near-alpha titanium alloy-Ti-6242Si. 2021 International Solid Freeform Fabrication Symposium.
Pendleton, E. G., Tehrani, K. F., Barrow, R. P., & Mortensen, L. J. (2020). Second harmonic generation characterization of collagen in whole bone. *Biomedical Optics Express, 11*(8), 4379-4396. 10.1364/BOE.391866
Petersen, D. N., Tkalcevic, G. T., Mansolf, A. L., Rivera-Gonzalez, R., & Brown, T. A. (2000). Identification of osteoblast/osteocyte factor 45 (OF45), a bone-specific cDNA encoding an RGD-containing protein that is highly expressed in osteoblasts and osteocytes. *Journal of Biological Chemistry, 275*(46), 36172-36180.
Pflanz, D., Birkhold, A. I., Albiol, L., Thiele, T., Julien, C., Seliger, A., Thomson, E., Kramer, I., Kneissel, M., & Duda, G. N. (2017). Sost deficiency led to a greater cortical bone formation response to mechanical loading and altered gene expression. *Scientific reports, 7*(1), 1-14.

Poondla, N., Srivatsan, T. S., Patnaik, A., & Petraroli, M. (2009). A study of the microstructure and hardness of two titanium alloys: Commercially pure and Ti–6Al–4V. *Journal of Alloys and Compounds, 486*(1-2), 162-167.
Prasadam, I., Zhou, Y., Du, Z., Chen, J., Crawford, R., & Xiao, Y. (2014). Osteocyte-induced angiogenesis via VEGF–MAPK-dependent pathways in endothelial cells. *Molecular and cellular biochemistry, 386*(1), 15-25.
Prideaux, M., Findlay, D. M., & Atkins, G. J. (2016). Osteocytes: the master cells in bone remodelling. *Current opinion in pharmacology, 28*, 24-30.
Qin, L., Ding, D., Cui, L., & Huang, Q. (2013). Expression and regulation of the SOST gene. *Yi chuan= Hereditas, 35*(8), 939-947.
Qiu, Z.-Y., Chen, C., Wang, X.-M., & Lee, I.-S. (2014). Advances in the surface modification techniques of bone-related implants for last 10 years. *Regenerative biomaterials, 1*(1), 67-79.
Radl, S., Klemes, J. J., Varbanov, P. S., & Wallek, T. (2018). *28th European Symposium on Computer Aided Process Engineering*. Elsevier.
Rahmani, N. (2018). *What is Osseointegration*. Manhattan Periodontics and implant dentistry. Retrieved 14 August 2018, from https://www.nycdentalimplantscenter.com/what-is-osseointegration/
Rangappa, R., Sajjan, S., & Kulkarni, M. (2015). selective laser sintering process - A review. *Technical Research Organisation India, 2*(10), 91-100.
Refaaq, F., Chen, X., & Pang, S. (2020). Effects of topographical guidance cues on osteoblast cell migration. *Scientific reports, 10*(1), 1-11.
Rho, J. Y., Ashman, R. B., & Turner, C. H. (1993). Young's modulus of trabecular and cortical bone material: ultrasonic and microtensile measurements. *Journal of biomechanics, 26*(2), 111-119.
Ribeiro, M., Monteiro, F. J., & Ferraz, M. P. (2012). Infection of orthopedic implants with emphasis on bacterial adhesion process and techniques used in studying bacterial-material interactions. *Biomatter, 2*(4), 176-194.
Rodriguez y Baena, R., Rizzo, S., Manzo, L., & Lupi, S. M. (2017). Nanofeatured Titanium Surfaces for Dental Implantology: Biological Effects, Biocompatibility, and Safety. *Journal of Nanomaterials, 2017*.
Roehling, S., Ghazal, G., Borer, T., Thieringer, F., & Gahlert, M. (2015). Implant Supported Fixed Dental Prostheses Using a New Monotype Zirconia Implant—A Case Report. *Dentistry journal, 3*(3), 79-92.
Roser, M., Ortiz-Ospina, E., & Ritchie, H. (2013). Life expectancy. *Our World in Data*.
Rosińczuk, J., Taradaj, J., Dymarek, R., & Sopel, M. (2018). Mechanoregulation of wound healing and skin homeostasis. *Chronic Wounds, Wound Dressings and Wound Healing*, 461-477.
Ru, J.-y., & Wang, Y.-f. (2020). Osteocyte apoptosis: the roles and key molecular mechanisms in resorption-related bone diseases. *Cell Death & Disease, 11*(10), 1-24.
Saeed, H., & Iqtedar, M. (2015). Aberrant gene expression profiles, during in vitro osteoblast differentiation, of telomerase deficient mouse bone marrow stromal stem cells (mBMSCs). *Journal of biomedical science, 22*(1), 11.
Salerno, M., Reverberi, A. P., & Baino, F. (2018). Nanoscale Topographical Characterization of Orbital Implant Materials. *Materials, 11*(5).
Sasaki, M., Kuroshima, S., Aoki, Y., Inaba, N., & Sawase, T. (2015). Ultrastructural alterations of osteocyte morphology via loaded implants in rabbit tibiae. *Journal of biomechanics, 48*(15), 4130-4141. https://doi.org/10.1016/j.jbiomech.2015.10.025
Sathish, S. (2016). Nanotubes: A step further in implants. *International Journal of Oral Health Dentistry, 2*(4), 213-216.
Sato, T., Verma, S., Andrade, C. D. C., Omeara, M., Campbell, N., Wang, J. S., Cetinbas, M., Lang, A., Ausk, B. J., & Brooks, D. J. (2020). A FAK/HDAC5 signaling axis controls osteocyte mechanotransduction. *Nature Communications, 11*(1), 3282.
Schett, G., Middleton, S., Bolon, B., Stolina, M., Brown, H., Zhu, L., Pretorius, J., Zack, D. J., Kostenuik, P., & Feige, U. (2005). Additive bone-protective effects of anabolic treatment when used in conjunction with RANKL and tumor necrosis factor inhibition in two rat arthritis models. *Arthritis & Rheumatism, 52*(5), 1604-1611.

Selinsky, C. L., & Howell, M. D. (2000). Soluble tumor necrosis factor receptor type I enhances tumor development and persistence in vivo. *Cellular immunology, 200*(2), 81-87.
Shapira, L., Klinger, A., Tadir, A., Wilensky, A., & Halabi, A. (2009). Effect of a niobium-containing titanium alloy on osteoblast behavior in culture. *Clinical oral implants research, 20*(6), 578-582.
Sheng, M. H., Lau, K., & Baylink, D. J. (2014). Role of osteocyte-derived insulin-like growth factor I in developmental growth, modeling, remodeling, and regeneration of the bone. *Journal of bone metabolism, 21*(1), 41-54.
Shih, N. R., Jo, O. D., & Yanagawa, N. (2002). Effects of PHEX antisense in human osteoblast cells. *Journal of the American Society of Nephrology, 13*(2), 394-399.
Shimabukuro, M., Ito, H., Tsutsumi, Y., Nozaki, K., Chen, P., Yamada, R., Ashida, M., Nagai, A., & Hanawa, T. (2019). The Effects of Various Metallic Surfaces on Cellular and Bacterial Adhesion. *Metals, 9*(11), 1145.
Sidambe, A. T. (2014). Biocompatibility of advanced manufactured titanium implants—A review. *Materials, 7*(12), 8168-8188.
Siemers, C., Wolter, D., & Sibum, H. (2016). New, Aluminum-and Vandium-Free Titanium Alloys for Osteosynthesis Applications. Proceedings of the 13th World Conference on Titanium.
Singaram, S., & Naidoo, M. (2019). The physical, psychological and social impact of long bone fractures on adults: A review. *African journal of primary health care & family medicine, 11*(1).
Singh, R., Singh, S., & Hashmi, M. S. J. (2016). Implant Materials and Their Processing Technologies. In *Reference Module in Materials Science and Materials Engineering*. Elsevier. https://doi.org/10.1016/B978-0-12-803581-8.04156-4
Sista, S., Wen, C., Hodgson, P. D., & Pande, G. (2013). Expression of cell adhesion and differentiation related genes in MC3T3 osteoblasts plated on titanium alloys: role of surface properties. *Materials Science and Engineering: C, 33*(3), 1573-1582. https://doi.org/10.1016/j.msec.2012.12.063
Sommer, N. G., Hahn, D., Okutan, B., Marek, R., & Weinberg, A.-M. (2019). Animal Models in Orthopedic Research: The Proper Animal Model to Answer Fundamental Questions on Bone Healing Depending on Pathology and Implant Material. In *Animal Models in Medicine and Biology*. IntechOpen.
Spatz, J. M., Wein, M. N., Gooi, J. H., Qu, Y., Garr, J. L., Liu, S., Barry, K. J., Uda, Y., Lai, F., & Dedic, C. (2015). The Wnt inhibitor sclerostin is up-regulated by mechanical unloading in osteocytes in vitro. *Journal of Biological Chemistry, 290*(27), 16744-16758.
Subramaniam, S., Breik, O., Cadd, B., Peart, G., Wiesenfeld, D., Heggie, A., Gibbons, S., & Nastri, A. (2018). Long-term outcomes of craniofacial implants for the restoration of facial defects. *International journal of oral and maxillofacial surgery, 47*(6), 773-782.
Subramanian, K., Tran, D., & Nguyen, K. T. (2012). Cellular responses to nanoscale surface modifications of titanium implants for dentistry and bone tissue engineering applications. In *Emerging Nanotechnologies in Dentistry* (pp. 113-136). Elsevier.
Sussman, H. I., & Volker, A. R. (2013). MDI Solutions for the Medically Compromised Patient. In *Mini Dental Implants* (pp. 101-116). Elsevier.
Takakubo, Y., Berce, A., Trebše, R., Tamaki, Y., Milošev, I., Al-Samadi, A., Tiainen, V.-M., & Konttinen, Y. (2013). Wear and corrosion in the loosening of total joint replacements (TJRs). In *Bio-Tribocorrosion in Biomaterials and Medical Implants* (pp. 74-110). Elsevier.
Tan, M. H., Baghi, A. D., Ghomashchi, R., Xiao, W., & Oskouei, R. H. (2019). Effect of niobium content on the microstructure and Young's modulus of Ti-xNb-7Zr alloys for medical implants. *Journal of the mechanical behavior of biomedical materials, 99*, 78-85.
Tanaka, Y., Nakayamada, S., & Okada, Y. (2005). Osteoblasts and osteoclasts in bone remodeling and inflammation. *Current Drug Targets-Inflammation & Allergy, 4*(3), 325-328.
Tasca, A., Astleford, K., Blixt, N. C., Jensen, E. D., Gopalakrishnan, R., & Mansky, K. C. (2018). SMAD1/5 signaling in osteoclasts regulates bone formation via coupling factors. *PloS one, 13*(9), e0203404.

TGA. (2021). *Personalised medical devices (including 3D-printed devices)* (5). (Personalised medical devices (including 3D-printed devices), Issue. https://www.tga.gov.au/sites/default/files/personalised-medical-devices-including-3d-printed-devices.pdf
Thi, M. M., Suadicani, S. O., Schaffler, M. B., Weinbaum, S., & Spray, D. C. (2013). Mechanosensory responses of osteocytes to physiological forces occur along processes and not cell body and require αVβ3 integrin. *Proceedings of the National Academy of Sciences, 110*(52), 21012-21017.
Thomas, P. C., Raghavan, S. R., & Forry, S. P. (2010). Monitoring and controlling oxygen levels in microfluidic devices. 26th Southern Biomedical Engineering Conference SBEC 2010, April 30-May 2, 2010, College Park, Maryland, USA.
Tomljenovic, L. (2011). Aluminum and Alzheimer's disease: after a century of controversy, is there a plausible link? *Journal of Alzheimer's Disease, 23*(4), 567-598.
Tsang, S. J., & Simpson, A. H. R. (2020). Pathogenesis of Biomaterial-Associated Infection. In *Racing for the Surface* (pp. 109-169). Springer.
Tunchel, S., Blay, A., Kolerman, R., Mijiritsky, E., & Shibli, J. A. (2016). 3D printing/additive manufacturing single titanium dental implants: a prospective multicenter study with 3 years of follow-up. *International journal of dentistry, 2016*.
Uggeri, J., Guizzardi, S., Scandroglio, R., & Gatti, R. (2010). Adhesion of human osteoblasts to titanium: A morpho-functional analysis with confocal microscopy. *Micron, 41*(3), 210-219. https://doi.org/10.1016/j.micron.2009.10.013
Van Bezooijen, R. L., Roelen, B. A., Visser, A., Van Der Wee-pals, L., De Wilt, E., Karperien, M., Hamersma, H., Papapoulos, S. E., Ten Dijke, P., & Lŏwik, C. W. (2004). Sclerostin is an osteocyte-expressed negative regulator of bone formation, but not a classical BMP antagonist. *The Journal of experimental medicine, 199*(6), 805-814.
Van Gastel, N., & Carmeliet, G. (2021). Metabolic regulation of skeletal cell fate and function in physiology and disease. *Nature Metabolism, 3*(1), 11-20.
Van Hal, S. J., Jensen, S. O., Vaska, V. L., Espedido, B. A., Paterson, D. L., & Gosbell, I. B. (2012). Predictors of mortality in Staphylococcus aureus bacteremia. *Clinical microbiology reviews, 25*(2), 362-386.
van Oers, R. F. M., Wang, H., & Bacabac, R. G. (2015). Osteocyte shape and mechanical loading. *Current osteoporosis reports, 13*(2), 61-66. 10.1007/s11914-015-0256-1
Varner, V. D., & Nelson, C. M. (2014). Cellular and physical mechanisms of branching morphogenesis. *Development, 141*(14), 2750-2759.
Vazouras, K. (2013). *Surface Analysis of SLA and SLActive Dental Implants*, The University of Manchester].
Veiga, C., Davim, J., & Loureiro, A. (2012). Properties and applications of titanium alloys: a brief review. *Rev. Adv. Mater. Sci, 32*(2), 133-148.
Verdins, G., Kanaska, D., & Kleinbergs, V. (2013). Selection of the method of hardness test. *Engineering for Rural Development*, 217-222.
Verissimo, N. C., Geilich, B. M., Oliveira, H. G., Caram, R., & Webster, T. J. (2015). R educing S taphylococcus aureus growth on T i alloy nanostructured surfaces through the addition of S n. *Journal of biomedical materials research Part A, 103*(12), 3757-3763.
Wadhwa, S., Godwin, S. L., Peterson, D. R., Epstein, M. A., Raisz, L. G., & Pilbeam, C. C. (2002). Fluid flow induction of cyclo-oxygenase 2 gene expression in osteoblasts is dependent on an extracellular signal-regulated kinase signaling pathway. *Journal of Bone and Mineral Research, 17*(2), 266-274.
Walters, B., Uynuk-Ool, T., Rothdiener, M., Palm, J., Hart, M. L., Stegemann, J. P., & Rolauffs, B. (2017). Engineering the geometrical shape of mesenchymal stromal cells through defined cyclic stretch regimens. *Scientific reports, 7*(1), 1-14.
Wang, D., Yu, C., Ma, J., Liu, W., & Shen, Z. (2017). Densification and crack suppression in selective laser melting of pure molybdenum. *Materials & Design, 129*, 44-52. https://doi.org/10.1016/j.matdes.2017.04.094

Wang, G., Moya, S., Lu, Z., Gregurec, D., & Zreiqat, H. (2015). Enhancing orthopedic implant bioactivity: refining the nanotopography. *Nanomedicine, 10*(8), 1327-1341.
Wang, G. C. (2016). *The utilization of slag in civil infrastructure construction*. Woodhead Publishing.
Wang, H., Zhao, Y., Mo, Z., Han, J., Chen, Y., Yu, H., Wang, Q., Liu, J., Li, C., & Zhou, Y. (2017). Comparison of short-segment monoaxial and polyaxial pedicle screw fixation combined with intermediate screws in traumatic thoracolumbar fractures: a finite element study and clinical radiographic review. *Clinics, 72*(10), 609-617.
Wang, X., He, Y., Tian, S., Zhu, F., Huang, B., Zhang, J., Chen, Z., & Wang, H. (2019). Fluid shear stress increases osteocyte and inhibits osteoclasts via downregulating receptor-activator of nuclear factor κB (RANK)/Osteoprotegerin expression in myeloma microenvironment. *Medical Science Monitor: International Medical Journal of Experimental and Clinical Research, 25*, 5961.
Wang, Y., Wan, C., Deng, L., Liu, X., Cao, X., Gilbert, S. R., Bouxsein, M. L., Faugere, M.-C., Guldberg, R. E., & Gerstenfeld, L. C. (2007). The hypoxia-inducible factor α pathway couples angiogenesis to osteogenesis during skeletal development. *The Journal of clinical investigation, 117*(6), 1616-1626.
Wei, M., Kuukasjärvi, P., Laurikka, J., Pehkonen, E., Kaukinen, S., Laine, S., & Tarkka, M. (2001). Inflammatory cytokines and soluble receptors after coronary artery bypass grafting. *Cytokine, 15*(4), 223-228.
Wen, C., Mabuchi, M., Yamada, Y., Shimojima, K., Chino, Y., & Asahina, T. (2001). Processing of biocompatible porous Ti and Mg. *Scripta Materialia, 45*(10), 1147-1153.
Wen, C., Yamada, Y., Shimojima, K., Chino, Y., Hosokawa, H., & Mabuchi, M. (2004). Compressibility of porous magnesium foam: dependency on porosity and pore size. *Materials Letters, 58*(3-4), 357-360.
Wood, C. L., Pajevic, P. D., & Gooi, J. H. (2017). Osteocyte secreted factors inhibit skeletal muscle differentiation. *Bone reports, 6*, 74-80.
Wu, C.-T., Chang, H.-T., Wu, C.-Y., Chen, S.-W., Huang, S.-Y., Huang, M., Pan, Y.-T., Bradbury, P., Chou, J., & Yen, H.-W. (2019). Machine learning recommends affordable new Ti alloy with bone-like modulus. *Materials Today*.
Wu, V., van Oers, R. F. M., Schulten, E. A. J. M., Helder, M. N., Bacabac, R. G., & Klein-Nulend, J. (2018). Osteocyte morphology and orientation in relation to strain in the jaw bone. *International journal of oral science, 10*(1), 2. 10.1038/s41368-017-0007-5
Xu, S., Wang, Y., Lu, J., & Xu, J. (2012). Osteoprotegerin and RANKL in the pathogenesis of rheumatoid arthritis-induced osteoporosis. *Rheumatology international, 32*(11), 3397-3403.
Xu, Z., Liang, Y., Lin, S., Chen, D., Li, B., Li, L., & Deng, Y. (2016). Crystal violet and XTT assays on Staphylococcus aureus biofilm quantification. *Current microbiology, 73*(4), 474-482.
Yan, Z., Wang, P., Wu, J., Feng, X., Cai, J., Zhai, M., Li, J., Liu, X., Jiang, M., & Luo, E. (2018). Fluid shear stress improves morphology, cytoskeleton architecture, viability, and regulates cytokine expression in a time-dependent manner in MLO-Y4 cells. *Cell Biology International, 42*(10), 1410-1422.
Yasuyuki, M., Kunihiro, K., Kurissery, S., Kanavillil, N., Sato, Y., & Kikuchi, Y. (2010). Antibacterial properties of nine pure metals: a laboratory study using Staphylococcus aureus and Escherichia coli. *Biofouling, 26*(7), 851-858.
You, L., Temiyasathit, S., Lee, P., Kim, C. H., Tummala, P., Yao, W., Kingery, W., Malone, A. M., Kwon, R. Y., & Jacobs, C. R. (2008). Osteocytes as mechanosensors in the inhibition of bone resorption due to mechanical loading. *Bone, 42*(1), 172-179.
Yu, J., Xi, S., Pan, S., Wang, Y., Peng, Q., Shi, R., Wang, C., & Liu, X. (2021). Machine learning-guided design and development of metallic structural materials. *Journal of Materials Informatics, 1*(2), 9.
Yuan, H. (2013). *Morphology of osteocyte cells in normal and hyper-gravity*, Queensland University of Technology].
Zareidoost, A., Yousefpour, M., Ghaseme, B., & Amanzadeh, A. (2012). The relationship of surface roughness and cell response of chemical surface modification of titanium. *Journal of Materials Science: Materials in Medicine, 23*(6), 1479-1488.

Zayed, A. (2018). *A Complete Overview Of Bone Cancer: From Symptoms To Treatment*. consumer health digest. Retrieved 14 August 2018, from https://www.consumerhealthdigest.com/bone-health/bone-cancer.html

Zhang, J.-M., & An, J. (2007). Cytokines, inflammation and pain. *International anesthesiology clinics, 45*(2), 27.

Zhang, X., Duyck, J., Vandamme, K., Naert, I., & Carmeliet, G. (2014). Ultrastructural characterization of the implant interface response to loading. *Journal of dental research, 93*(3), 313-318.

Zhang, Z. H., Jia, X. Y., Fang, J. Y., Chai, H., Huang, Q., She, C., Jia, P., Geng, D. C., & Xu, W. (2020). Reduction of SOST gene promotes bone formation through the Wnt/β-catenin signalling pathway and compensates particle-induced osteolysis. *Journal of Cellular and Molecular Medicine, 24*(7), 4233-4244.

Zimmerman, S. M., Heard-Lipsmeyer, M. E., Dimori, M., Thostenson, J. D., Mannen, E. M., O'Brien, C. A., & Morello, R. (2018). Loss of RANKL in osteocytes dramatically increases cancellous bone mass in the osteogenesis imperfecta mouse (oim). *Bone reports, 9*, 61-73.

Zysset, P. K., Guo, X. E., Hoffler, C. E., Moore, K. E., & Goldstein, S. A. (1999). Elastic modulus and hardness of cortical and trabecular bone lamellae measured by nanoindentation in the human femur. *Journal of biomechanics, 32*(10), 1005-1012.

# 10. Appendix

## 10.1 Housekeeping genes (GAPDH) for both osteoblast and osteocytes gene expression characterised on the three different titanium alloy substrates.

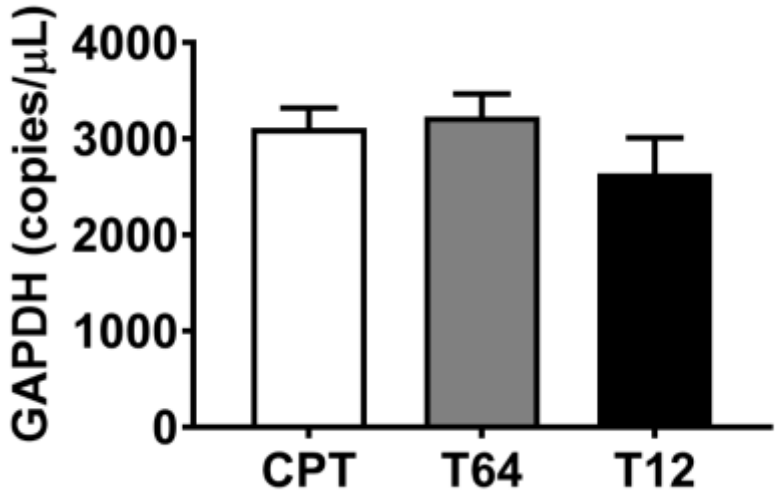


**Figure 46.** Housekeeping gene GAPDH for osteocyte cells characterised on titanium alloy substrates CPT, T64 and T12. Analysed following ddPCR. n = 3 independent biological replicates. Data is presented as mean ± SEM. Statistical significance was determined using One-Way ANOVA (with Turkey's post hoc analysis).

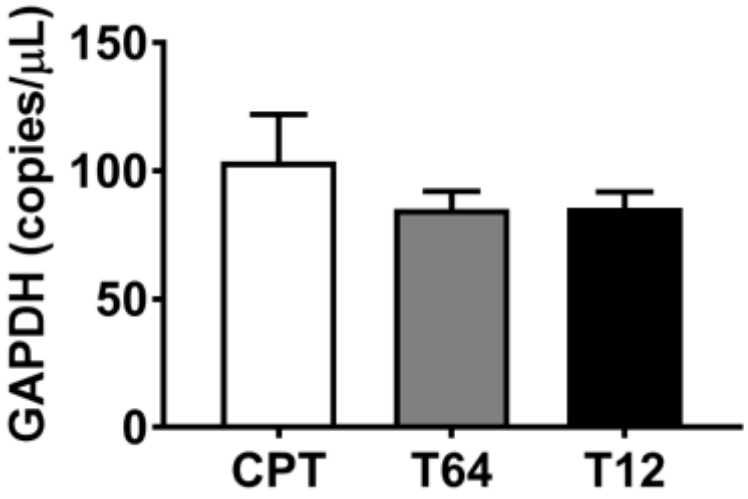


**Figure 47.** Housekeeping gene GAPDH for osteoblast cells characterised on titanium alloy substrates CPT, T64 and T12. Analysed following ddPCR. n = 3 independent biological replicates. Data is presented as mean ± SEM. Statistical significance was determined using One-Way ANOVA (with Turkey's post hoc analysis).

## 10.2 Housekeeping genes (GAPDH) for both osteoblast and osteocytes gene expression characterised on the porous 3D printed titanium alloy substrates.

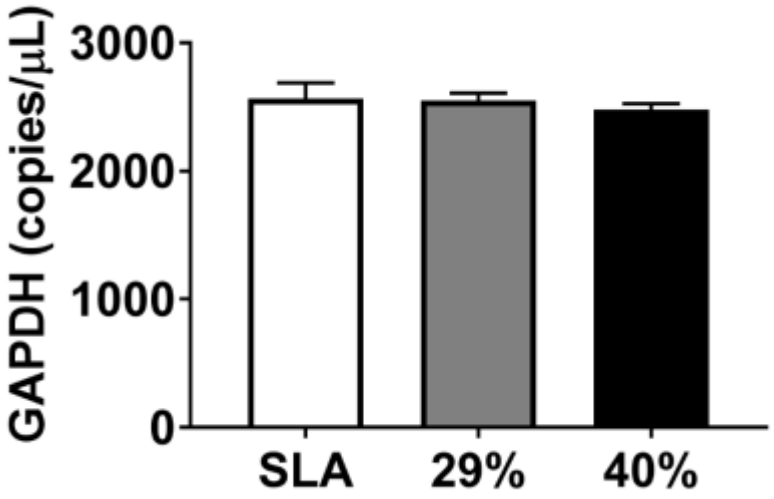


**Figure 48.** Housekeeping gene GAPDH for osteocyte cells characterised on titanium alloy substrates SLA, 29% and 40%. Analysed following ddPCR. n = 3 independent biological replicates. Data is presented as mean ± SEM. Statistical significance was determined using One-Way ANOVA (with Turkey's post hoc analysis).

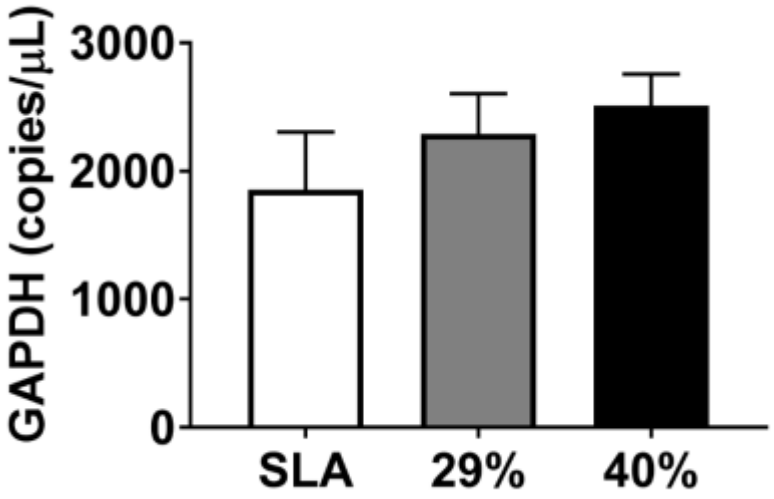


**Figure 49.** Housekeeping gene GAPDH for osteoblast cells characterised on titanium alloy substrates SLA, 29% and 40%. Analysed following ddPCR. n = 3 independent biological replicates. Data is presented as mean ± SEM. Statistical significance was determined using One-Way ANOVA (with Turkey's post hoc analysis).

## 10.3 Housekeeping genes (GAPDH) for osteocytes gene expression characterised on the three different titanium alloy substrates under FSS conditions.

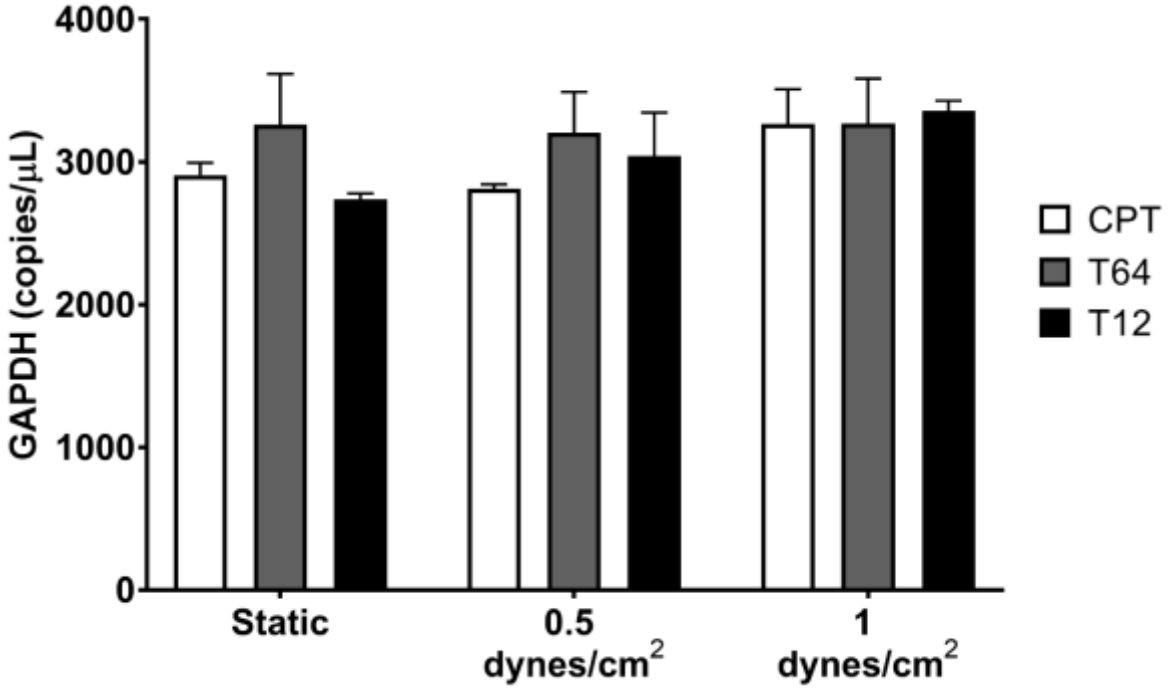


**Figure 50.** Housekeeping gene GAPDH for osteocyte cells characterised on titanium alloy substrates (CPT, T64 and T12) under fluid shear stress condition for 24 hours. Comparison of static control, fluid shear stress of 0.5 dynes/cm$^2$ and 1 dynes/cm$^2$ for the OCY454 gene expression of OPG, cultured on titanium alloy substrates. n = 3 independent biological replicates. Data is presented as mean ± SEM. Statistical significance was determined using Two-Way ANOVA (with Turkey's post hoc analysis).